AD-753 469

STRESS ANALYSIS OF AN ADHESIVE LAP JOINT SUBJECTED TO TENSION, SHEAR FORCE AND BENDING MOMENTS

Murlidhar H. Pahoja

Illinois University

Prepared for:

Naval Air Systems Command

August 1972

UILU-ENG 72 6009

T.&A.M. REPORT NO. 361

STRESS ANALYSIS OF AN ADHESIVE LAP JOINT SUBJECTED TO TENSION, SHEAR FORCE AND BENDING MOMENTS

by

Murlidhar H. Pahoja

Sponsored by

Contract No. N00019-72-C-0274
Department of the Navy
Naval Air Systems Command

DEPARTMENT OF THEORETICAL AND APPLIED MECHANICS
UNIVERSITY OF ILLINOIS
URBANA, ILLINOIS

T. & A. M. Report 361

STRESS ANALYSIS OF AN ADHESIVE LAP JOINT SUBJECTED TO TENSION, SHEAR FORCE AND BENDING MOMENTS

by

Murlidhar H. Pahoja

Contract No. NOOO19-72-C-0274

Department of the Navy

Naval Air Systems Command

Department of Theoretical and Applied Mechanics

University of Illinois at Urbana-Champaign

August, 1972

I

II

ELASTIC STRESS ANALYSIS OF AN ADHESIVE LAP JOINT SUBJECTED TO TENSION, SHEAR FORCE AND BENDING MOMENTS

Murlidhar H. Pahoja, Ph.D.
Department of Theoretical and Applied Mechanics
University of Illinois at Urbana-Champaign, 1972

A stress analysis of the lap joint is presented treating the problem as one of plane strain. The joint is subjected to a general loading, consisting of tension, shear force and bending moments. The variation in the material properties and thickness of the two adherends is considered. The displacement field in the adhesive layer is expressed in series form and the compatibility condition at the interface is used to express the displacement field in the adherends. The potential energy of the joint is calculated and minimized to obtain linear, ordinary differential equations and boundary conditions. The differential equations are solved on the computer.

Photoelasticity is used to confirm the theory. Two specimens of lap joint using a 1/4 in. layer of a photoelastic plastic simulating the adhesive, are tested photoelastically. The agreement between the theoretical and the experimental results is found to be good.

Design recommendations for the lap joint are made based on the results of this investigation.

ACKNOWLEDGEMENT

The author is grateful to his advisor, Professor H. T. Corten for his able guidance and encouragement throughout the course of the study. Thanks are due to Professor M. Stippes for his very helpful suggestions regarding theoretical stress analysis and to Professor C. E. Taylor for his guidance in setting up the experiments. Help and guidance from Professors R. E. Miller and J. W. Phillips regarding computer programming is greatly appreciated.

Recognition is due to Miss Karen Hageman for her efficient preparation of the final manuscript. Appreciation is also due to Eddie Terrell and Hardin T. James, Jr. for their assistance in preparing the figures.

नमः सरस्वति महाभागे ज्ञानदे विज्ञानदे ।
विश्वरूपे विद्ये सुमतिं देहि नमोस्तुते ।।
इयं या श्रेष्ठिनी विज्ञानविद्या तवप्रदत्ता ।
यैव बसृजे घोरं तयैव शान्तिरस्तु नः ।।

Hail! O, Saraswati! Giver of Knowledge,
Giver of Sciences,
All pervading, Grant us Wisdom,
May the Sciences that you give us,
Bring not destruction but Peace.

TABLE OF CONTENTS

			Page
1.	INTRODUCTION		1
2.	REVIEW OF PREVIOUS THEORETICAL AND EXPERIMENTAL WORK		6
	2.1	Introduction	6
	2.2	Volkersen's Theory	6
	2.3	Theory of Goland and Reissner	8
	2.4	Plantema's Modification	12
	2.5	Modification by Kelsey and Benson	13
	2.6	Cornell's Modification	14
	2.7	Stepped Joint of Erdogan and Ratwani	15
	2.8	Finite Element Analysis	17
	2.9	Experimental Stress Analysis	18
	2.10	Conclusion	20
3.	ANALYSIS OF LAP JOINT		21
	3.1	Problem	21
	3.2	Assumptions	21
	3.3	Derivation of Differential Equations	21
	3.4	Parameters of Similarity	35
	3.5	Case of Identical Adherends	36
	3.6	Condition for Uniform Shear Stress in an Antisymmetric Joint	45
	3.7	Solution for the General Case	48
4.	EXPERIMENTAL INVESTIGATION		49
	4.1	Introduction	49
	4.2	Material and Specimen Preparation	49
	4.3	Test Equipment and Procedure	50

TABLE OF CONTENTS (Continued)

		Page
5.	ANALYTICAL AND EXPERIMENTAL RESULTS	52
	5.1 General	52
	5.2 Effect of m and n	52
	5.3 Comparison with Experiment	54
	5.4 Case of Identical Adherends	55
	5.4.1 Shear Stress	56
	5.4.2 Normal Stresses	58
	5.4.3 Effect of V_f	61
	5.4.4 Design of Lap Joint	61
	5.5 Case of Pure Moment	62
	5.6 Non-Identical Adherends	63
6.	SUMMARY AND CONCLUSIONS	65
REFERENCES		67
APPENDIX A	SOLUTION OF DIFFERENTIAL EQUATIONS IN THE GENERAL CASE	69
APPENDIX B	FORTRAN PROGRAM BASED ON IBM SYSTEM 360/75 FOR GENERAL CASE	76
APPENDIX C	FORTRAN PROGRAM BASED ON IBM SYSTEM 360/75 FOR THE IDENTICAL ADHEREND CASE	85
FIGURES		90
VITA		157

LIST OF FIGURES

Figure		Page
1.	Stress Due to Stretching of Adherends (a) Joint Prior to Stretching (b) Joint After Stretching	90
2.	System Considered by Goland and Reissner (a) Forces Acting on Adherends (b) Forces at Joint Edges	91
3.	Lap Joint Under a General Loading (a) Forces Acting on Adherends (b) Forces at Joint Edges	92
4.	Joint Considered by Cornell	93
5.	Step Joint of Erdogan and Ratwani (a) Multiple Step Joint (b) Single Step Joint	94
6.	Dimensions of Test Models	95
7.	Photoelastic Test Bench	96
8.	Loading the Specimen at an Angle	97
9.	Calibration of Araldite 6020 Epoxy to Determine Fringe Value	98
10.	Theoretical Distribution of τ_{xy} at Midplane for Different Values of m	99
11.	Theoretical Distribution of τ_{xy} at Interfacial Plane for Different Values of m	100
12.	Theoretical Distribution of σ_y at Midplane for Different Values of m.	101
13.	Theoretical Distribution of σ_y at Interfacial Plane for Different Values of m	102
14.	Theoretical Distribution of σ_x at Midplane for Different Values of m	103
15.	Theoretical Distribution of σ_x at Interfacial Plane for Different Values of m	104
16.	Fringe Pattern at No Load (a) 2 in. Overlap Specimen (b) 3 in. Overlap Specimen	105
17.	Comparison of Theory and Experiment (y = 0 plane) a = 2 in., V/P = 0	106

LIST OF FIGURES (Continued)

Figure — Page

18. Comparison of Theory and Experiment (y = t/2 plane) a = 2 in., V/P = 0 . . . 107

19. Comparison of Theory and Experiment (y = 0 plane) a = 3 in., V/P = 0 . . . 108

20. Comparison of Theory and Experiment (y = t/2 plane) a = 3 in., V/P = 0 . . . 109

21. Comparison of Theory and Experiment (y = 0 plane) a = 2 in., V/P = 0.8 . . . 110

22. Comparison of Theory and Experiment (y = t/2 plane) a = 2 in., V/P = 0.8 . . . 111

23. Comparison of Theory and Experiment (y = 0 plane) a = 3 in., V/P = 0.6 . . . 112

24. Comparison of Theory and Experiment (y = t/2 plane) a = 3 in., V/P = 0.6 . . . 113

25. Comparison of Experimental and Theoretical Fringe Patterns (a = 2 in., V/P = 0.0, 0.4) 114

26. Comparison of Experimental and Theoretical Fringe Patterns (a = 2 in., V/P = 0.5, 0.6) 115

27. Comparison of Experimental and Theoretical Fringe Patterns (a = 2 in., V/P = 0.7, 0.8) 116

28. Comparison of Experimental and Theoretical Fringe Patterns (a = 3 in., V/P = 0.0, 0.4) 117

29. Comparison of Experimental and Theoretical Fringe Patterns (a = 3 in., V/P = 0.5, 0.6) 118

30. Comparison of Experimental and Theoretical Fringe Patterns (a = 3 in., V/P = 0.7, 0.8) 119

31. Shear Stress Concentration Factor at the Mid-plane of Adhesive Layer as a Function of t_1/t, E_1/E, and S_f, for $V_f = 0$ 120

32. Shear Stress Concentration Factor at the Interfacial Plane as a Function of t_1/t, E_1/E, and S_f, for $V_f = 0$ 121

33. Shear Stress Concentration Factor at the Mid-plane of the Adhesive Layer as Function of t_1/t, E_1/E, and S_f, for $V_f = 2$ 122

34. Shear Stress Concentration Factor at the Interfacial Plane as a Function of t_1/t, E_1/E, and S_f, for $V_f = 2$ 123

35. Maximum Shearing Stress Factor as a Function of t_1/t, E_1/E, and S_f, for $V_f = 0$ 124

LIST OF FIGURES (Continued)

Figure		Page
36.	Maximum Shearing Stress Factor as a Function of t_1/t, E_1/E, and S_f, for $V_f = 2$	125
37.	Shear Stress Concentration Factor at the Midplane as a Function of S_f and V_f	126
38.	Shear Stress Concentration Factor at the Interfacial Plane as a Function of S_f and V_f	127
39.	Maximum Shearing Stress Factor as a Function of S_f and V_f	128
40.	σ_y Concentration Factor at the Mid-plane as a Function of t_1/t, E_1/E, N_f, and V_f	129
41.	σ_y Concentration Factor at the Interfacial Plane as a Function of t_1/t, E_1/E, N_f, and V_f	130
42.	σ_x Concentration Factor at the Mid-plane as a Function of t_1/t, E_1/E, N_f and V_f	131
43.	σ_x Concentration Factor at the Interfacial Plane as a Function of t_1/t, E_1/E, N_f, and V_f	132
44.	Maximum Principal Stress Factor as a Function of t_1/t, E_1/E, N_f, and V_f	133
45.	σ_y Concentration Factor at the Mid-plane as a Function of N_f and V_f	134
46.	σ_y Concentration Factor at the Interfacial Plane as a Function of N_f and V_f	135
47.	σ_x Concentration Factor at the Mid-plane as a Function of N_f and V_f	136
48.	σ_x Concentration Factor at the Interfacial Plane as a Function of N_f and V_f	137
49.	Maximum Principal Stress Factor as a Function of N_f and V_f	138
50.	σ_y Concentration Factor at the Mid-plane as a Function of $(N_f)^2$ and V_f	139
51.	σ_y Concentration Factor at the Interfacial Plane as a Function of $(N_f)^2$ and V_f	140
52.	σ_x Concentration Factor at the Mid-plane as a Function of $(N_f)^2$ and V_f	141

LIST OF FIGURES (Continued)

Figure		Page
53.	σ_x Concentration Factor at the Interfacial Plane as a Function of $(N_f)^2$ and V_f	142
54.	Maximum Principal Stress Factor as a Function of $(N_f)^2$ and V_f	143
55.	τ_{xy} Distribution at Interfacial Plane (y = t/2) As a Function of V_f	144
56.	σ_y Distribution at Interfacial Plane (y = t/2) As a Function of V_f	145
57.	σ_x Distribution at Interfacial Plane (y = t/2) As a Function of V_f	146
58.	Design of Lap Joint (a) Pull Along the Adherends (b) Loading for $V_f = 1$	147
59.	τ_{xy} for Joint Loaded in Pure Moment	148
60.	σ_y for Joint Loaded in Pure Moment	149
61.	σ_x for Joint Loaded in Pure Moment	150
62.	$(\tau_{xy})_{max}$ in Non-Identical Adherend Joint for V = 0	151
63.	$(\sigma_y)_{max}$ in Non-Identical Adherend Joint for V = 0	152
64.	$(\sigma_x)_{max}$ in Non-Identical Adherend Joint for V = 0	153
65.	$(\tau_{xy})_{max}$ in Non-Identical Adherend Joint for $M_1 = M_2 = 0$	154
66.	$(\sigma_y)_{max}$ in Non-Identical Adherend Joint for $M_1 = M_2 = 0$	155
67.	$(\sigma_x)_{max}$ in Non-Identical Adherend Joint for $M_1 = M_2 = 0$	156

NOMENCLATURE

Adherends I and II	As defined in Fig. 3
a	Overlap length
E	Young's modulus of adhesive material
E_1 , E_2	Young's modulii of adherends I and II
G	Shear modulus of adhesive material
G_1 , G_2	Shear modulii of adherends I and II
I_0	Strain energy of the adhesive
I_1 , I_2	Strain energy of adherends I and II
I	Strain energy of the joint
M_1 , M_2	Bending moments per unit width of joint
m	Integer defined in Eq. (3.1)
n	Integer defined in Eq. (3.2)
N_f	Dimensionless parameter defined in Eq. (5.3)
P	Tensile force per unit width of joint
$Q = \lambda + 2G$	
$Q_1 = E_1 / (1 - \mu_1^2)$	
$Q_2 = E_2 / (1 - \mu_2^2)$	
S_f	Dimensionless parameter defined in Eq. (5.2)
t	Thickness of adhesive layer
t_1 , t_2	Thicknesses of adherends I and II
u	Displacement in x-direction in adhesive
U_1 , U_2	Displacement in x-direction in adherends I and II

NOMENCLATURE (Continued)

v	Displacement in y-direction in adhesive
V_1 , V_2	Displacements in y-direction in adherends I and II
V	Shear force per unit width of joint
V_f	Dimensionless parameter defined in Eq. (5.1)
x , y	Rectangular coordinates
α_{ij} , β_{ij} , δ_{ij}	Variables defined in Eq. (3.7)
ϵ_x , ϵ_y	Normal strains in adhesive
ϵ_{1x} , ϵ_{1y} , ϵ_{2x} , ϵ_{2y}	Normal strains in adherends I and II
γ_{xy}	Shear strain in adhesive
γ_{1xy} , γ_{2xy}	Shear strain in adherends I and II
λ	Lame's constant for adhesive material
λ_1 , λ_2	Lame's constants for adherends I and II
μ	Poisson ratio of adhesive material
μ_1 , μ_2	Poisson ratios of adherends I and II
σ_x , σ_y	Normal stresses in adhesive
σ_{1x} , σ_{1y} , σ_{2x} , σ_{2y}	Normal stresses in adherends I and II
τ_{xy}	Shear stress in adhesive
τ_{1xy} , τ_{2xy}	Shear stress in adherends I and II
ϕ	Force defined on page 46

1. INTRODUCTION

In the last two decades, adhesive bonding has become more and more common in engineering structures. The advantages of the adhesive joint over the conventional mechanical fasteners are, savings in weight and cost and elimination of holes which can cause excessive stress concentration.

The commonest type of joint in use today, is the lap joint where two adherends overlap and are fixed together by a layer of adhesive between them (Fig. 1a). The main advantage of this joint is its simplicity in design. Further, where the surfaces need chemical preparation, the adherends are easy to handle. It is also a simple type of joint to cure. The chief disadvantage of this type of joint is that when loaded in tension, varying shearing and tearing stresses are produced in the adhesive as well as the adherends, and very high peak stresses are produced at or very near the ends of the overlap.

Failure in a joint may occur either in the adherend or in the adhesive or at the interface. A failure at the interface is termed as 'adhesive,' since it involves the failure of the bond between the adhesive and the adherend. When the fracture occurs either inside the adhesive or inside the adherend, the failure is then termed as 'cohesive.' In a cohesive failure, the material at the two fracture surfaces is the same. The interfacial adhesion of modern adhesives is high so that failure mostly occurs either in the adhesive as in the case of metal to metal joints, or in the adherends as happens with wood joints.

The stress in the adhesive layer is dependent on the geometrical proportions and the elastic constants of the materials of the joint, and on the nature of the forces acting on the joint. When loaded in tension, non-uniform shear and tearing stresses are developed in the adhesive layer. The shear stress is parallel to the interface

while the tearing stresses are normal to the adhesive face. It has been predicted theoretically and confirmed experimentally that the peak shear and tearing stresses occur at the two ends of the overlap. This concentration of stresses at the ends of the overlap is due to two main causes, namely to the differential strain of the adherends and their bending.

Fig. 1a shows a lap joint loaded in tension. Each adherend bears the full load P just before the joint and transmit it gradually to the other through the adhesive. Thus the stress in adherend (I) will be the highest at A and gradually diminish towards B where it will be zero. On the contrary the stress in adherend (II) will be the highest at B and diminish to zero at A. The adherends (I) and (II) will develop tensile strains proportional to the stresses resulting in the deformation as shown in Fig. 1b. The displacement is the highest at the two ends of the overlap and therefore the highest shear stress in the adhesive can be expected to occur at these two points.

As can be seen in Fig. 1a, the two equal and opposite tensile forces acting on the joint are not colinear, and the joint therefore, is not in equilibrium. In order to overcome this difficulty, it is generally assumed that the line of action of the two forces is oblique and passes through the midpoint of the joint. This is equivalent to the addition of a shear force V (Fig. 2) so that the moment due to P is balanced by the moment due to V. This configuration of forces produces bending along the joint. The stresses developing in this way are normal to the interface, and are called "tearing" stresses; they are highest at the areas adjoining the ends of the overlap.

The earliest theoretical analysis of lap joints is that done by Volkersen (1), in which the stresses arising from the differential straining are considered but the tearing stresses are ignored. The next analysis is that of Goland and Reissner (2) who took the bending deformation of the adherends into account as well as the tearing stresses in the adhesive. Subsequent modifications to the theories of Volkersen and

Goland and Reissner have been made by Plantema (3) and Kelsey and Benson (4). These theories are reviewed and discussed in detail in Chapter II.

The results from these theories indicate a non-uniform distribution of shear stress with peaks at the ends of the overlap. While in a qualitative sense this distribution is in agreement with what has been observed experimentally, the magnitude of the shear stress in the vicinity of the ends of the overlap is found to be in error. This is a serious shortcoming since the highest stresses occur in the same area. This inaccuracy is mainly due to the assumption made in these analyses that the stresses do not vary in the direction of the thickness of the adhesive. Irrespective of how small the thickness of the adhesive layer may be, it has to be taken under consideration for the stress distribution in the areas distant by the same order of magnitude from the edge. Another important limitation of the above theories is that the joint is considered to be loaded in tension only. In a general case, the lap joint could be subject to shear forces and bending moments as shown in Fig. 3, the only restriction being that the external forces and bending moments be in equilibrium.

The objective of the present work is to analyze the lap joint when subjected to the general loading (Fig. 3) and to predict the stresses more accurately by allowing them to vary through the thickness of the adhesive layer. The analysis does not put any restriction on the thickness of the adhesive and is therefore, valid for thin as well as thick adhesives. The thickness of the adhesive however, is required to be much smaller than the length of the overlap which of course, is realistic. One major limitation of the previous theories as well as the present analysis is the assumption that the adhesive is isotropic and linearly elastic. The behavior of most adhesives is viscoelastic depending on time, temperature and previous history. Even when an adhesive can be considered to be elastic, it is more likely that the stress-strain curve is a non linear one. Furthermore, as the adhesive sets in between the adherends, it may do

so in an uneven fashion so that it would be strictly inadmissible to consider the adhesive layer as homogeneous and isotropic. The nature of such variations is however, uncertain and any attempt to incorporate the viscoelasticity or the non-homogeneity of the adhesive into the analysis would render the analysis extremely complicated. Further, any plastic flow of the adhesive would have a relieving effect on the peak stresses in the adhesive and an elastic analysis would therefore, provide a built-in factor of safety. It is felt that once a reasonable analysis based on linear elasticity of the adhesive is available for comparison, it would then be possible to use such tools as finite element analysis to incorporate the non-linear elastic or plastic behavior of the adhesive.

As regards the adherends, they are assumed to behave as beams or in other words the lateral stress σ_y in the adherends is considered negligible and their mechanical behavior is assumed to be isotropic and linearly elastic. While in the case of metal adherends this assumption holds good, it is not strictly valid for wood and plastic adherends. Wood, although linearly elastic, is anisotropic and its mechanical properties vary with the direction relative to the grain and the way of loading. Yet for the relative comparison between similar joints the theoretical results are expected to be sufficient, since the nature and directions of the developing stresses do not vary considerably from joint to joint. In the case of adherends which exhibit plastic behavior, the theoretical results may not be applicable since the yield in the adherends will greatly increase the differential strain and consequently the shear stress in the adhesive layer.

The analysis is based on the theory of elasticity treating the joint as a plane strain problem and therefore, it goes without saying that the results are valid only for small deformations, and for joints with sufficiently large widths.

The experimental part of the present investigation is designed to check and confirm the theoretical results, both along the length of the overlap as well as through the

thickness of the adhesive. The stresses in the adhesive layer are determined photoelastically since the photoelastic methods provide a simple and effective means for handling plane problems such as the one under consideration.

2. REVIEW OF PREVIOUS THEORETICAL AND EXPERIMENTAL WORK

2.1 Introduction

Several papers have been published analyzing stresses in various types of adhesive joints. In the case of double lap joints and scarf joints the analysis is relatively simple because of the inherent symmetry of the joints. The single lap joint presents a special case where the eccentricity in loading produces a bending moment which has to be accounted for in the stress analysis. Theories specifically dealing with the single lap joint will therefore, be reviewed here. Theories dealing with joints such as double lap joint, scarf joint, butt joint or tubular joints will not be included in the review.

Experimental works have been published describing tests to determine the strength of lap joints. Such works will be referred to when useful in demonstrating a point in relation to a theory. Of greater interest are experimental works where the main interest is the distribution stresses in the joint. These works will be reviewed in some detail.

2.2 Volkersen's Theory

The simplest approximate theory is that attributed to Volkersen (1). This analysis is concerned only with the stresses arising from the differential straining in lap joints and does not examine the tearing stresses resulting from the bending of the adherends. The bonded members are assumed to be in pure tension and the elongation of the adherends ϵ_x and the shear deformations of the adhesive γ_{xy} are taken into account as in shear lag problems. It is further assumed that ϵ_y in the adhesive is zero so that the shear stress τ_{xy} is constant over the thickness of the adhesive layer. The results indicate a non-uniform distribution of shear stress with peaks at the ends of the overlap. Volkersen compared the maximum shearing stress at the end

of the overlap with the mean stress and evaluated the stress concentration factor η, which is given by,

$$\eta = \sqrt{D/W} \quad \frac{W - 1 + \cosh \sqrt{DW}}{\sinh \sqrt{DW}}$$

where,

$$D = Ga^2 / E_2 t_2 t$$

$$W = (E_1 t_1 + E_2 t_2) / E_1 t_1$$

Here $E_1 t_1 > E_2 t_2$, and the maximum stress occurs at the interface with adherend (II).

For identical adherends W reduces to 2 and the factor of stress concentration can be written as,

$$\eta = \sqrt{D/2} \coth \sqrt{D/2}$$

Thus it is seen that for identical adherends the factor η of stress concentration is a function of a single dimensionless coefficient D.

In the case of a joint between adherends that are not identical, the values of D and W are different at the two interfaces. At the interface with an adherend of higher rigidity, D is smaller and W larger than the corresponding values of D and W at the interface with less rigid member. Mylonas and deBruyne (5) show in the form of a graph the variation of Volkersen's stress concentration factor η in terms of D for various values of W. It can be readily seen from this graph that η is smaller for lower values of D and higher values of W. Thus the stress concentration would be higher at the interface with the less rigid member. The same result is shown by Greenwood (6) by calculating the factors of stress concentration at the two interfaces

of a joint between steel and rubber adherends. The conclusion then would be that it is disadvantageous to have joints between adherends that greatly differ in rigidity since this would result in a much greater stress concentration at one interface.

Volkersen's theory, while it indicates in a general way the distribution of shear stress in the adhesive layer and the importance of various parameters which have an effect on this distribution, has the following shortcomings.

(1) Bending deformation of the adherends and the associated tearing stresses in the adhesive are ignored.

(2) The assumption that the stress does not vary through the thickness of the adhesive is shown to be untrue in the proximity of the ends of the overlap, by Mylonas (7) and by Tuzi and Shimada (8) in their photoelastic experiments. This assumption results in inaccurate prediction of stresses in the area where the maximum stress occurs, and the factor of stress concentration obtained by this theory is therefore, unreliable.

(3) The analysis limits itself to the case when the members are subjected to tensile loads only. Shear force and bending loads are not considered.

2.3 Theory of Goland and Reissner (2)

This theory takes into account the bending deformation of the adherends and also the tearing stresses in the adhesive. The system considered is that shown in Fig. 2a. The line of action of the tensile force R is assumed to pass through the mid-point of the adhesive layer. This is equivalent to a system where a small shear force V acts normal to P so that the couple due to P is balanced by the couple due to V. The adherends are identical in terms of mechanical properties as well as geometry.

Goland and Reissner recognized that the bending of the adherends outside the joint region has a pronounced effect upon the stress distribution in the joint itself. This effect is expressed via their bending moment factor k which is obtained by treating the

adherends as cylindrically bent plates. The value of k is given by:

$$\frac{1}{k} = 1 + 2\sqrt{2} \tanh \left[\frac{a}{4t_1}\sqrt{6(1-\mu_1^2) \cdot P/(E_1 t_1)}\right]$$

The system can now be reduced to that shown in Fig. 2b where,

$$M = \frac{kPt_1}{2}$$

$$P \simeq R$$

and

$$V = kP\sqrt{3(1-\mu_1^2) \cdot P/(E_1 t_1)}$$

Goland and Reissner considered two cases.

(1) In the first approximation, where $t/t_1 \ll E/E_1$, the presence of the adhesive layer is ignored and the joint is assumed to be a homogeneous isotropic rectangular slab. The calculated stresses are those of the adherends along the glue line, and are assumed to be equal to those of the adhesive layer. The values of the shear stress τ and the tearing stress σ are given as converging series. The results show that while the tearing stress is high at the edge of the joint, the shear stress is zero. The shear stress however, rises rapidly to a maximum in close proximity to the edge.

(2) In the second case where $t/t_1 \gg E/E_1$, the adhesive layer is considered to be flexible so that the transverse normal strain and the shear strain in the adherends may be neglected in comparison with the corresponding strains in the adhesive. In this approximation the adhesive is assumed to behave like a system of infinitesimal springs placed between two plates. The distributions of shear stress τ and the tearing stress σ are obtained as follows:

$$\frac{\tau}{p} \cdot \left(\frac{a}{t_1}\right) = \frac{1}{4} \left[\frac{\beta a}{2t_1} (1+3k) \cdot \frac{\cosh(\beta x/t_1)}{\sinh(\beta a/2t_1)} + 3(1-k) \right]$$

and

$$\frac{\sigma}{p}\left(\frac{a}{2t_1}\right)^2 = \frac{1}{\Delta} \left[(R_2\lambda^2 \cdot k/2 + \lambda k_1 \cdot \cosh\lambda \cdot \cos\lambda) \cdot \cosh\left(\frac{2\lambda x}{a}\right) \cdot \cos\left(\frac{2\lambda x}{a}\right) + (R_1\lambda^2 \cdot k/2 + \lambda k_1 \cdot \sinh\lambda \cdot \sin\lambda) \cdot \sinh\left(\frac{2\lambda x}{a}\right) \cdot \sin\left(\frac{2\lambda x}{a}\right) \right]$$

where,

$$\beta^2 = \frac{8Gt_1}{E_1 t}$$

$$\lambda = \frac{a}{2t_1} \left(\frac{6Et_1}{E_1 t}\right)^{\frac{1}{4}}$$

$$R_1 = \cosh\lambda \cdot \sin\lambda + \sinh\lambda \cdot \cos\lambda$$

$$R_2 = \sinh\lambda \cdot \cos\lambda - \cosh\lambda \cdot \sin\lambda$$

$$\Delta = \tfrac{1}{2}(\sinh 2\lambda + \sin 2\lambda)$$

$$k_1 = Va/(2Pt_1)$$

$$p = P/t_1$$

The maximum values of τ and σ are found at the edge of the joint and are given by,

$$\frac{\tau_{max}}{p} \cdot \left(\frac{a}{t_1}\right) = \frac{1}{4} \left[\frac{\beta a}{2t_1} (1 + 3k) \coth \frac{\beta a}{2t_1} + 3(1 - k) \right]$$

and

$$\frac{\tau_{max}}{p} \cdot \left(\frac{a}{2t_1}\right)^2 = \frac{\lambda^2 k}{2} \cdot \frac{\sinh 2\lambda - \sin 2\lambda}{\sinh 2\lambda + \sin 2\lambda} + \lambda k_1 \frac{\cosh 2\lambda + \cos 2\lambda}{\sinh 2\lambda + \sin 2\lambda}$$

The first expression gives the ratio of maximum shear stress to mean shear stress which of course, is the factor of stress concentration. As is seen, this factor is a function of $\beta a/2t_1$ and k. Comparing with the factor D of Volkersen's theory, it can be readily seen that $\beta a/2t_1 = \sqrt{2D}$. As in Volkensen's analysis, the shear stress distribution obtained through Goland and Reissner's theory is uniform irrespective of the value of D as long as this is smaller than about 0.1, but the stress concentration increases rapidly for higher values of D and for $D \geq 2$ becomes practically proportional to $\sqrt{D}$. This is because for large values of D, $\coth\sqrt{2D}$ approaches the value 1 and in fact the factor η of stress concentration can then by written as,

$$\eta \simeq \frac{1}{4} (1 + 3k) \sqrt{2D} + 3(1 - k) / 4$$

The bending of the members (k small) is seen to have a reducing effect on the highest stresses. For small values of k, the shear stress distribution is of similar form to that obtained by Volkensen. In the limiting case of $k = 1$ i.e. when the bending deformation of the adherends is negligible, the Goland and Reissner theory yields $\eta = \sqrt{2D} \coth \sqrt{2D}$, whereas the Volkersen result was $\eta = \sqrt{D/2x} \coth \sqrt{D/2}$. For $D \geq 2$ i.e. for long overlaps, the stress concentration factor is therefore twice as large as predicted by Volkersen.

The theory of Goland and Reissner, though an improvement over Volkersen's analysis in that it takes into account the bending deformation of the adherends and the tearing stresses in the adhesive, has certain limitations which can be summarized as follows.

(1) This theory is valid only for adherends of the same material and of identical length and thickness.

(2) The first case is valid for $t/t_1 << E/E_1$ while the second case requires the condition $t/t_1 >> E/E_1$.

(3) The joint edge loads are not in equilibrium except when $k = 1$.

(4) The stresses in the adhesive are not considered to vary through its thickness which as in the case of Volkersen's theory, results in inaccurate prediction of stresses in the area adjacent to the overlap edge.

(5) The theory does not consider external shear force or bending loads.

2.4 Plantema's Modification

Plantema (3) has attempted to combine the Goland and Reissner theory with the Volkersen theory. Volkersen's theory is employed to calculate the differential strain of the members and the stress distribution at the edges of the overlap. The factor k of Goland and Reissner theory is then introduced to calculate the differential strain of the members due to bending. The total strain of the members due to both tension and bending is used for the correction of Volkersen's formula. The factor of stress concentration is given by,

$$\eta = \sqrt{D(1+3k)/2} \cdot \coth \sqrt{D(1+3k)/2}$$

No calculation is made of the tearing stresses.

Mylonas and deBruyne (5) show that for inflexible adherends ($k = 1$) and long joints, Plantema's results approach those of Goland and Reissner whereas for flexible

adherends ($k \ll 1$) Plantema's results are closer to those of Volkersen.

2.5 Modification by Kelsey and Benson (4, 9)

Kelsey and Benson employ the complimentary energy method to determine the shear and tearing stresses in a lap joint. In this method, the equilibrium is taken into account, but the necessary compatibility is only approximately satisfied. Treatment of the lap joint as a shear lag problem results in a second order differential equation, but allowance for the complimentary energy due to the tearing stresses inflates the equation to one of fourth order. The boundary condition that the shear stress vanishes at the two ends of the overlap is then applied. The expressions for shear and tearing stress are obtained as follows,

$$\tau = \tfrac{1}{4} P m_1 m_2 a \cdot \frac{(\cosh m_1 x) \cdot (\cosh \frac{m_2 a}{2}) - (\cosh \frac{m_1 a}{2}) \cdot (\cosh m_2 x)}{(m_1 \cosh \frac{m_1 a}{2}) \cdot (\sinh \frac{m_2 a}{2}) - (m_2 \sinh \frac{m_1 a}{2}) \cdot (\cosh \frac{m_2 a}{2})}$$

and

$$\sigma = \frac{1}{8} P m_1 m_2 a t \cdot \frac{(m_1 \sinh m_1 x) \cdot (\cosh \frac{m_2 a}{2}) - (m_2 \cosh \frac{m_1 a}{2}) \cdot (\sinh \frac{m_2 a}{2})}{(m_1 \cosh \frac{m_1 a}{2}) \cdot (\sinh \frac{m_2 a}{2}) - (m_2 \sinh \frac{m_1 a}{2}) \cdot (\cosh \frac{m_2 a}{2})}$$

where,

$$m_1 = \frac{6E}{t^2 G} (1 + m_3)$$

$$m_2 = \frac{6E}{t^2 G} (1 - m_3)$$

$$m_3 = (1 - \frac{2G^2 t}{3EE_1 t_1})^{\frac{1}{2}}$$

The shear stress distribution shows no appreciable difference from that obtained by Volkersen's analysis, except that at the two ends of the overlap it rapidly falls to zero. This of course, because the boundary conditions used in the analysis require that the shear stress be zero at these two points. Since the two end surfaces of the adhesive are stress free, it is argued that for equilibrium, the shear stress must vanish at the two ends. However, it should be noted that the lap joint has a discontinuity at the two leading corners of the adhesive and the stress at these points can be expected to be singular for an elastic analysis. There is no such discontinuity at the two trailing corners however, and the shear stress at these two points can be expected to be zero. Since Kelsey and Benson do not allow the stresses to vary over the adhesive thickness, the imposition of the boundary condition that the shear stress be zero at the two ends of the overlap only results in the shear stress falling rapidly to zero at these two points. The shear stress distribution cannot however, be considered an improvement over that obtained by Volkersen.

The tearing stress distribution obtained by Kelsey and Benson shows these stresses to be concentrated almost entirely at the two ends of the overlap. Through most of the length of the overlap, this stress is almost zero.

2.6 Cornell's Modification (10)

The system considered by Cornell is shown in Fig. 4. This joint is fixed at one end and it is some what different from the conventional lap joint. Cornell's interest lay in brazed joints where a thin tab is brazed to a thick base bar. The base bar is subjected to tension, bending moment and shear force. Cornell assumed that the two adherends act like simple beams and the adhesive layer consists of an infinite number of shear and tension springs. Differential equations for σ and τ are combined into a tenth order linear differential equation in the transverse deflection of each adherend. The mathematical analysis is fundamentally simple but the expressions involved

are complicated. Results indicate a high concentration of shear and transverse tensile stress in the vicinity of the joint edge.

Cornell has compared his theoretical results with the results of photoelastic and brittle lacquer experiments and found them in good agreement. It should however, be noted that the joints investigated by Cornell both theoretically and experimentally, are brazed joints where the adhesive modulii are 1/3 to 1/2 as large as those of the adherends, whereas in an adhesive joint the ratio might be 1/20 or smaller. The error in the predicted stresses due to the assumption that the stresses do not vary over the thickness of the adhesive, may be more serious in the case of the adhesive joints than it would be for brazed joints.

Cornell's theory applies to joints between adherends differing in material properties and thickness. Application of external shear force and bending loads are also considered. The configuration considered by Cornell is however, of a special type and the theory cannot be applied to a general case of lap joint.

2.7 Stepped Joint of Erdogan and Ratwani (11)

In this analysis a stepped joint between two plates is considered (Fig. 5). Plate (1) is considered to be isotropic while Plate (2) is orthotropic. A uniform tensile force P is applied to the plates away from the joint. The tensile stresses, $\sigma_1(x)$ and $\sigma_2(x)$, in the two plates and the shear stress, τ, at the interface are determined under the following assumptions:

(1) The thicknesses of the two plates are small compared to the other dimensions of the composite structure so that the individual layers and the composite plate may be considered to be under generalized plane stress (i.e. $\sigma_{1y} = \sigma_{2y} = 0$).

(2) The thickness variation of the stresses in the plates is neglected.

(3) In the z direction (Fig. 5a), it is assumed that either $\epsilon_{1z} = \epsilon_{2z}$ or

$\bar{\sigma}_z = 0$, $\bar{\sigma}_z$ being the average stress in the composite.

The results of this analysis are then applied to a special case of one single step (Fig. 5b) which of course is a single lap joint. The shear stress in the adhesive layer is given by,

$$\tau = \frac{P\beta}{\alpha}\left[\sinh \alpha x + (1 - \cosh \alpha a + \frac{\alpha^2}{\beta})\frac{\cosh \alpha x}{\sinh \alpha a}\right]$$

where,

$$\alpha^2 = \frac{G}{t}\left[\frac{1 - \mu_1^2}{E_1 t_1} + \frac{1 - \mu_{2x} \cdot \mu_{2z}}{E_{2x} t_2}\right]$$

$$\beta = -\frac{G(1 - \mu_1^2)}{E_1 t_1 t}$$

For both plates isotropic and identical,

$$\alpha^2 = \frac{2G}{t}\left[\frac{1 - \mu_1^2}{E_1 t_1}\right]$$

$$\beta = -\frac{\alpha^2}{2}$$

and

$$\tau = -\frac{P\alpha}{2}\left[\sinh \alpha x - (1 + \cosh \alpha a)\frac{\cosh \alpha x}{\sinh \alpha a}\right]$$

This result is similar to that obtained by Volkersen. This theory assumes that the tearing stresses are nonexistant in the adhesive layer.

2.8 Finite Element Analysis

Problems in structural mechanics can be numerically solved by using the finite element method (12). Wooley and Carver (13) have attempted to apply this method to the case of a single lap joint. The lap joint is loaded in tension and shear and tearing stresses are determined. The adhesive layer was divided into two equal layers through its thickness, giving an indication of the variation of stresses in the direction normal to the bondline. The solution is obtained by a plane stress analysis. The shear and tearing stress distribution obtained by this method is similar to that obtained by Goland and Reissner. Wooley and Carver compare the stress concentration factors with those obtained by Goland and Reissner theory. They are shown to compare favorably.

The joint considered by Wooley and Carver is loaded in tension only. The finite element method is however, a promising one and can be extended to a more general case

Another attempt to use the finite element analysis in the case of adhesive joints is that by Harrison and Harrison (14). It is assumed that the displacements at the two interfaces are known and are uniform. This is a very special case and the closest practical case would be one where the adherends are rigid. It is further assumed that in a region of the adhesive layer, away from the two ends, the stress field is uniform This uniform stress field is determined from the known displacement field at the two interfaces Finite element analysis is then applied to determine stresses near the ends of the adhesive layer.

In practice, the relative displacements of the interfaces are not known, only the external loads are given. Furthermore, the displacements at the interfaces are far from being uniform, especially at the ends of the joint. This method needs to be further developed in order to be applicable to practical problems in adhesive joints.

2.9 Experimental Stress Analysis

Several works have been published where the stress distribution was determined experimentally. These works will be reviewed here briefly.

Unpublished extensometer tests made by Copper have been referred to by Mylonas and deBruyne (5). In these tests, the shear stress developing at various points of the 3 inch long overlap was estimated from the relative displacement of the adherends measured by an optical lever. The load applied was tensile and was kept very low so that Hooke's law could be assumed to hold even in the region of high stress. The stress distribution so obtained was compared with the results of Volkersen's theory and also with the results of Goland and Reissner theory. Experimental results were found to be in better agreement with the theory of Goland and Reissner than with the theory of Volkersen.

Mylonas (7) applied the method of photoelastic analysis to investigate the stresses in a lap joint. The adherends were made of $\frac{1}{2}$ in. square Bakelite bars reinforced longitudinally with stainless steel studdings. The adherends were made practically rigid. The adhesive used was an Araldite resin which is also a photoelastic material. The thickness of the adhesive layer was appreciable.

The main purpose of Mylonas' work was to study the effect on the peak stress of the shape of the free boundary of the adhesive at the edge of the overlap. Models with concave edges with varying radii of curvature and with straight edges of various inclinations were studied.

The practically infinite stiffness of the adherends in these experiments leads theoretically to a uniform shear throughout the adhesive layer. For this reason Mylonas' results are of limited interest from the stress analysis point of view. The work is however, of great importance as a pioneering work describing techniques for making stress free adhesive joints to be used as models for photoelastic analysis.

McLaren and MacInnes (15) studied the effect of bending of the adherends in their photoelastic tests. Two series of tests were made. In the first, a lap joint consisting of $\frac{1}{2}$ in. thick adherends and an adhesive layer varying in thickness from zero to $\frac{1}{2}$ in. was simulated by a model cast whole in Araldite; in the second series of tests the adherends had a Young's modulus twenty times greater than that of the adhesive layer.

In the homogeneous models the 'adhesive layer' was always rectangular and ran the whole length of the overlap. In every case in which $k > 0$ the fringe pattern had the same general character: the order was a minimum at the center of the joint and increased towards a maximum at the leading corner. Change of the value k produced an approximately proportional change in the value of the peak fringe without appearing to affect the order at the center. For negative ($k = -\frac{1}{2}$), the fringe order at the free end of the glue line reduced to a minimum, the fringe order was a maximum at the center.

In composite models which were geometrically similar to the homogeneous ones, similar fringe patterns were obtained. For $k > 0$ the fringe order rose from a minimum at the center of the adhesive layer to a maximum at the leading corner. The high tensile stress in the free surface at the leading corner decreased on traversing the end but gave way to slight compression at the other extreme. Increase in the value of k again produced no change at the center but led to an increased fringe order at the leading corner. When k was made sufficiently negative, it was found that the highest-order fringe appeared at the center of the adhesive and then there was a fall in order towards the free surfaces.

The main significance of this work by McLaren and MacInnes is that it clarifies the contribution made to the distribution of stress by the bending of adherends. The results tend to support the Goland and Reissner theory.

Tuzi and Shimada (8) use both the adhesive and the adherends made of photo-

elastic materials. The adherends are made of an epoxy resin while the adhesive is made of epoxy rubber. The ratio of the Young's modulii for the two materials is 6. The fringe pattern obtained for rectangular adhesive layer is similar to that obtained by Melaren and MacInnes. Tuzi and Shimada study adhesive layers with concave and canvex ends and joints with a fillet at the leading corners. The results indicate that convex ends tend to produce excessive stress concentration at the leading corner whereas the use of a fillet tends to reduce the stress concentration considerably.

The photoelastic investigations by Mylonas, McLaren and MacInnes, and Tuzi and Shimada, all show a significant variation of stress through the thickness of the adhesive layer, especially in areas where the maximum stress occurs.

2.10 Conclusion

Amongst the theoretical works, Goland and Reissner's theory is the most rigorous study of the stress distribution in lap joints and is in good agreement with experimental results except at and near the two ends of the joint where the maximum stress occurs. This error results mainly from the assumption that the stress does not vary through the thickness of the adhesive layer. In fact, photoelastic tests show this variation to be quite significant especially in those areas where the maximum stress occurs. Furthermore, the theoretical analyses consider the joint to be loaded in tension alone and the effects of shear force and bending moment are not studied. Photoelastic stress analysis by McLaren and MacInnes shows that application of shear force and bending moment can be advantageous from the point of view of obtaining a more uniform stress distribution along the overlap.

The objective of the present work is to analyze the lap joint subjected to a generalized load configuration consisting of tensile and shear forces and bending moments (Fig. 3). The stresses are allowed to vary through the thickness of the adhesive layer. The analytical results are to be checked by means of photoelastic tests.

3. ANALYSIS OF LAP JOINT

3.1 Problem

Given are two rectangular sheets of thickness t_1 and t_2 and of unit width, lap-jointed over a length 'a' by means of an adhesive layer of thickness t (Fig. 3b). It is assumed that the loads P, V, M_1, and M_2 are given at the joint edges. The main problem is the determination of the shear stress τ_{xy}, and the normal stresses σ_x and σ_y in the adhesive layer.

3.2 Assumptions

The following assumptions are made:

(1) The adherend and the adhesive materials are isotropic and linearly elastic.

(2) The adherends behave according to simple beam theory, i.e. the lateral stress in the adherends can be neglected, and plane sections remain plane.

(3) The adhesive thickness t is small compared to the overlap length a.

(4) The displacements in the joint are small, i.e. the strains are considerably less than 1.

(5) The joint width is large compared to adherend and adhesive thicknesses, so that this may be considered as a problem in plane strain.

3.3 Derivation of Differential Equations

The coordinate axes x and y are shown in Fig. 3. The x-axis is parallel to the plane of the adhesive layer and passes through its center. The y-axis is normal to the plane of the adhesive layer at the left edge of the joint.

Let u(x, y) and v(x, y) represent the displacements of the point (x, y) in the adhesive, in the x and y direction respectively. Further, let

$$u(x,y) = u_o(x) + yu_1(x) + y^2u_2(x) + \ldots\ldots\ldots + y^m u_m(x) = \sum_{j=0}^{m} y^j u_j(x) \tag{3.1}$$

and

$$v(x,y) = v_o(x) + y v_1(x) + y^2 v_2(x) + \ldots\ldots + y^n v_n(x) = \sum_{j=0}^{n} y^j v_j(x) \tag{3.2}$$

where m and n are integers.

A perfect solution would require m and n to approach infinity. However, since the adhesive thickness t (dimension in the y-direction) is small compared to the overlap length a (dimension in x-direction), m and n could be terminated at values 2, 3, or 4 and the results could be expected to be reasonably accurate.

The strains in the adhesive layer can now be written as,

$$\epsilon_x = \frac{\partial u(x,y)}{\partial x} = \sum_{j=0}^{m} y^j u_j(x) \tag{3.3}$$

$$\epsilon_y = \frac{\partial v(x,y)}{\partial y} = \sum_{j=1}^{n} j y^{(j-1)} v_j(x) \tag{3.4}$$

$$\gamma_{xy} = \frac{\partial u(x,y)}{\partial y} + \frac{\partial v(x,y)}{\partial x} = \sum_{j=1}^{m} j y^{(j-1)} u_j(x) + \sum_{j=0}^{n} y^j v'_j(x) \tag{3.5}$$

For the plane strain problem, the strain energy I_o of the adhesive is given by,

$$I_o = \int_o^a \int_{-t/2}^{t/2} \left[(Q/2)(\epsilon_x^2 + \epsilon_y^2) + \lambda \epsilon_x \epsilon_y + \frac{G}{2} \gamma_{xy}^2 \right] dy\, dx$$

$$= \int_o^a \int_{-t/2}^{t/2} \left\{ \left(\frac{Q}{2}\right) \left[\left(\sum_{j=0}^{m} y^j u'_j \right)^2 + \left(\sum_{j=1}^{n} j y^{(j-1)} v_j \right)^2 \right] \right.$$

$$+ \lambda \left(\sum_{j=0}^{m} y^j u'_j \right) \left(\sum_{j=1}^{n} j y^{(j-1)} v_j \right) + \frac{G}{2} \left(\sum_{j=1}^{m} j y^{(j-1)} u_j + \sum_{j=0}^{n} y^j v'_j \right)^2 \Bigg\} \, dy \, dx$$

$$= \int_0^a \int_{-t/2}^{t/2} \Bigg\{ \left(\frac{Q}{2} \right) \left[\sum_{i=0}^{m} \sum_{j=0}^{m} y^{(i+j)} u'_i u'_j + \sum_{i=1}^{n} \sum_{j=1}^{n} ij y^{(i+j-2)} v_i v_j \right]$$

$$+ \lambda \left[\sum_{i=0}^{m} \sum_{j=1}^{n} j y^{(i+j-1)} u'_i v_j \right] + \frac{G}{2} \left[\sum_{i=1}^{m} \sum_{j=1}^{m} ij y^{(i+j-2)} u_i u_j \right.$$

$$\left. + \sum_{i=0}^{n} \sum_{j=0}^{n} y^{(i+j)} v'_i v'_j + 2 \sum_{i=1}^{m} \sum_{j=0}^{n} i y^{(i+j-1)} u_i v'_j \right] \Bigg\} \, dy \, dx$$

Integration over the thickness of the adhesive yields,

$$I_o = \int_0^a \Bigg\{ \frac{Q}{2} \left[\sum_{i=0}^{m} \sum_{j=0}^{m} \left(\frac{t}{2} \right)^{i+j+1} \alpha_{ij} u'_i u'_j \right.$$

$$\left. + \sum_{i=1}^{n} \sum_{j=1}^{n} ij \left(\frac{t}{2} \right)^{i+j-1} \delta_{ij} v_i v_j \right] + \lambda \left[\sum_{i=0}^{m} \sum_{j=1}^{n} j \left(\frac{t}{2} \right)^{i+j} \beta_{ij} u'_i v_j \right]$$

$$+ \frac{G}{2} \left[\sum_{i=1}^{m} \sum_{j=1}^{m} ij \left(\frac{t}{2} \right)^{i+j-1} \delta_{ij} u_i u_j + \sum_{i=0}^{n} \sum_{j=0}^{n} \left(\frac{t}{2} \right)^{i+j+1} \alpha_{ij} v'_i v'_j \right.$$

$$\left. + 2 \sum_{i=0}^{m} \sum_{j=0}^{n} i \left(\frac{t}{2} \right)^{i+j+1} \alpha_{ij} u_i v_j \right] \Bigg\} \, dx \qquad (3.6)$$

where,

$$\alpha_{ij} = \frac{1 - (-1)^{i+j+1}}{i+j+1} , \qquad \beta_{ij} = \frac{1 - (-1)^{i+j}}{i+j} , \qquad \delta_{ij} = \frac{1 - (-1)^{i+j-1}}{i+j-1}$$

(3.7)

The condition of compatibility at the two interfaces can be used to determine the displacement field and the strain energy of the two adherends.

Let $U_1(x,y)$ and $V_1(x,y)$ represent the displacements in the x and y directions respectively in adherend (I).

Since plane sections remain plane,

$$U_1(x,y) = U_1(x, \tfrac{t}{2}) - (y - \tfrac{t}{2}) \frac{\partial V_1}{\partial x}(x, \tfrac{t}{2}) \tag{3.8}$$

Now, conditions for compatibility at the interface are,

$$U_1(x, \tfrac{t}{2}) = u(x, \tfrac{t}{2}) \tag{3.9}$$

and

$$V_1(x, \tfrac{t}{2}) = v(x, \tfrac{t}{2}) \tag{3.10}$$

Eqs. (3.8), (3.9) and (3.10) yield

$$U_1(x,y) = u(x, \tfrac{t}{2}) - (y - \tfrac{t}{2}) \frac{\partial v(x, \frac{t}{2})}{\partial v} \tag{3.11}$$

or

$$U_1(x,y) = \sum_{j=0}^{m} \left(\frac{t}{2}\right)^j u_j - \left(y - \frac{t}{2}\right) \sum_{j=0}^{n} \left(\frac{t}{2}\right)^j v'_j \qquad (3.12)$$

Similarly for adherend (II) the displacements $U_2(x,y)$ and $V_2(x,y)$ in the x and y directions respectively can be written as,

$$U_2(x,y) = \sum_{j=0}^{m} \left(-\frac{t}{2}\right)^j u_j - \left(y + \frac{t}{2}\right) \sum_{j=0}^{n} \left(-\frac{t}{2}\right)^j v'_j \qquad (3.13)$$

The strain field for adherend (I) is,

$$\epsilon_{1x} = \frac{\partial U_1}{\partial x} = \sum_{j=0}^{m} \left(\frac{t}{2}\right)^j u'_j - \left(y - \frac{t}{2}\right) \sum_{j=0}^{n} \left(\frac{t}{2}\right)^j v''_j \qquad (3.14)$$

$$\gamma_{1xy} = 0 \qquad (3.15)$$

And the strain field for adherend (II) is,

$$\epsilon_{2x} = \sum_{j=0}^{m} \left(-\frac{t}{2}\right)^j u'_j - \left(y + \frac{t}{2}\right) \sum_{j=0}^{n} \left(-\frac{t}{2}\right)^j v''_j \qquad (3.16)$$

$$\gamma_{2xy} = 0 \qquad (3.17)$$

The strain energy I_1 for adherend (I) is given by,

$$I_1 = \int_0^a \int_{\frac{t}{2}}^{(\frac{t}{2}+t_1)} \frac{Q_1}{2} \epsilon_{1x}^2 \, dy \, dx$$

$$= \int_0^a \int_{\frac{t}{2}}^{(\frac{t}{2}+t_1)} \frac{Q_1}{2} \left[\sum_{j=0}^{m} (\frac{t}{2})^j \dot{u}'_j - (y - \frac{t}{2}) \left\{ \sum_{j=0}^{n} (\frac{t}{2})^j v''_j \right\} \right]^2 dy \, dx$$

$$= \int_0^a \int_{\frac{t}{2}}^{(\frac{t}{2}+t_1)} \frac{Q_1}{2} \left[\sum_{i=0}^{m} \sum_{j=0}^{m} (\frac{t}{2})^{i+j} u'_i u'_j \right.$$

$$+ (y - \frac{t}{2})^2 \left\{ \sum_{i=0}^{n} \sum_{j=0}^{n} (\frac{t}{2})^{i+j} v''_i v''_j \right\}$$

$$\left. - 2(y - \frac{t}{2}) \left\{ \sum_{i=0}^{m} \sum_{j=0}^{n} (\frac{t}{2})^{i+j} u'_j v''_j \right\} \right] dy \, dx$$

Integrating in the y-direction,

$$I_1 = \int_0^a \frac{Q_1}{2} \left[\sum_{i=0}^{m} \sum_{j=0}^{m} t_1 (\frac{t}{2})^{i+j} u'_i u'_j \right.$$

$$+ \frac{t_1^3}{3} \left\{ \sum_{i=0}^{n} \sum_{j=0}^{n} (\frac{t}{2})^{i+j} v''_i v''_j \right\}$$

$$\left. - t_1^2 \left\{ \sum_{i=0}^{m} \sum_{j=0}^{n} (\frac{t}{2})^{i+j} u'_i v''_j \right\} \right] dx \qquad (3.18)$$

Similarly, the strain energy I_2 for adherend (II) is given by,

$$I_2 = \int_0^a \frac{Q_2}{2} \left[\sum_{i=0}^{m} \sum_{j=0}^{m} t_2 \left(-\frac{t}{2}\right)^{i+j} u'_i u'_j + \frac{t_2^3}{3} \left\{ \sum_{i=0}^{n} \sum_{j=0}^{n} \left(-\frac{t}{2}\right)^{i+j} v''_i v''_j \right\} + t_2^2 \left\{ \sum_{i=0}^{m} \sum_{j=0}^{n} \left(-\frac{t}{2}\right)^{i+j} u'_i v''_j \right\} \right] dx \qquad (3.19)$$

Work done by the boundary forces P and V and moments M_1 and M_2 can now be calculated. Let W_{P1}, W_{V1}, and W_{M1} represent the work done by P, V, and M_1 respectively on adherend (I). And let W_{P2}, W_{V2}, and W_{M2} represent the work done by P, V, and M_2 respectively on adherend (II).

Assuming P to be uniformly distributed over the cross-sectional area of each adherend,

$$W_{P1} = \int_{\frac{t}{2}}^{(\frac{t}{2} + t_1)} \frac{P}{t_1} U_1(a,y)\,dy$$

$$= \frac{P}{t_1} \int_{\frac{t}{2}}^{(\frac{t}{2} + t_1)} \left[\sum_{j=0}^{m} \left(\frac{t}{2}\right)^j u_j(a) - \left(y - \frac{t}{2}\right) \left\{ \sum_{j=0}^{n} \left(\frac{t}{2}\right)^j v'_j(a) \right\} \right] dy$$

$$= P \left[\sum_{j=0}^{m} \left(\frac{t}{2}\right)^j u_j(a) - \frac{t_1}{2} \sum_{j=0}^{n} \left(\frac{t}{2}\right)^j v'_j(a) \right] \qquad (3.20)$$

Similarly,

$$W_{P2} = -P \left[\sum_{j=0}^{m} (-\frac{t}{2})^j u_j(o) + \frac{t_2}{2} \sum_{j=0}^{n} (-\frac{t}{2})^j v'_j(o) \right] \tag{3.21}$$

$$W_{V1} = V \cdot V_1(a) = V \sum_{j=0}^{n} (\frac{t}{2})^j v_j(a) \tag{3.22}$$

$$W_{V2} = -V \cdot V_2(o) = -V \sum_{j=0}^{n} (-\frac{t}{2})^j v_j(o) \tag{3.23}$$

$$W_{M1} = M_1 \frac{\partial v\,(a, t/2)}{\partial x} = M_1 \sum_{j=0}^{n} (\frac{t}{2})^j v'_j(a) \tag{3.24}$$

$$W_{M2} = -M_2 \sum_{j=0}^{n} (-\frac{t}{2})^j v'_j(o) \tag{3.25}$$

The total work done by external forces is given by,

$$W = W_{P1} + W_{P2} + W_{V1} + W_{V2} + W_{M1} + W_{M2} \tag{3.26}$$

Let I_0, I_1, and I_2 be expressed as,

$$I_0 = \int_0^a F_0(u_i, u'_i, v_j, v'_j, v''_j)\, dx \tag{3.27}$$

$$I_1 = \int_0^a F_1(u_i, u'_i, v_j, v'_j, v''_j)\, dx \tag{3.28}$$

$$I_2 = \int_0^a F_2(u_i, u'_i, v_j, v'_j, v''_j)\, dx \tag{3.29}$$

where $i = 0, 1, 2, \ldots\ldots, m$ and $j = 0, 1, 2, \ldots\ldots, n$

The functions F_0, F_1, F_2 are given by the expressions on the right hand side of the equations (3.6), (3.18), and (3.19) respectively. Let

$$F(u_i, u'_i, v_j, v'_j, v''_j) = F_0 + F_1 + F_2 \tag{3.30}$$

so that the total potential energy I can be written as,

$$I = \left[\int_0^a F(u_i, u'_i, v_j, v'_j, v''_j)\, dx \right] - W \tag{3.31}$$

Now, equilibrium requires that I be minimized. Application of the principle of calculus of variations yields the following differential equations; also known as Euler equations.

$$\frac{\partial F}{\partial u_i} - \frac{d}{dx}\left(\frac{\partial F}{\partial u'_i}\right) = 0 \qquad i = 0, 1, 2, \ldots\ldots, m \tag{3.32}$$

and

$$\frac{\partial F}{\partial v_j} - \frac{d}{dx}\left(\frac{\partial F}{\partial v'_j}\right) + \frac{d^2}{dx^2}\left(\frac{\partial F}{\partial v''_j}\right) = 0 \qquad j = 0, 1, 2, \ldots\ldots, n \tag{3.33}$$

In order to eliminate the rigid body displacements of the joint, it will be convenient to let the displacement and slope at the origin be zero. This would yield the forced boundary conditions (3.34).

$$u_0(0) = 0 \qquad v_0(0) = 0 \qquad \text{and} \qquad v'_0(0) = 0 \tag{3.34}$$

The natural boundary conditions are given by Eqs. (3.35) to (3.40).

$$\left(\frac{\partial F}{\partial u'_i}\right)_{x=0} - P\left(-\frac{t}{2}\right)^i = 0 \qquad i = 1, 2, \ldots\ldots, m \tag{3.35}$$

$$\left(\frac{\partial F}{\partial u'_i}\right)_{x=a} - P\left(\frac{t}{2}\right)^i = 0 \qquad i = 0, 1, 2, \ldots\ldots, m \tag{3.36}$$

$$\left(\frac{\partial F}{\partial v'_j}\right)_{x=0} - \left[\frac{d}{dx}\left(\frac{\partial F}{\partial v''_j}\right)\right]_{x=0} - V\left(-\frac{t}{2}\right)^j = 0$$

$$j = 1, 2, \ldots\ldots, n \tag{3.37}$$

$$\left(\frac{\partial F}{\partial v'_j}\right)_{x=a} - \left[\frac{d}{dx}\left(\frac{\partial F}{\partial v''_j}\right)\right]_{x=a} - V\left(\frac{t}{2}\right)^j = 0$$

$$j = 0, 1, 2, \ldots\ldots, n \tag{3.38}$$

$$\left(\frac{\partial F}{\partial v''_j}\right)_{x=0} - \left(-\frac{t}{2}\right)^j \left(\frac{Pt_2}{2} + M_2\right) = 0 \qquad j = 1, 2, \ldots., n \tag{3.39}$$

and

$$\left(\frac{\partial F}{\partial v''_j}\right)_{x=a} + \left(\frac{t}{2}\right)^j \left(\frac{Pt_1}{2} - M_1\right) = 0 \qquad j = 0, 1, 2, \ldots., n \tag{3.40}$$

Differentiation of F yields Eqs. (3.41) to (3.50).

$$\frac{\partial F}{\partial u_0} = 0 \tag{3.41}$$

$$\frac{\partial F}{\partial u_i} = G\left[\sum_{j=1}^{m} ij\left(\frac{t}{2}\right)^{i+j-1} \delta_{ij} u_j + \sum_{j=0}^{n} i\left(\frac{t}{2}\right)^{i+j} \beta_{ij} v_j\right]$$

$$i = 1, 2, \ldots\ldots, m \tag{3.42}$$

$$\frac{\partial F}{\partial u'_i} = \frac{Q}{2}\left[\sum_{j=0}^{m} 2\left(\frac{t}{2}\right)^{i+j+1} \alpha_{ij} u'_j\right] + \lambda\left[\sum_{j=0}^{n} j\left(\frac{t}{2}\right)^{i+j} \beta_{ij} v_j\right]$$

$$+ \frac{Q_1}{2} \left[\sum_{j=0}^{m} 2t_1 \left(\frac{t}{2}\right)^{i+j} u''_j - t_1^2 \sum_{j=0}^{n} \left(\frac{t}{2}\right)^{i+j} v'''_j \right]$$

$$+ \frac{Q_2}{2} \left[\sum_{j=0}^{m} 2t_2 \left(-\frac{t}{2}\right)^{i+j} u''_j + t_2^2 \sum_{j=0}^{n} \left(-\frac{t}{2}\right)^{i+j} v'''_j \right]$$

$$i = 0, 1, 2, \ldots\ldots, m \qquad (3.43)$$

$$\frac{d}{dx}\left(\frac{\partial F}{\partial u'_i}\right) = \frac{Qt}{2} \left[\sum_{j=0}^{m} \left(\frac{t}{2}\right)^{i+j} \alpha_{ij} u'''_j \right]$$

$$+ \frac{\lambda t}{2} \left[\sum_{j=1}^{n} j\left(\frac{t}{2}\right)^{i+j-1} \beta_{ij} v'_j \right]$$

$$+ \frac{Q_1 t_1}{2} \left[\sum_{j=0}^{m} 2\left(\frac{t}{2}\right)^{i+j} u''_j - t_1 \sum_{j=0}^{n} \left(\frac{t}{2}\right)^{i+j} v'''_j \right]$$

$$+ \frac{Q_2 t_2}{2} \left[\sum_{j=0}^{m} 2\left(-\frac{t}{2}\right)^{i+j} u''_j + t_2 \sum_{j=0}^{n} \left(-\frac{t}{2}\right)^{i+j} v'''_j \right]$$

$$i = 0, 1, 2, \ldots\ldots, m \qquad (3.44)$$

$$\frac{\partial F}{\partial v_o} = 0 \qquad (3.45)$$

$$\frac{\partial F}{\partial v_j} = \frac{Q}{2} \left[\sum_{i=1}^{n} 2ij\left(\frac{t}{2}\right)^{i+j-1} \delta_{ij} v_i \right] + \lambda \left[\sum_{i=0}^{m} j\left(\frac{t}{2}\right)^{i+j} \beta_{ij} u'_i \right]$$

$$j = 1, 2, \ldots\ldots, n \qquad (3.46)$$

$$\frac{\partial F}{\partial v'_j} = G\left[\sum_{i=0}^{n}\left(\frac{t}{2}\right)^{i+j+1}\alpha_{ij}v'_i + \sum_{i=1}^{m} i\left(\frac{t}{2}\right)^{i+j}\beta_{ij}u_i\right]$$

$$j = 0, 1, 2, \ldots\ldots, n \qquad (3.47)$$

$$\frac{d}{dx}\left(\frac{\partial F}{\partial v'_j}\right) = G\left[\sum_{i=0}^{n}\left(\frac{t}{2}\right)^{i+j+i}\alpha_{ij}v''_i + \sum_{i=1}^{m} i\left(\frac{t}{2}\right)^{i+j}\beta_{ij}u'_i\right]$$

$$j = 0, 1, 2, \ldots\ldots, n \qquad (3.48)$$

$$\frac{\partial F}{\partial v''_j} = \frac{Q_1}{2}\left[\frac{2t_1^3}{3}\sum_{i=0}^{n}\left(\frac{t}{2}\right)^{i+j}v''_i - t_1^2\sum_{i=0}^{m}\left(\frac{t}{2}\right)^{i+j}u'_i\right]$$

$$+\frac{Q_2}{2}\left[\frac{2t_2^3}{3}\sum_{i=0}^{n}\left(-\frac{t}{2}\right)^{i+j}v''_i + t_2^2\sum_{i=0}^{m}\left(-\frac{t}{2}\right)^{i+j}u'_i\right]$$

$$j = 0, 1, 2, \ldots\ldots, n \qquad (3.49)$$

$$\frac{d^2}{dx^2}\left(\frac{\partial F}{\partial v''_j}\right) = \frac{Q_1t_1^2}{2}\left[\frac{2t_1}{3}\sum_{i=0}^{n}\left(\frac{t}{2}\right)^{i+j}v_i^{iv} - \sum_{i=0}^{m}\left(\frac{t}{2}\right)^{i+j}u'''_i\right]$$

$$+\frac{Q_2t_2^2}{2}\left[\frac{2t_2}{3}\sum_{i=0}^{n}\left(-\frac{t}{2}\right)^{i+j}v_i^{iv} + \sum_{i=0}^{m}\left(-\frac{t}{2}\right)^{i+j}u_i'''\right]$$

$$j = 0, 1, 2, \ldots\ldots, n \qquad (3.50)$$

Differential equations (3.32) can now be rewritten as Eqs, (3.51) and (3.52).

$$\sum_{j=0}^{m}\left[\frac{Q}{2}t\alpha_{oj} + 2Q_1t_1 + 2Q_2t_2(-1)^j\right]\left(\frac{t}{2}\right)^j u''_j$$

$$+ \sum_{j=1}^{n} \lambda j \left(\frac{t}{2}\right)^j \beta_{oj} v'_j + \sum_{j=0}^{n} \left[\left(\frac{Q_2}{2}\right) t_2^2 (-1)^j - \left(\frac{Q_1}{2}\right) t_1^2 \right] \left(\frac{t}{2}\right)^j v'''_j = 0$$

(3.51)

$$G \sum_{j=1}^{m} ij \left(\frac{t}{2}\right)^{j-1} \delta_{ij} u_j - \sum_{j=0}^{m} \left[\frac{Qt}{2} \alpha_{ij} + Q_1 t_1 + Q_2 t_2 (-1)^{i+j} \right] \left(\frac{t}{2}\right)^j u''_j$$

$$+ \sum_{j=0}^{n} (Gi - \lambda j) \left(\frac{t}{2}\right)^j \beta_{ij} v'_j - \sum_{j=0}^{n} \left[\left(\frac{Q_2}{2}\right) t_2^2 (-1)^{i+j} \right.$$

$$\left. - \left(\frac{Q_1}{2}\right) t_1^2 \right] \left(\frac{t}{2}\right)^j v'''_j = 0 \qquad i = 1, 2, \ldots\ldots, m \qquad (3.52)$$

Differential Eqs. (3.33) can be rewritten as Eqs. (3.53) and (3.54).

$$-G \sum_{i=1}^{m} i \left(\frac{t}{2}\right)^i \beta_{io} u'_i + \sum_{i=0}^{m} \left[\left(\frac{Q_2}{2}\right) t_2^2 (-1)^i - \left(\frac{Q_1}{2}\right) t_1^2 \right] \left(\frac{t}{2}\right)^i u'''_i$$

$$-G \sum_{i=0}^{n} \left(\frac{t}{2}\right)^{i+1} \alpha_{io} v''_i + \sum_{i=0}^{n} \left[\frac{Q_1 t_1^3}{3} + \frac{Q_2 t_2^3}{3} (-1)^i \right] \left(\frac{t}{2}\right)^i v_1^{iv} = 0$$

(3.53)

$$\sum_{i=0}^{m} (\lambda j - Gi) \left(\frac{t}{2}\right)^i \beta_{ij} u'_i + \sum_{i=0}^{m} \left[\left(\frac{Q_2}{2}\right) t_2^2 (-1)^{i+j} - \left(\frac{Q_1}{2}\right) t_1^2 \right]$$

$$\left(\frac{t}{2}\right)^i u'''_i + \left(\frac{Q}{2}\right) \sum_{i=1}^{n} 2ij \left(\frac{t}{2}\right)^{i-1} \delta_{ij} v_i - G \sum_{i=0}^{n} \left(\frac{t}{2}\right)^{i+1} \alpha_{ij} v''_i$$

$$+ \sum_{i=0}^{n} \left[\frac{Q_1 t_1^3}{3} + \frac{Q_2 t_2^3}{3} (-1)^{i+j} \right] \left(\frac{t}{2}\right)^i v_i^{iv} = 0$$

$$j = 1, 2, \ldots\ldots, n \qquad (3.54)$$

The forced boundary conditions are,

$$u_o(0) = 0 \qquad v_o(0) = 0 \qquad v'_o(0) = 0 \tag{3.55}$$

The natural boundary conditions can be rewritten as Eqs. (3.56) to (3.61).

$$\sum_{j=0}^{m} \left[\frac{Qt}{2} \alpha_{ij} + Q_1 t_1 + Q_2 t_2 (-1)^{i+j} \right] \left(\frac{t}{2}\right)^j u'_j(0) + \sum_{j=1}^{n} \lambda_j \left(\frac{t}{2}\right)^j \beta_{ij} v_j(0)$$

$$+ \sum_{j=0}^{n} \left[\left(\frac{Q_2}{2}\right) t_2^2 (-1)^{i+j} - \left(\frac{Q_1}{2}\right) t_1^2 \right] \left(\frac{t}{2}\right)^j v''_j(0) - (-1)P = 0$$

$$i = 1, 2, \ldots\ldots, m \tag{3.56}$$

$$\sum_{j=0}^{m} \left[\left(\frac{Q}{2}\right) t\alpha_{ij} + Q_1 t_1 + Q_2 t_2 (-1)^{i+j} \right] \left(\frac{t}{2}\right)^j u'_j(a) + \sum_{j=1}^{n}$$

$$\lambda_j \left(\frac{t}{2}\right)^j \beta_{ij}(a) + \sum_{j=0}^{n} \left[\left(\frac{Q_2}{2}\right) t_2^2 (-1)^{i+j} - \left(\frac{Q_1}{2}\right) t_1^2 \right] \left(\frac{t}{2}\right)^j v''_j(a) - P = 0$$

$$i = 0, 1, 2, \ldots\ldots, m \tag{3.57}$$

$$\sum_{i=1}^{m} Gi \left(\frac{t}{2}\right)^i \beta_{ij} u_i(0) - \sum_{i=0}^{m} \left[\left(\frac{Q_2}{2}\right) t_2^2 (-1)^{i+j} - \left(\frac{Q_1}{2}\right) t_1^2 \right]$$

$$\left(\frac{t}{2}\right)^i u''_i(0) + \sum_{i=0}^{n} G \left(\frac{t}{2}\right)^{i+1} \alpha_{ij} v'_i(0) - \sum_{i=0}^{n} \left[\frac{Q_1 t_1^3}{3} + \frac{Q_2 t_2^3}{3} (-1)^{i+j} \right]$$

$$\left(\frac{t}{2}\right)^i v'''_i(0) - (-1) V = 0 \qquad j = 1, 2, \ldots\ldots, n \tag{3.58}$$

$$\sum_{i=1}^{m} Gi\left(\frac{t}{2}\right)^{i} \beta_{ij} u_i(a) - \sum_{i=0}^{m} \left[\left(\frac{Q_2}{2}\right) t_2^{\,2} (-1)^{i+j} - \left(\frac{Q_1}{2}\right) t_1^{\,2} \right] \left(\frac{t}{2}\right)^{i} u''_i(a)$$

$$+ \sum_{i=0}^{n} G\left(\frac{t}{2}\right)^{i+1} \alpha_{ij} v'_i(a) - \sum_{i=0}^{n} \left[\frac{Q_1 t_1^{\,3}}{3} + \frac{Q_2 t_2^{\,3}}{3} (-1)^{i+j} \right] \left(\frac{t}{2}\right)^{i} v'''_i(a) - V = 0$$

$$j = 0, 1, 2, \ldots\ldots, n \qquad (3.59)$$

$$\sum_{i=0}^{m} \left[\left(\frac{Q_2}{2}\right) t_2^{\,2} (-1)^{i+j} - \left(\frac{Q_1}{2}\right) t_1^{\,2} \right] \left(\frac{t}{2}\right)^{i} u'_i(0)$$

$$+ \sum_{i=0}^{n} \left[\frac{Q_1 t_1^{\,3}}{3} + \frac{Q_2 t_2^{\,3}}{3} (-1)^{i+j} \right] \left(\frac{t}{2}\right)^{i} v''_i(0) - (-1)^{j} \left(\frac{Pt_2}{2} + M_2\right) = 0$$

$$j = 1, 2, \ldots\ldots, n \qquad (3.60)$$

$$\sum_{i=0}^{m} \left[\left(\frac{Q_2}{2}\right) t_2^{\,2} (-1)^{i+j} - \left(\frac{Q_1}{2}\right) t_1^{\,2} \right] \left(\frac{t}{2}\right)^{i} u'_i(a)$$

$$+ \sum_{i=0}^{n} \left[\frac{Q_1 t_1^{\,3}}{3} + \frac{Q_2 t_2^{\,3}}{3} (-1)^{i+j} \right] \left(\frac{t}{2}\right)^{i} v''_i(a) + \left(\frac{Pt_1}{2} - M_1\right) = 0$$

$$j = 0, 1, 2, \ldots\ldots, n \qquad (3.61)$$

3.4 Parameters of Similarity

Inspection of the differential equations and the boundary conditions shows that the displacement field in the adhesive layer is a function of G, λ, Q_1, Q_2, t, t_1, t_2, a, P, V, M_1 and M_2. The equilibrium of the external forces however, gives M_2 as a function of P, V and M_1.

$$M_2 = M_1 + Va - P\left(\frac{t_1}{2} + \frac{t_2}{2} + t\right) \qquad (3.62)$$

Further, it can safely be assumed that the Poisson's ratio μ does not vary appreciably for different adhesive materials. G and λ could then, be considered as functions of Q. Also, the various dimensions and the loads can be expressed in dimensionless form. The parameters of similarity then, are, Q, Q_1, Q_2, $\frac{t}{a}$, $\frac{t_1}{a}$, $\frac{t_2}{a}$, $\frac{P}{a}$, $\frac{V}{P}$, and $\frac{M_1}{Pa}$.

The stresses σ_x and σ_y are dependent on the modulus of elasticity E, while the shear stress τ_{xy} is determined by the shear modulus G. Since μ does not vary greatly, G can be considered as a function of E. Also, if we assume that μ, μ_1, and μ_2 are approximately equal then, $\frac{Q_1}{E} \alpha \frac{Q_1}{G} \alpha \frac{E_1}{E}$ and $\frac{Q_2}{E} \alpha \frac{Q_2}{G} \alpha \frac{E_2}{E}$. The stress field in the adhesive layer is then determined by the factors, $\frac{E_1}{E}$, $\frac{E_2}{E}$, $\frac{t}{a}$, $\frac{t_1}{a}$, $\frac{t_2}{a}$, $\frac{P}{a}$, $\frac{V}{P}$ and $\frac{M_1}{Pa}$.

A special case of identical adherends with antisymmetric loading configuration can be considered here. In this case,

$$M_1 = -M_2 = \tfrac{1}{2}\left[P(t_1 + t) - Va\right] \quad \text{and} \quad t_1 = t_2\,;\; E_1 = E_2 \tag{3.63}$$

The stress field in this case, is a function of $\frac{E_1}{E}$, $\frac{t}{t_1}$, $\frac{t_1}{a}$, $\frac{P}{a}$, $\frac{V}{P}$.

3.5 Case of Identical Adherends

The differential equations and the boundary conditions can be greatly simplified if the two adherends are identical and m and n are taken to be equal to 1. An analytical solution of the differential equations is possible in this case. Since, the adherends are identical,

$$t_2 = t_1\,; \text{ and } Q_2 = Q_1 \tag{3.64}$$

The four differential equations in this case are:

$$(Qt + 2Q_1t_1)u_o'' + \lambda t v_1' - (\frac{Q_1}{2})t_1^2 t v_1''' = 0 \tag{3.65}$$

$$2Gu_1 - \left(\frac{Qt}{3} + 2Q_1t_1\right)\frac{t}{2}u_1'' + 2Gv_o' + Q_1t_1^2v_o''' = 0 \tag{3.66}$$

$$-Gtu_1' - Q_1t_1^2\frac{t}{2}u_1''' - Gtv_o'' + Q_1\frac{2t_1^3}{3}v_o^{iv} = 0 \tag{3.67}$$

$$2\lambda u_o' - Q_1t_1^2u_o''' + 2Qv_1 - \frac{Gt^2}{6}v_1'' + Q_1\frac{t_1^3t}{3}v_1^{iv} = 0 \tag{3.68}$$

The boundary conditions in this case are given by Eqs. (3.69) to (3.78).

$$u_o(0) = 0 \qquad v_o(0) = 0 \qquad v_o'(0) = 0 \tag{3.69}$$

$$\left(\frac{Qt}{3} + 2Q_1t_1\right)\frac{t}{2}u_1'(0) - Q_1t_1^2v_o''(0) + P = 0 \tag{3.70}$$

$$(Qt + 2Q_it_1)u_o'(a) + \lambda tv_j(a) - Q_1\frac{t_1^2t}{2}v_1''(a) - P = 0 \tag{3.71}$$

$$\left(\frac{Qt}{3} + 2Q_1t_1\right)\frac{t}{2}u_1'(a) - Q_1t_1^2v_o''(a) - P = 0 \tag{3.72}$$

$$Q_1t_1^2u_o''(0) + \frac{Gt_2}{6}v_1'(0) - Q_1\frac{t_1^3t}{3}v_1''(0) + V = 0 \tag{3.73}$$

$$Gtu_1(a) + Q_1\frac{t_1^2t}{2}u_1''(a) + Gtv_o'(a) - Q_1\frac{2t_1^3}{3}v_o'''(a) - V = 0 \tag{3.74}$$

$$Q_1t_1^2u_o''(a) + \frac{Gt^2}{6}v_1'(a) - Q_1\frac{t_1^3t}{3}v_1'''(a) - V = 0 \tag{3.75}$$

$$-Q_1t_1^2u_o'(0) + Q_1\frac{t_1^3t}{3}v_1''(0) + \left(\frac{Pt_1}{2} + M_2\right) = 0 \tag{3.76}$$

$$-Q_1 \frac{t_1^2 t}{2} u_1'(a) + Q_1 \frac{2t_1^3}{3} v_o''(a) + \left(\frac{Pt_1}{2} - M_1\right) = 0 \tag{3.77}$$

$$-Q_1 t_1^2 u_o'(a) + Q_1 \frac{t_1^3 t}{3} v_1''(a) + \left(\frac{Pt_1}{2} - M_1\right) = 0 \tag{3.78}$$

The solution for the differential equations can be found as follows:

From (3.65) we have,

$$u_o'' = A_1 \cdot v_1''' + A_2 \cdot v_1' \tag{3.79}$$

where,

$$A_1 = \frac{Q_1 t_1^2 t}{2(Qt + 2Q_1 t_1)} \tag{3.80}$$

and

$$A_2 = \frac{-\lambda t}{(Qt + 2Q_1 t_1)} \tag{3.81}$$

Integrating (3.79),

$$u_o' = A_1 \cdot v_1'' + A_2 \cdot v_1 + c_1 \tag{3.82}$$

where c_1 is a constant.

Substituting (3.79) and (3.82) in (3.68) and rearranging the coefficients, we get,

$$v_1^{iv} + A_3 v_1'' + A_4 v_1 = \left(\frac{2\lambda}{A_5}\right) c_1 \tag{3.83}$$

where,

$$A_3 = \left(\frac{Gt^2}{6} - 4\lambda A_1\right) / A_5$$

$$A_4 = -2(\lambda A_2 + Q) / A_5$$

$$A_5 = A_1 Q_1 t_1^2 - \frac{Q_1 t_1^3 t}{3}$$

(3.83) is an ordinary linear differential equation with constant coefficients and yields,

$$v_1 = c_2 e^{k_1 x} + c_3 e^{-k_1 x} + c_4 e^{k_2 x} + c_5 e^{-k_2 x} + \frac{2\lambda c_1}{A_4 A_5} \qquad (3.84)$$

where k_1 , $-k_1$, k_2 , $-k_2$ are roots of the polynomial $k^4 + A_3 k^2 + A_4 = 0$; and c_2 , c_3 , c_4 , c_5 are constants of integration.

Substituting (3.84) in (3.82) we get,

$$u_o' = A_1(c_2 k_1^2 e^{k_1 x} + c_3 k_1^2 e^{-k_1 x} + c_4 k_2^2 e^{k_2 x} + c_5 k_2^2 e^{-k_2 x})$$

$$+ A_2\left(c_2 e^{k_1 x} + c_3 e^{-k_1 x} + c_4 e^{k_2 x} + c_5 e^{-k_2 x} + \frac{2\lambda c_1}{A_4 A_5}\right) + c_1$$

or

$$u_o = \left(A_1 c_2 k_1 + \frac{A_2 c_2}{k_1}\right) e^{k_1 x} - \left(A_1 c_3 k_1 + \frac{A_2 c_3}{k_1}\right) e^{-k_1 x}$$

$$+ \left(A_1 c_4 k_2 + \frac{A_2 c_2}{k_2}\right) e^{k_1 x} - \left(A_1 c_5 k_2 + \frac{A_2 c_5}{k_2}\right) e^{-k_2 x} + \left(\frac{2A_2\lambda}{A_4 A_5} + 1\right) c_1 x + c_6$$

(3.85)

where c_6 is a constant of integration.

Now, v_1 and u_o are known functions of x from (3.84) and (3.85) if the constants c_1, c_2, c_3, c_4, c_5, and c_6 are known. These constants can be determined from the boundary conditions (3.69), (3.71), (3.73), (3.75), (3.76), and (3.78). These boundary conditions yield the following set of simultaneous equations.

From (3.69), i.e. for $u_o(0) = 0$,

$$(A_1k_1 + \frac{A_2}{k_1})c_2 - (A_1k_1 + \frac{A_2}{k_1})c_3 + (A_1k_2 + \frac{A_2}{k_2})c_4 - (A_1k_2 + \frac{A_2}{k_2})c_5 + c_6 = 0 \tag{3.86}$$

From (3.71),

$$(Qt + 2Q_1t_1)c_1 = P \tag{3.87}$$

From (3.73),

$$(A_6k_1 + A_7k_1^3)c_2 - (A_6k_1 + A_7k_1^3)c_3 + (A_6k_2 + A_7k_2^3)c_4 - (A_6k_2 + A_7k_2^3)c_5 = -V \tag{3.88}$$

where,

$$A_6 = \frac{Gt^2}{6} + A_2Q_1t_1^2$$

and

$$A_7 = Q_1t_1^2(A_1 - \frac{t_1t}{3})$$

From (3.75),

$$(A_6k_1 + A_7k_1^3)e^{k_1a} c_2 - (A_6k_1 + A_7k_1^3)e^{-k_1a} c_3$$

$$+ (A_6k_2 + A_7k_2^3)e^{k_2a} c_4 - (A_6k_2 + A_7k_2^3)e^{-k_2a} c_5 = V \qquad (3.89)$$

From (3.76),

$$A_9c_1 + (A_7k_1^2 + A_8)c_2 + (A_7k_1^2 + A_8)c_3 + (A_7k_2^2 + A_8)c_4$$

$$+ (A_7k_2^2 + A_8)c_5 = (\frac{Pt_1}{2} + M_2) \qquad (3.90)$$

where,

$$A_8 = -Q_1t_1^2A_2$$

and

$$A_9 = -(1 + \frac{2\lambda A_2}{A_4A_5})Q_1t_1^2$$

From (3.78),

$$A_9c_1 + (A_7k_1^2 + A_8)e^{k_1a} c_2 + (A_7k_1^2 + A_8)e^{-k_1a} c_3$$

$$+ (A_7k_2^2 + A_8)e^{k_2a} c_4 + (A_7k_2^2 + A_8)e^{-k_2a} c_5 = M_1 - \frac{Pt_1}{2} \qquad (3.91)$$

The above six simultaneous linear equations can be solved to obtain the six constants which when substituted in (3.84) and (3.85) would give $v_1(x)$ and $u_o(x)$.

Now, to determine $u_1(x)$ and $v_o(x)$, differential equations (3.66) and (3.67) should be solved.

Differentiating (3.66) once, multiplying by $t/2$ and then adding to (3.67) gives,

$$Q_1 t_1^2 \left(\frac{2t_1}{3} + \frac{t}{2}\right) v_o^{iv} - \left[\left(\frac{Qt}{3} + 2Q_1 t_1\right) \frac{t^2}{4} + Q_1 \frac{t_1^2 t}{2} \right] u_1''' = 0$$

or

$$u_1''' = B_1 v_o^{iv} \tag{3.92}$$

where,

$$B_1 = \frac{Q_1 t_1^2 \left(\frac{2t_1}{3} + \frac{t}{2}\right)}{\left[\left(\frac{Qt}{3} + 2Q_1 t_1\right) \frac{t^2}{4} + Q_1 \frac{t_1^2 t}{2} \right]}$$

Integrating (3.92), we have,

$$u_1 = B_1 v_o' + \frac{c_7}{2} x^2 + c_8 x + c_9 \tag{3.93}$$

where c_7, c_8, c_9 are constants of integration.

Substituting (3.93) in (3.66) and rearranging coefficients, we get,

$$v_o''' + B_2 v_o' = B_3 c_7 x^2 + 2B_3 c_8 x + 2B_3 c_9 + B_4 c_7 \tag{3.94}$$

where,

$$B_2 = \frac{-2G(B_1 + 1)}{B_5}$$

$$B_3 = \frac{G}{B_5}$$

$$B_4 = - \frac{(\frac{Qt}{6} + Q_1 t_1)t}{B_5}$$

$$B_5 = (\frac{Qt}{6} + Q_1 t_1)tB_1 - Q_1 t_1^2$$

The solution of (3.94) is,

$$v_o = c_7 \frac{B_3}{3B_2} x^3 + c_8 \frac{B_3}{B_2} x^2 + \left\{ (\frac{B_4}{B_2} - \frac{2B_3}{B_2^2}) c_7 + \frac{2B_3}{B_2} c_9 \right\} x$$

$$+ c_{10} e^{kx} + c_{11} e^{-kx} + c_{12} \qquad (3.95)$$

where c_{10} , c_{11} , c_{12} are constants and $k = \sqrt{- B_2}$.

The six constants c_7 , c_8 , c_9 , c_{10} , c_{11} and c_{12} are determined from the boundary conditions (3.69), (3.70), (3.72), (3.74), and (3.77).

From (3.69), for $v_o(0) = 0$ we get,

$$c_{10} + c_{11} + c_{12} = 0 \qquad (3.96)$$

From (3.69) for $v_o'(0) = 0$ we get,

$$(\frac{B_4}{B_2} - \frac{2B_3}{B_2^2}) c_7 + \frac{2B_3}{B_2} c_9 + kc_{10} - kc_{11} = 0 \qquad (3.97)$$

From (3.70),

$$B_6 \cdot c_8 + B_7 k^2 \cdot c_{10} + B_7 k^2 \cdot c_{11} = -P \qquad (3.98)$$

where,

$$B_6 = \frac{2B_7B_3}{B_2} + B_8$$

$$B_7 = \frac{Q_1t_1^3}{3} \quad \frac{(\frac{2Qt}{3} + Q_1t_1)}{(Q_1t_1^2 + B_8)}$$

$$B_8 = (\frac{Qt}{6} + Q_1t_1)t$$

From (3.72),

$$B_6ac_7 + B_6c_8 + B_7k^2e^{ka} \cdot c_{10} + B_7k^2e^{-ka} \cdot c_{11} = P \qquad (3.99)$$

From (3.74),

$$B_9c_7 + (B_{10}k + B_{11}k^3)e^{ka} \cdot (B_{10}k + B_{11}k^3)e^{-ka}\, c_{11} = V \qquad (3.100)$$

where,

$$B_9 = \left\{ B_8 - \frac{B_5}{(B_1 + 1)} \right\} \frac{t}{2} - \frac{Q_1t_1^2(B_1t - \frac{4}{3}t_1)}{2(B_1 + 1)} + \frac{Q_1t_1^2t}{2}$$

$$B_{10} = Gt(B_1 + 1)$$

$$B_{11} = \frac{Gt}{2}(Q_1t_1^2tB_1 - \frac{4}{3}Q_1t_1^3)$$

From (3.77),

$$B_{12}ac_7 + B_{12}c_8 + B_{13}k^2e^{ka}c_{10} + B_{13}k^2e^{-ka}c_{11} = M_1 - \frac{Pt_1}{2} \qquad (3.101)$$

where,

$$B_{12} = - \frac{B_{13}}{(B_1 + 1)} - \frac{Q_1 t_1^2 t}{2}$$

and

$$B_{13} = \frac{Q_1 t_1^2}{2} \left(\frac{4}{3} t_1 - B_1 t\right)$$

The above six simultaneous linear equations can be solved to obtain the six constants which when substituted in (3.95) would give $v_o(x)$. $u_1(x)$ can then be obtained from (3.93).

3.6 Condition for Uniform Shear Stress in an Antisymmetric Joint

If, in a joint, the two adherends are identical and the moment M_2 is equal to $-M_1$, then the joint is antisymmetric about the middle of the adhesive layer, i.e. about the x-axis. In such a case, it is possible to require a uniform distribution of shear stress along the x-axis, and derive an expression for the ratio (V/P) as a necessary and sufficient condition for this requirement. It is required that,

$$(\tau_{xy})_{y=0} = \frac{P}{a}$$

or

$$G(u_1 + v_o') = \frac{P}{a}$$

or

$$v_o' = \frac{P}{Ga} - u_1 \qquad (3.102)$$

Substituting (3.102) in (3.66),

$$\frac{2P}{a} - \left(\frac{Qt}{3} + 2Q_1t_1\right)\frac{t}{2}u_1'' + Q_1t_1^2(-u_1'') = 0$$

or

$$u_1'' = \frac{2P}{a'/} \tag{3.103}$$

where,

$$'/ = \frac{Qt^2}{6} + Q_1t_1t + Q_1t_1^2$$

(3.103) yields,

$$u_1 = \frac{P}{a'/}x^2 + b_1x + b_2 \tag{3.104}$$

b_1 and b_2 are constants of integration.

(3.102) yields,

$$v_o' = \frac{P}{Ga} - \left(\frac{P}{a'/}x^2 + b_1x + b_2\right) \tag{3.105}$$

From (3.69), since $v_o'(0) = 0$,

$$b_2 = \frac{P}{Ga}$$

$$\therefore \quad v_o' = \frac{P}{a'/}x^2 - b_1x \tag{3.106}$$

and

$$u_1 = \frac{P}{a'/}x^2 + b_1x + \frac{P}{Ga} \tag{3.107}$$

The above expressions for v_o' and u_1 satisfy the differential equation (3.67) identically. From (3.70),

$$(\frac{Qt^2}{6} + Q_1t_1t)b_1 + Q_1t_1^2b_1 = -P$$

or

$$b_1 = \frac{-P}{(\frac{Qt^2}{6} + Q_1t_1t + Q_1t_1^2)} = -\frac{P}{\text{illegible}} \tag{3.108}$$

From (3.74),

$$\frac{Pt}{a} + \frac{Q_1t_1^2t}{\text{illegible}} - \frac{2}{3}Q_1t_1^3(\frac{-2P}{\text{illegible}}) - V = 0$$

or

$$\frac{Pt}{a} + (Q_1t_1^2t + \frac{4}{3}Q_1t_1^3)\frac{P}{\text{illegible}} - V = 0$$

or

$$\frac{V}{P} = \frac{t}{a} + \frac{(Q_1t_1^2t + \frac{4}{3}Q_1t_1^3)}{a(\frac{Qt^2}{6} + Q_1t_1t + Q_1t_1^2)} \tag{3.109}$$

Boundary conditions (3.72) and (3.77) are identically satisfied. Two special cases can be considered.

Case (1): $\frac{Q}{Q_1} \ll 1$

The ratio (V/P) then reduces to

$$\frac{V}{P} = \frac{t}{a} + \frac{t_1 (t + \frac{4}{3} t_1)}{a(t + t_1)} \tag{3.110}$$

Case (2) : $\frac{t}{t_1} << 1$

In this case we have

$$\frac{V}{P} = \frac{4}{3} \frac{t_1}{a} \tag{3.111}$$

It can be seen that as the ratios $\frac{t}{t_1}$ and $\frac{Q}{Q_1}$ increase, the required value of (V/P) also increases. Eq. (3.111) thus provides the minimum value of V/P for which a uniform distribution of shear stress can be obtained.

A similar attempt at requiring the tearing stress σ_y to be uniform along the x-axis results in the trival case of $P = V = M_1 = M_2 = 0$ indicating that the tearing stress distribution cannot be completely uniform under any given load configuration.

3.7 Solution for the General Case

In the case where the adherends are not identical and where m and n are integers greater than 1, the differential equations still remain linear and homogeneous but their number is larger and therefore their analytical solution becomes more complex. These differential equations are therefore, solved numerically using the method of linear conversion. The details of this method and the computer program for IBM 360 are given in Appendix A.

4. EXPERIMENTAL INVESTIGATION

4.1 Introduction

The main purpose of the experimental work was to check the analytical results and establish confidence in the theory. The analysis considers the variation of stresses through the thickness of the adhesive and treats the problem as one of plane strain. Photoelasticity presents the most suitable means of experimentally determining stresses over an area in a plane problem and was therefore employed in this case. In order to check all the stress distributions and results that the analytical work gives would require the construction and testing of many complex specimens. For the limited purpose of checking the validity of the theory however, testing of two specimens of varying overlap lengths was thought to be sufficient. In order to obtain a reasonably good fringe pattern for the adhesive, it was necessary that the adhesive layer be sufficiently thick. For this reason the joints ere made of a $\frac{1}{4}$" laver of a photoelastic plastic simulating the adhesive, bonded between two identical 1" thick metal adherends. The joints were made 1" wide to approximate the condition of plane strain.

One important result that the theory predicts is the effect of the ratio V/P on the distribution of stress. This effect was tested experimentally by subjecting the specimens to loads at different angles with respect to the plane of the adhesive layer.

4.2 Material and Specimen Preparation

Araldite 6020 epoxy was used to simulate the adhesive layer. This epoxy is available in solid form and can be machined to the required shape. Araldite 6020 was preferred over the other photoelastic plastics for two main reasons. Firstly, compared to the other plastics, Araldite 6020 has a lower fringe value which means a good number of fringes can be obtained with small loads thus improving the accuracy of the experimental results. Secondly and more importantly, Araldite 6020 can be

easily bonded to aluminum with a thin layer of adhesive of the same material, setting at room temperature. Araldite 6020 adhesive sets at room temperature when used with Ciba hardener 951. This aids in keeping the initial stresses to a minimum. In fact with a little care, the joints can be made practically free of initial stresses. This fact is important because the presence of high initial stresses would render the model useless for a photoelastic investigation.

Adherends were made of 1" square 2024 T4 aluminum alloy. In order to prepare the aluminum surface for adhesive application, the adherends were treated in a hot acid bath at 150 - 160^{o} F for about 10 - 12 minutes. The hot acid bath was made with 66 ml. of sulphuric acid (H_2SO_4), 315 ml. of water and 13.5 gms. of sodium dichromate ($Na_2Cr_2O_7$).

Two pieces of Araldite 6020 epoxy were machined, one to the dimensions, $\frac{1}{4}$" x 1" x 2" for the 2" overlap model and another to the dimensions, $\frac{1}{4}$" x 1" x 3", for the 3" overlap model. Each piece was bonded first to one adherend by means of an adhesive consisting of 10 pbw of Ciba 6020 and 1 pbw of Ciba hardener 951. The joint was allowed to set at room temperature for 24 hours. The other surface of the epoxy was bonded to the second adherend in the similar manner and allowed to set 24 hours. The joint was tested immediately after it was hardened, because the epoxy starts absorbing mositure from the air and high initial stresses develop. The dimensions of the two specimens are shown in Fig. 6.

4.3 Test Equipment and Procedure

Fig. 7 shows the photoelastic bench. A circular polariscope with a mercury green monochromatic light source was used. The model was photographed in light background. The model was loaded by means of dead weights at the end of a lever arm with a mechanical advantage of 4:1. The direction of the load with respect to the plane of the adhesive layer was varied by rotating the model to the desired angle. This was

achieved by means of two aluminum plates fastened to the model, one at each end (Fig. 8), each plate provided nine loading points allowing the tangent of the angle (or the ratio V/P) to vary from zero to 0.8 in steps of 0.1.

At first the model was photographed with no load. For the photoelastic tests to be reliable it was necessary that nothing in excess of a half order fringe be present at zero load. The model was then gradually loaded to R = P + V = 309 lbs. The movement of the fringe was observed and the model was photographed.

In order to obtain the stress distribution from the fringe patterns photographed, it was necessary that the Araldite epoxy be calibrated for its fringe value. A circular disc of the material was loaded in compression and the fringe order at the center of the disc was obtained by using Tardy's method of compensation (16). This procedure was repeated with different loads and a calibration curve was obtained (Fig. 9). Theoretically the shear stress at the center of the disc is given by, $\tau = \frac{4P_c}{\pi d}$ where, P_c = compressive load, and d = diameter of the disc. The fringe value, f, of the material was then calculated from $f = \frac{4P_c}{\pi dN}$ where N is the fringe order at the center of the disc.

The modulus of elasticity for Araldite 6020 ($E = 4.5 \times 10^5$ psi) was taken from Leven (17). This value was used for the theoretical stress analysis of the models. The results are discussed in the following chapter.

5. ANALYTICAL AND EXPERIMENTAL RESULTS

5.1 General

The behavior of a lap joint depends on a number of factors including the relative properties of the two adherends. The case of identical adherends is of special interest and will be discussed in detail. The performance of the non-identical-adherend-joint will be compared with that of the identical-adherend-joint. The case where the joint is subjected to pure moment, will also be discussed.

5.2 Effect of m and n

The displacements u, and v, have been expressed in Eqs. (3.1) and (3.2) as power series in y. For an exact elastic solution m and n should approach infinity. It should, however, be possible to terminate the series after a certain number of terms and arrive at a solution reasonable close to the elastic solution.

Fig. 10 shows the shear stress distribution at the mid-plane (y = 0 plane) of the adhesive layer with varying values of m. At m = 1, the displacement u is a linear function of y, while at m = 2 and 3, the displacement u is expressed respectively as a quadratic and a cubic in y. Qualitatively it is seen that in all the three cases, the maximum stress occurs at the joint edges, decreasing rapidly to a minimum in the middle. It is also seen that as m increases, there is a decrease in the maximum stress concentration. The effect of m is, however, much more clear in Fig. 11 where the distribution of interfacial shear stress is shown. For m = 2 and 3, the highest stress is seen to occur at the leading corner, there is a rapid decrease in the stress towards the middle of the joint and then another smaller peak occurs near but not at the trailing corner. The stress is in fact, seen to decrease at the trailing corner. This qualitative distribution is not seen in m = 1 curve. Theoretically the stress at the trailing corner should be expected to be zero whereas the singularity at the leading

corner should produce a high shear stress at that corner. It is interesting to note that rising values of m produce a higher stress at the leading corner. This indicates that if m is made sufficiently large the ideal solution may be approached. The real materials, however, do not behave as perfectly elastic materials and some plastic deformation may occur at the leading corners, the extent of such deformation would depend on the properties of the adhesive material. The stress distribution obtained for m = 2 or 3 can be expected to be reasonably close to the actual case both qualitatively and quantitatively.

The distribution of σ_y at the mid-plane and at the interfacial plane is shown in Figs. 12 and 13. At the interface the three curves are in good agreement, but at the mid-plane, m = 2 and 3 show σ_y to be much lower. This indicates that σ_y varies appreciably through the thickness of the adhesive. Similar conclusions can be drawn about the longitudinal stress σ_x shown in Figs. 14 and 15.

It can be concluded from these results that for m equal to 2 or higher the qualitative and quantitative distribution of stress is better, compared to the distribution obtained for m equal to 1. Also, the quantitative results for m equal to 2, can be considered sufficiently close to the elastic solution.

In all cases discussed above, the value of n was kept constant at 1. The thickness, t, of the adhesive is small compared to the overlap length, a. For this reason the numerical integration of the differential equations for n greater than 1, becomes extremely inaccurate. In order to obtain reasonably good results, the step size for integration has to be made extremely small. The computer time and cost involved would in such a case be high. It must, however, be noted that for the very fact that t/a is small, the displacement v can be assumed to be approximately a linear function in y, and n can therefore, be taken as 1.

5.3 Comparison with Experiment

In Fig. 16 are shown the fringe patterns for the two models at no load. It is seen that the zero and half order fringes are present. Under load, fringes of up to eighth order are found. The models can be considered to be adequately free of initial stresses.

The experimental results were obtained in the form of photoelastic fringe patterns. The computer was programmed to convert the maximum shear stress at each point in the adhesive layer, into the corresponding fringe order. The comparison of these results is shown in Figs. 17 and 18 for the 2 inch specimen and in Figs. 19 and 20 for the 3 inch specimen. The theoretical results shown in these figures are for $m = 2$ and $n = 1$. At the mid-plane (Figs. 17 and 19), the theoretical and experimental results are in good agreement except at the two ends, where, the experimental results show a rapid decrease in stress. At the interfacial plane ($y = t/2$), again, the two results are in excellent agreement except at the trailing end, where the experimental results show lower stress concentrations. It can be argued here again, as has been done in Article 5.2, that as m is made greater, the theoretical stress distribution can be expected to approach the experimental pattern.

The analysis predicts that the ratio V/P has a significant effect on the stress distribution, and in fact for a certain value of V/P given by Eq. (3.109), the shear stress distribution can be made uniform. This value of V/P turns out to be 0.76 for the 2 inch specimen and 0.51 for the 3 inch specimen. Experimental results for $V/P = 0.8$ for the 2 inch specimen are compared in Figs. 21 and 22 with the corresponding theoretical results. At the mid-plane (Fig. 21), it is again seen that the two results are in good agreement except at the ends where the experimental stress decreases rapidly. At the interfacial plane (Fig. 22), the experimental stress shows a rapid decrease at the trailing edge but is otherwise, in good agreement with the theory. Simi-

lar results are shown in Figs. 23 and 24, for the 3 inch specimen for V/P = 0.60. It must be emphasized here, again, that the theoretical results are for m = 2, and can be expected to approach the experimental results for greater values of m.

In order to compare the theoretical and experimental results over the whole area of the adhesive layer, the computer was programmed to plot theoretical fringe patterns for m = 2. These fringe patterns are compared against the experimental fringe patterns in Figs. 25 to 27 for the 2 inch specimen and Figs. 28 to 30 for the 3 inch specimen. Similar conclusions can be drawn from these results as have been discussed above.

5.4 Case of Identical Adherends

In this section, the analytical results for a joint with identical adherends and antisymmetric loading will be discussed. Theoretically it has been found that the stresses in the adhesive layer depend on the factors, E_1/E, t_1/t, t_1/a, V/P and P/a. The stresses can be expressed in dimensionless form by dividing them by the mean shear stress P/a. The number of joint parameters then reduces to four, E_1/E, t_1/t, t_1/a and V/P.

The condition for a uniform distribution of shear stress at the mid-plane of the adhesive layer is given by Eq. (3.109). Let V_f be a factor defined as follows

$$V_f = \frac{V}{P} \cdot \frac{a}{\left[t + \frac{Q_1 t_1^2 (t + \frac{4}{3} t_1)}{\psi} \right]} \tag{5.1}$$

Then the condition for uniform distribution of stress is, $V_f = 1$. The factor V_f can therefore, be used as a parameter of comparison. The joint parameters then are, E_1/E, t_1/t, t_1/a, V_f.

Let S_f and N_f be parameters defined as follows.

$$S_f = \frac{a}{t_1} \sqrt{\frac{Et_1}{E_1 t}} \tag{5.2}$$

$$N_f = \frac{a}{t_1} \left[\frac{E t_1}{E_1 t} \right]^{\frac{1}{3}} \tag{5.3}$$

The factor S_f is similar to $\sqrt{D}$ of Volkersen (1) and $\frac{\beta a}{t_1}$ of Goland and Reissner (2). The shear stress can be expressed as a function of S_f.

$$\frac{(\tau_{xy})_{max}}{\tau_{av}} = F_1 (S_f, V_f, E_1/E, t_1/t) \tag{5.4}$$

where,

$$\tau_{av} = \text{average shear stress} = P/a \tag{5.5}$$

The factor N_f is similar to the parameter λ of Goland and Reissner (2). The normal stresses can be expressed as functions of N_f.

$$\frac{(\sigma_y)_{max}}{\tau_{av}} \cdot \frac{a}{t_1} = F_2 (N_f, V_f, E_1/E, t_1/t) \tag{5.6}$$

$$\frac{(\sigma_x)_{max}}{\tau_{av}} \cdot \frac{a}{t_1} = F_3 (N_f, V_f, E_1/E, t_1/T) \tag{5.7}$$

In the following discussion on the shear and normal stresses in the adhesive layer, the theoretical data has been calculated for $m = n = 1$ and $\mu = \mu_1 = 0.30$. It has been discussed in Article 5.2, that $m = 2$ gives better results from the viewpoint of accuracy of stresses. $m = 1$, however, provides a simpler and adequate means for comparison of joints.

5.4.1 Shear Stress: Figs. 31 and 32 show the shear stress concentration factor as a function of the parameter t_1/t. Curves are shown for various values of E_1/E and

S_f, keeping V_f constant at zero. Figs. 33 and 34 show the same curves for $V_f = 2$. It can be concluded from these diagrams, that for $t_1/t \geq 10$ and $E_1/E \geq 10$, the shear stress concentration factor is independent of t_1/t and E_1/E, and is a function of V_f and S_f alone.

From design point of view, the maximum shearing stress, τ_{max}, is even more important and is shown in Figs. 35 and 36 as a function of t_1/t. For $t_1/t \geq 10$ and $E_1/E \geq 20$, the maximum shearing stress can be considered as a function of S_f and V_f only.

From the above discussion, it is observed that the shear stress concentration factor and the maximum shearing stress concentraion factor are independent of t_1/t and E_1/E for $t_1/t \geq 10$ and $E_1/E \geq 20$, and are functions of V_f and S_f only. It must be mentioned here that the peak stress, whether positive or negative, is found to occur at the leading corner when stresses at the interfacial plane are being considered, and at the two ends when stresses at the mid-plane are being considered.

In Fig. 37 is shown the shear stress concentration factor at the mid-plane of the adhesive layer as a function of S_f and V_f. It is interesting to note that the shear stress varies approximately linearly with S_f, and also with V_f. For $S_f > 6$ the shear stress concentration factor can be approximately expressed as follows.

$$\frac{(\tau_{xy})_{max}}{\tau_{av}} = 1 + \frac{4}{5}(S_f - 1)(1 - V_f), \qquad \text{at } y = 0 \text{ plane} \qquad (5.8)$$

Fig. 38 shows shear stress at the plane of the interface, as a function of S_f and V_f. Again, the shear stress is approximately a linear function of S_f and V_f. The approximate formula in this case is,

$$\frac{(\tau_{xy})_{max}}{\tau_{av}} = 1 + \frac{7}{8}(S_f - 1)(1 - V_f), \qquad \text{at } y = \pm \frac{t}{2} \qquad (5.9)$$

τ_{max} is shown as a function of S_f and V_f in Fig. 39. The maximum shearing stress can be approximately expressed by the following two equations.

For $V_f \leq 1$ and $S_f > 4$,

$$\frac{\tau_{max}}{\tau_{av}} = 1 + \frac{6}{7}\left(\frac{19}{18} - V_f\right)(S_f - 1) \qquad (5.10)$$

For $V_f \geq 1.5$ and $S_f > 5$

$$\frac{\tau_{max}}{\tau_{av}} = -1 + \frac{18}{19}\left(V_f - \frac{17}{18}\right)(S_f - 1) \qquad (5.11)$$

5.4.2 Normal Stresses: The maximum tearing stress, $(\sigma_y)_{max}$, is shown in Figs. 40 and 41 as a function of the parameters t_1/t, E_1/E, N_f and V_f. It is observed that for $t_1/t \geq 10$ and $E_1/E \geq 10$, the tearing stress factor is independent of the parameters t_1/t and E_1/E, and is a function of N_f and V_f alone.

Figs. 42 and 43 show that the variation of the stress $(\sigma_x)_{max}$ is quite appreciable for $E_1/E < 20$. However, it can be concluded from these diagrams that, for $E_1/E \geq 20$ and $t_1/t \geq 10$, $(\sigma_x)_{max}$ is a function of the parameters N_f and V_f only.

The maximum normal stress at any given point acts on one of the principal planes. Fig. 44 shows the maximum principal stress, σ_{max}, as a function of the parameters t_1/t, E_1/E, N_f and V_f. Again, it can be concluded that, for $t_1/t \geq 10$, and $E_1/E \geq 20$, σ_{max} can be considered to be a function of two parameters, N_f and V_f only.

The maximum tearing stress is shown in Figs. 45 and 46 as a function of N_f and V_f. These diagrams are drawn for $t_1/t = 10$, and $E_1/E = 20$. As has been discussed above, these graphs would be applicable for all joints where $t_1/t \geq 10$ and $E_1/E \geq 20$. It must be noted here that this range is the one that is most frequently

encountered in practice. The data shown in Figs. 45 and 46 are therefore, applicable to the majority of the practical lap joints.

Similar graphs are shown in Figs. 47 and 48 for $(\sigma_x)_{max}$, and in Fig. 49 for σ_{max}. It is observed that for a given V_f, the normal stress factors vary approximately as square functions of N_f. This is more clearly seen in Figs. 50 through 54, where the stress factors are shown as functions of N_f^2. These graphs consist of almost straight lines. The stresses can be approximately expressed as follows.

$$\frac{(\sigma_y)_{max}}{\tau_{av}} \cdot \frac{a}{t_1} = (1.325 - 1.6\, V_f)\, N_f^2 , \qquad \text{at } y = 0 \text{ plane} \tag{5.12}$$

$$\frac{(\sigma_y)_{max}}{\tau_{av}} \cdot \frac{a}{t_1} = (1.4 - 1.675\, V_f)\, N_f^2 , \qquad \text{at } y = \pm \frac{t}{2} \tag{5.13}$$

$$\frac{(\sigma_x)_{max}}{\tau_{av}} \cdot \frac{a}{t_1} = (0.85 - 0.95\, V_f)\, N_f^2 , \qquad \text{at } y = 0 \tag{5.14}$$

$$\frac{(\sigma_x)_{max}}{\tau_{av}} \cdot \frac{a}{t_1} = (0.85 - 0.95\, V_f)\, N_f^2 , \qquad \text{at } y = \pm \frac{t}{2} \tag{5.15}$$

$$\frac{(\sigma_{max})}{\tau_{av}} \cdot \frac{a}{t_1} = (2.0 - 2.2\, V_f)\, N_f^2 , \qquad \text{at } y = \pm \frac{t}{2} \tag{5.16}$$

Now, Eqs. (5.2) and (5.3) yield,

$$N_f^2 = \frac{a}{t_1} \cdot S_f \tag{5.17}$$

Substituting (5.17) in (5.12) through (5.15),

$$\frac{(\sigma_y)_{max}}{\tau_{av}} = (1.325 - 1.6\, V_f)\, S_f , \qquad \text{at } y = 0 \tag{5.18}$$

$$\frac{(\sigma_y)_{max}}{\tau_{av}} = (1.4 - 1.675\ V_f)\, S_f, \qquad \text{at } y = \pm \frac{t}{2} \tag{5.19}$$

$$\frac{(\sigma_x)_{max}}{\tau_{av}} = (0.7 - 0.8\ V_f)\, S_f, \qquad \text{at } y = 0 \tag{5.20}$$

$$\frac{(\sigma_x)_{max}}{\tau_{av}} = (0.85 - 0.95\ V_f)\, S_f, \qquad \text{at } y = \pm \frac{t}{2} \tag{5.21}$$

$$\frac{\sigma_{max}}{\tau_{av}} = (2.0 - 2.2\ V_f)\ S_f, \qquad \text{at } y = \pm \frac{t}{2} \tag{5.22}$$

Thus it is seen that the normal stresses are approximately linear functions of V_f and S_f. Eqs. (5.18) through (5.22) show another interesting development if both sides of these equations are multiplied by t_1/a, which yields,

$$\frac{(\sigma_y)_{max}\, t_1}{P} = (1.35 - 1.6\ V_f) \cdot \frac{E t_1}{E_1 t}, \qquad \text{at } y = 0 \tag{5.23}$$

$$\frac{(\sigma_y)_{max}\, t_1}{P} = (1.4 - 1.675\ V_f) \cdot \frac{E t_1}{E_1 t} \qquad \text{at } y = \pm \frac{t}{2} \tag{5.24}$$

$$\frac{(\sigma_x)_{max}\, t_1}{P} = (0.7 - 0.8\ V_f) \cdot \frac{E t_1}{E_1 t}, \qquad \text{at } y = 0 \tag{5.25}$$

$$\frac{(\sigma_x)_{max}\, t_1}{P} = (0.85 - 0.95\ V_f)\ \frac{E t_1}{E_1 t}, \qquad \text{at } y = \pm \frac{t}{2} \tag{5.26}$$

$$\frac{\sigma_{max}\, t_1}{P} = (2.0 - 2.2\ V_f)\ \frac{E t_1}{E_1 t}, \qquad \text{at } y = \pm \frac{t}{2} \tag{5.27}$$

Since V_f is a linear function of the overlap length, a (Eq. 5.1), it can be concluded that the normal stresses are also linear functions of the overlap length.

5.4.3 Effect of V_f: It has been observed that V_f is an important factor controlling the stress concentrations. It would therefore, be of interest to look at the stress distributions along the overlap length for different values of V_f. Fig. 55 shows the shear stress distribution at the interfacial plane for three values of V_f. The maximum shear stress occurs at the leading corner and is in the positive direction for $V_f = 0$, and in the negative direction for $V_f = 2$. At $V_f = 1$, the shear stress at the interfacial plane is nearly uniform. Figs. 56 and 57 show the distribution of σ_y and σ_x. Again for $V_f = 0$ and 2, the maximum stress occurs at the leading corner and is positive for $V_f = 0$, and negative for $V_f = 2$. At $V_f = 1$, the normal stresses are nearly uniform over much of the overlap length except near the leading corner, where a negative maximum occurs.

5.4.4 Design of Lap Joint: The importance of the factors S_f and V_f in relation to the stresses in the adhesive layer, has been demonstrated. The stresses are greatly reduced as the factor V_f is brought closer to 1. This fact can be usefully employed in designing lap joints. In practice, lap joints are used to fasten two sheets subjected to pull. The pull can be applied at any angle θ along the length of the adherends (Fig. 58a). The equilibrium of the joint requires that the pull at the two ends be colinear. In this case the ratio V/P is given by,

$$\frac{V}{P} = \tan\theta = \frac{(t_1 + t)}{\ell} \qquad (5.28)$$

ℓ is the length defined in Fig. 58a. The minimum value of ℓ that can be used, is equal to the overlap length, a. The maximum value of the ratio V/P therefore, in this case is given by,

$$\frac{V}{P} = \frac{(t_1 + t)}{a} \tag{5.29}$$

Further, if t/t_1 is small then the maximum value is,

$$\frac{V}{P} = \frac{t_1}{a} \tag{5.30}$$

Eq. (3.111) gives the required value of the ratio V/P for uniform distribution of stress as,

$$\frac{V}{P} = \frac{4}{3} \cdot \frac{t_1}{a}$$

Thus the maximum value of V/P obtainable by means of simple bending of adherends, is less than that required for uniform shear stress distribution. In other words, the factor V_f for the joint shown in Fig. 58a, is less than 1. The value of this factor V_f is approximately 0.75 for $\ell = a$. This value is fairly close to 1, and the stress curves show that this design provides an excellent improvement over the conventional straight adherend design. It is, however, possible to further improve the design by applying the pull at angle to the adherend (Fig. 58b) and requiring that the condition for $V_f = 1$ be satisfied.

5.5 Case of Pure Moment

A lap joint is under pure moment when $P = 0$, $V = 0$, and $M_1 = M_2$. In Figs. 59, 60, and 61 are shown the stresses in a joint subjected to pure moment. The stresses were determined for $m = 2$. The peak stresses are found to occur at the two ends of the joint. The highest stress occurs at the leading corner, as would indeed be expected. The stresses are positive at that end of the joint where the moment produces tensile stresses in the adherend at the interfacial plane. The peak stresses are negative at the other end.

5.6 Non-Identical Adherends

The case of identical adherends has been discussed in detail. The performance of the non-identical adherend joint will now, be compared with that of the identical adherend joint. The two adherends in a joint, can differ in their material properties as well as in their thicknesses. Theoretical results were obtained for a case where t_2 and E_2 were varied while holding t_1 and E_1 constant. The case of $t_2 = t_1$ and $E_2 = E_1$ provided the identical adherend joint as the base for comparison. The ratios t_2/t_1 and E_2/E_1 were increased from their initial value of 1. The stress at the leading corner of adherend (I), which is also the highest stress in the joint, was obtained.* This stress is presented in Figs. 62 through 67, as a multiple of the stress for the base joint. The results are shown for two different loading conditions, (i) $V = 0$, and (ii) $M_1 = M_2 = 0$. It was found, in both cases, that for $E_2/E_1 = 1$, 10, and 100, the results were almost identical indicating that the factor E_2/E_1 has no appreciable effect on the maximum stress in the joint. The factor t_2/t_1 however, has a marked effect on the maximum stress, which increases as t_2/t_1 increases. The ratio of this increase is much greater in the case where $V = 0$, as compared to the case where $M_1 = M_2 = 0$. The moments M_1 and M_2 when $V = 0$, are given by,

$$M_1 = -M_2 = \frac{P}{2}\left(\frac{t_1}{2} + \frac{t_2}{2} + t\right) \qquad (5.30)$$

Thus M_1 is proportional to t_2, which explains the rapid increase in stresses as t_2 increases. This also indicates that the increase in M_1, rather than the increase in stiffness of the adherend (II), is responsible for the increase in stresses. One important

---

* For $t_2/t_1 \leq 1$, and $E_2/E_1 \leq 1$, the maximum stress would occur at the adherend (II) interface at its leading corner.

conclusion from these results, is that the joint with identical adherends is the most efficient joint and that any difference in the thicknesses of the two joints tends to increase the maximum stress.

6. SUMMARY AND CONCLUSIONS

An elastic analysis of the lap joint has been presented. The two adherends are allowed to differ in their thicknesses and mechanical properties. The joint is subjected to a general loading, consisting of tension, shear force and bending moments. The stresses in the adhesive layer are determined treating the problem as one of plane strain. The analysis is therefore, applicable to joints with large widths. The main limitation of the theory is that it requires the adhesive material to be isotropic and linearly elastic.

In order to check the analytical results, and to establish confidence in the theory, two specimens of lap joint of varying overlap lengths were made and tested photoelastically. Excellent agreement was found between the theoretical and the experimental results, thus establishing validity of the theory.

The case of a joint with identical adherends and subjected to antisymmetric loading, was analytically studied in detail. The following conclusions can be drawn for this joint.

(1) The maximum shear stress and the maximum normal stresses are approximately linear functions of two parameters, S_f and V_f. Simplified formulas giving the maximum stresses as functions of S_f and V_f are obtained.

(2) The maximum normal stresses are linearly dependent on the overlap length.

(3) A nearly uniform distribution of the shear stress can be obtained for $V_f = 1$. The normal stresses, although not uniformly distributed, are minimized in this case. Thus $V_f = 1$ provides the most efficient joint.

(4) Design of the lap joint based on the above results, has been discussed and recommendations made.

The analytical results for a joint with identical adherends, and subjected to pure moment, show high stress concentrations at the two leading corners. The adherend that is subjected to an anticlockwise bending moment has at its leading corner, high positive stresses. The stresses at the other leading corner are negative.

Following conclusions can be drawn from the analysis of joints with non-identical adherends,

(1) The difference between the modulii of elasticity of the two adherends, has no appreciable effect on the maximum stress in the joint.

(2) An increase in the thickness of one adherend as compared to that of the other, results in an increase in the maximum stress.

(3) Considering variation in the adherends, the joint with identical adherends is the most efficient.

REFERENCES

1. Volkersen, O., "Die Nietkraftverteilung in zugbeanspruchten Nietverbindungen mit konstanten Laschenquerschnitten," Luftfahrtforschung, Vol. 15, 1938, pp. 41-47.

2. Goland, M., and Reissner, E., "The Stresses in Cemented Joints," Journal of Applied Mechanics, Vol. 11, No. 1, March 1944, pp. A-17-27.

3. Plantema, F. J., De Schuifspanning in eme lijmnaad, Report M1181, Nat Luchtvaartlaboratorium, Amsterdam, 1949.

4. Kelsey, S., and Benson, N. K., Institut für Statik und Dynamik, Technische Hochschule, Stuttgart, ISD Report No. 10, 1966.

5. Mylonas, C., and de Bruyne, N. A., "Static Problems," Adhesion and Adhesives, Ed. de Bruyne, N. A., and Houwink, R., Elsevier, Amsterdam, 1951.

6. Greenwood, L., "The Strength of a Lap Joint," Aspects of Adhesion, Ed. Alner, D. J., Vol. 5, University of London Press Ltd., London, 1969, p. 40.

7. Mylonas, C., "Experiments on Composite Models with Application to Cemented Joints," Proc. Soc. Exp. Stress Analysis, Vol. 12, No. 2, 1955, pp. 129-142.

8. Tuzi, I., and Shimada, H., "Photoelastic Investigation of the Stresses in Cemented Joints," Bulletin of JSME, Vol. 7., No. 26, 1964, pp. 263-267.

9. Benson, N. K., "Influence of Stress Distribution on the Strength of Bonded Joints," Adhesion-Fundamentals and Practice, Ministry of Technology, Maclaren, London, 1969, pp. 191-205.

10. Cornell, R. W., "Determination of Stresses in Cemented Lap Joints," Journal of Applied Mechanics, Vol. 20, No. 1, March 1953, pp. 355-364.

11. Erdogan, F., and Ratwani, M., "Stress Distribution in Bonded Joints," Journal of Composite Materials, Vol. 5, July 1971, pp. 378-393.

12. Zienkiewicz, O. C., The Finite Element Method in Structural and Continuum Mechanics, McGraw-Hill Publishing Co. Ltd., Gt. Britain, 1967.

13. Wooley, G. R., and Carver, D. R., "Stress Concentration Factors for Bonded Lap Joints," J. Aircraft, Vol. 8, No. 10, Oct. 1971, pp. 817-820.

14. Harrison, N. L., and Harrison, W. J., "The Stresses in an Adhesive Layer," J. Adhesion, Vol. 3, No. 3, Jan. 1972, pp. 195-212.

15. McLaren, A. S., MacInnes, I., "The Influence on the Stress Distribution in an Adhesive Lap Joint of Bending of the Adherend Sheets," British Journal of Applied Mechanics, Vol. 9, Feb. 1958, pp. 72-77.

16. Durelli, A.J., and Riley, W.F., Introduction to Photomechanics, Prentice-Hall Inc., N.J., 1965, pp. 88-92.

17. Leven, M.M., "Epoxy Resins for Photoelastic Use," Photoelasticity, Ed. Frocht, M.M., Pergamon Press Inc., New York, 1963, p. 164.

APPENDIX A

SOLUTION OF DIFFERENTIAL EQUATIONS IN THE GENERAL CASE

Equations (3.51) through (3.54) are linear, homogeneous, ordinary differential equations. The boundary conditions are partly at one end and partly at the other. The problem can be transformed into an initial value problem by using linear conversion. The equations are, at first, reduced to first order differential equations by the following substitution.

$$\left.\begin{aligned} w_i &= u_i \\ w_{i_1} &= u_i' \\ w_{i_2} &= u_i'' \\ w_{j_3} &= v_j \\ w_{j_4} &= v_j' \\ w_{j_5} &= v_j'' \\ w_{j_6} &= v_j''' \end{aligned}\right\} \qquad (A.1)$$

where,

$$i = 0, 1, 2, \ldots\ldots, m$$

$$j = 0, 1, 2, \ldots\ldots, n$$

$$i_1 = i + (m+1)$$

$$i_2 = i + 2(m+1)$$

$$j_3 = j + 3(m+1)$$

$$j_4 = j + 3(m + 1) + (n + 1)$$

$$j_5 = j + 3(m + 1) + 2(n + 1)$$

$$j_6 = j + 3(m + 1) + 3(n + 1)$$

Equations (3.51) and (3.52) reduce to $(m + 1)$ algebraic equations, given by,

$$- \sum_{i=0}^{m} b_{10}(i, k)\, w_i + \sum_{i=0}^{m} b_{12}(i, k)\, w_{i_2} - \sum_{j=0}^{n} b_{14}(j, k)\, w_{j_4}$$

$$+ \sum_{j=0}^{n} b_{16}(j, k)\, w_{j_6} = 0 \qquad \text{for } k = 0, 1, 2, \ldots\ldots m \qquad \text{(A 2)}$$

where,

$$b_{10}(i, 0) = 0, \qquad i = 0, 1, 2, \ldots\ldots, m$$

$$b_{10}(0, k) = 0, \qquad k = 0, 1, 2, \ldots\ldots, m$$

$$b_{10}(i, k) = -Gik \left(-\frac{t}{2}\right)^{i + k - 1} \delta_{ik}, \qquad i = 1, 2, \ldots., m \quad k = 1, 2, \ldots., m$$

$$b_{12}(i, 0) = \left(\frac{t}{2}\right)^{i} \left[\frac{Q_i}{2} a_{io} + Q_1 t_1 + Q_2 t_2 (-1)^{i} \right] \qquad i = 0, 1, 2, \ldots., m$$

$$b_{12}(i, k) = -\left(\frac{t}{2}\right)^{i + k} \left[-\frac{Q_i}{2} a_{ik} + Q_1 t_1 + Q_2 t_2 (-1)^{i + k} \right]$$

$$i = 0, 1, 2, \ldots., m; \quad k = 1, 2, \ldots., m$$

$$b_{14}(0, 0) = 0$$

$$b_{14}(j, 0) = -\lambda_j \left(\frac{t}{2}\right)^{j} \beta_{j0}, \qquad j = 1, 2, \ldots., n$$

$$b_{14}(0, k) = -Gk\left(\frac{t}{2}\right)^{k} \beta_{ok}, \qquad k = 1, 2, \ldots, m$$

$$b_{14}(j, k) = (\lambda j - Gk)\left(\frac{t}{2}\right)^{j+k} \beta_{jk}, \qquad j = 1, 2, \ldots, n \quad k = 1, 2, \ldots, m$$

$$b_{16}(j, 0) = \tfrac{1}{2}\left(\frac{\tau}{2}\right)^{j} \left[-Q_1 t_1^{2} + (-1)^{j} Q_2 t_2^{2}\right], \qquad j = 0, 1, 2, \ldots, n$$

$$b_{16}(j, k) = \tfrac{1}{2}\left(\frac{\tau}{2}\right)^{j+k} \left[Q_1 t_1^{2} - (-1)^{j+k} Q_2 t_2^{2}\right], \qquad j = 0, 1, 2, \ldots, n \quad k = 1, 2, \ldots, m$$

Equations (3.53) and (3.54) are reduced to $(n+1)$ first order differential equations, given by,

$$\sum_{i=0}^{m} b_{22}(i, k)\, w_{i_2}' + \sum_{j=0}^{n} b_{26}(j, k)\, w_{j_6}' = \sum_{i=0}^{m} b_{21}(i, k)\, w_{i_1}$$

$$+ \sum_{j=0}^{n} b_{23}(j, k)\, w_{j_3} + \sum_{j=0}^{n} b_{25}(j, k)\, w_{j_5} = 0, \qquad k = 0, 1, 2, \ldots, n \qquad (A.3)$$

where,

$$b_{21}(0, 0) = G$$

$$b_{21}(i, 0) = G_1\left(\frac{t}{2}\right)^{i} \beta_{io}, \qquad i = 1, 2, \ldots, m$$

$$b_{21}(i, k) = (G_1 - \lambda k)\left(\frac{t}{2}\right)^{i+k} \beta_{ik}, \qquad i = 0, 1, 2, \ldots, m \quad k = 1, 2, \ldots, n$$

$$b_{22}(i, 0) = \tfrac{1}{2}\left(\frac{t}{2}\right)^{i} \left[Q_1 t_1^{2} - (-1)^{i} Q_2 t_2^{2}\right], \qquad i = 0, 1, 2, \ldots$$

$$b_{22}(i, k) = \tfrac{1}{2}\left(\frac{t}{2}\right)^{i+k}\left[-Q_1 t_1^{\,2} + (-1)^{i+k} Q_2 t_2^{\,2}\right] \quad \begin{matrix} i = 0, 1, 2, \ldots, m \\ k = 1, 2, \ldots, n \end{matrix}$$

$$b_{23}(0, k) = 0, \qquad k = 0, 1, 2, \ldots, n$$

$$b_{23}(j, 0) = 0, \qquad j = 0, 1, 2, \ldots, n$$

$$b_{23}(j, k) = -Q_{jk}\left(\frac{t}{2}\right)^{j+k-1} \delta_{jk}, \qquad \begin{matrix} j = 1, 2, \ldots, n \\ k = 1, 2, \ldots, n \end{matrix}$$

$$b_{25}(j, 0) = -G\left(\frac{t}{2}\right)^{j+1} \alpha_{jo}, \qquad j = 0, 1, 2, \ldots, n$$

$$b_{25}(j, k) = G\left(\frac{t}{2}\right)^{j+k+1} \alpha_{jk} \qquad j = 0, 1, 2, \ldots, n; \quad k = 1, 2, \ldots, n$$

$$b_{26}(j, 0) = -\frac{1}{3}\left(\frac{t}{2}\right)^{j}\left[Q_1 t_1^{\,3} + (-1)^{j} Q_2 t_2^{\,3}\right], \qquad j = 0, 1, 2, \ldots, n$$

$$b_{26}(j, k) = \frac{1}{3}\left(\frac{t}{2}\right)^{j+k}\left[Q_1 t_1^{\,3} + (-1)^{j+k} Q_2 t_2^{\,3}\right] \quad \begin{matrix} j = 0, 1, 2, \ldots, n \\ k = 1, 2, \ldots, n \end{matrix}$$

Equations (A.2) can be differentiated once to give additional $(m + 1)$ first order differential equations as follows.

$$\sum_{i=0}^{m} b_{12}(i, k)\, w_{i_2}' + \sum_{j=0}^{n} b_{16}(j, k)\, w_{j_6}' = \sum_{i=0}^{m} b_{10}(i, k)\, w_{i_1}$$

$$+ \sum_{j=0}^{n} b_{14}(j, k)\, w_{j_5} \qquad \text{for } k = 0, 1, 2, \ldots, m \tag{A.4}$$

Equations (A.3) and (A.4) can be treated as simultaneous equations in w_{i_2} and

w_{j_6}' and can be solved as such, to obtain the following system of equations.

$$w_{i_2}' = f_{i_2}(w_0, w_1, \ldots\ldots, w_q) \tag{A.5}$$

and

$$w_{j_6}' = f_{j_6}(w_0, w_1, \ldots\ldots, w_q) \tag{A.6}$$

where, $q = 3m + 4n + 6$

Also, equations (A.1) can be written in the form,

$$\left.\begin{aligned}
w_i' = w_{i_1} &= f_i(w_0, w_1, \ldots\ldots, w_q) \\
w_{i_1}' = w_{i_2} &= f_{i_1}(w_0, w_1, \ldots\ldots, w_q) \\
w_{j_3}' = w_{j_4} &= f_{j_3}(w_0, w_1, \ldots\ldots, w_q) \\
w_{j_4}' = w_{j_5} &= f_{j_4}(w_0, w_1, \ldots\ldots, w_q) \\
w_{j_5}' = w_{j_6} &= f_{j_5}(w_0, w_1, \ldots\ldots, w_q)
\end{aligned}\right\} \tag{A.7}$$

Now, the method of linear conversion can be applied to obtain $w_i(0)$, for $i = 0, 1, 2, \ldots\ldots q$. The following equations are used.

$$w_i(a) = \sum_{j=0}^{q} a_{ij} w_j(0) + p_i, \qquad i = 0, 1, 2, \ldots\ldots, q \tag{A.8}$$

In order to determine the constants a_{ij} and p_i, the following steps are followed.

(1) Set $w_o(0) = w_1(0) = w_2(0) = \ldots\ldots = w_q(0) = 0$ and integrate equations (A.5), (A.6), and (A.7) using Runge-Kutta fourth order formula. This gives,

$$p_i = w_i(a), \qquad i = 0, 1, 2, \ldots\ldots, q$$

In this case all the p_i are zero.

(2) Set $w_o(0) = 1$, $w_1(0) = w_2(0) = \ldots\ldots = w_q(0) = 0$ and integrate equations (A.5), (A.6), and (A.7). This yields,

$$a_{i1} = w_i(a) - p_i = w_i(a), \qquad i = 0, 1, 2, \ldots\ldots, q.$$

This step is repeated for $w_1(0) = 1$ and all other zero, etc., until all a_{ij} are determined.

(3) $(4n + 2m + 6)$ boundary conditions are known. Equations (A.2) supply another $(m + 1)$ boundary conditions, so that a total of $(q + 1)$ boundary conditions are known. Equations (A.8) provide an additional set of $(q + 1)$ equations. These $(2q + 2)$ equations can be solved for $(2q + 2)$ initial and final conditions.

(4) Using the initial conditions from step 3, integrate equations (A.5), (A.6), and (A.7) a final time to get the answers. As a check, $w_i(a)$ obtained via this integration must agree with those obtained previously in step 3.

The Runge-Kutta fourth order formula to be used for integration, can be stated as follows.

$$w_i(x + h) = w_i(x) + \frac{1}{6}(a_i + 2b_i + 2c_i + d_i)$$

where,

h = step size

$$a_i = hf_i\left[w_0(x), w_i(x), w_2(x), \ldots\ldots, w_q(x)\right]$$

$$b_i = hf_i \quad w_o(x) + \frac{a_o}{2}, \left[w_i(x) + \frac{a_1}{2}, \ldots\ldots, w_q(x) + \frac{a_q}{2} \right]$$

$$c_i = hf_i \quad \left[w_o(x) + \frac{b_o}{2}, \; w_1(x) + \frac{b_1}{2}, \ldots\ldots\ldots, w_q(x) + \frac{b_q}{2} \right]$$

$$d_i = hf_i \quad \left[w_o(x) + c_o, \; w_1(x) + c_1, \ldots\ldots\ldots, w_q(x) + c_q \right]$$

The computer program using the above method for solving the differential equations, is given in Appendix B.

APPENDIX B

FORTRAN PROGRAM BASED ON IBM SYSTEM 360/75 FOR THE GENERAL CASE

Notation:

E,E1,E2 =	E, E_1, E_2 respectively
D,D1,D2 =	G, G_1, G_2 respectively
B,B1,B2 =	Q/2, $Q_1/2$, $Q_2/2$ respectively
T,T1,T2 =	t, t_1, t_2 respectively
A =	Overlap length, a
P,V,C1,C2 =	P, V, M_i, M_2 respectively
M =	m + 1
N =	n + 1
MM =	Number of data points along x-axis, (M M-1). $\Delta x = a$
NN =	Number of data points along y-axis, (NN-1). $\Delta y = t$
L=	Integer denoting number of divisions of Δx for integration
H =	Step size for integration
L*H*(MM-1.0) =	A, i.e. $L \cdot H = \Delta x$
SIGMAX =	σ_x
SIGMAY =	σ_y
TAUXY =	τ_{xy}
TAUMAX =	τ_{max}

```
C      THE PURPOSE OF THIS PROGRAM IS TO DETERMINE STRESSES IN THE
C      ADHESIVE LAYER OF A LAP JOINT OF GIVEN GEOMETRY AND LOADING.
C
C      INPUT = E,E1,E2,D,D1,D2,B,B1,B2,T,T1,T2,P,V,C1,A,H,M,N,MM,NN,L
C
C      OUTPUT = SIGMAX, SIGMAY, TAUXY, TAUMAX
```

```
C
      IMPLICIT REAL*8(A-H,O-Z)
      DIMENSION F(NW2,NW2),G(NW2),B10(M,M),B12(M,M),AA(MN,MN),W(NW,MM)
     1,B14(N,M),B16(N,M),B22(M,N),B26NN,N),B21(M,N),B23(N,N),B25(N,N),
     2AU2(M,M),AV1(N,M),AV3(N,M),CV1(N,N),CUO(M,N),DU1(M,N),DV2(N,N)
     3AX(NW),BX(NW),CX(NW),DX(NW),GX(NW2,1)
     4GG(MN,MN2),ALFA(MN,MN),BETA(MN,MN),DELT(MN,MN),SIGMAX(MM,NN)
     5,SIGMAY(MM,NN),TAUXY(MM,NN),TAUMAX(MM,NN)
      MN=M+N
      MN2=M+2*N
      NW=3*M+4*N
      NW2=2*NW
      C2=C1+V*A-P*(T1/2.0+T2/2.0+T)
      BB=2.0*(B-D)
C     DETERMINE THE COEFFICIENTS FOR THE BOUNDARY CONDITIONS AND
C     THE DIFFERENTIAL EQUATIONS
      B21(1,1)=0.0
      DO 6 I=1,M
      DO 2 J=1,M
      AU2(I,J)=2.0*(T/2.0)**(I+J-2)*(B*T/2.0*(1.0+(-1.0)**(I+J-2))/
     1(I+J-1.0)+B1*T1+B2*T2*(-1.0)**(I+J-2))
    2 CONTINUE
      DO 3 J=1,N
      AV3(J,I)=(T/2.0)**(I+J-2)*(-B1*T1**2+(-1.0)**(I+J-2)*B2*T2**2)
      DU1(I,J)=(T/2.0)**(I+J-2)*(-B1*T1**2+(-1.0)**(I+J-2)*B2*T2**2)
    3 CONTINUE
      AV1(1,I)=0.0
      B22(I,1)=-DU1(I,1)
      DO 4 J=2,N
      BETA(I,J)=(1.0-(-1.0)**(I+J-2))/(I+J-2.0)
      AV1(J,I)=BB*(J-1.0)*(T/2.0)**(I+J-2)*BETA(I,J)
      B22(I,J)=DU1(I,J)
    4 CONTINUE
      B10(I,1)=0.0
      B10(1,I)=0.0
      B12(I,1)=AU2(I,1)
      DO 5 J=2,M
      B12(I,J)=-AU2(I,J)
    5 CONTINUE
    6 CONTINUE
      DO 10 I=2,M
      DO 7 J=2,M
      DELT(I,J)=(1.0-(-1.0)**(I+J-3))/(I+J-3.0)
      B10(I,J)=-D*(I-1.0)*(J-1.0)*(T/2.0)**(I+J-3)*DELT(I,J)
    7 CONTINUE
      B14(1,I)=-D*(T/2.0)**(I-1)*(1.0-(-1.0)**(I-1))
      DO 8 J=1,N
      BETA(I,J)=(1.0-(-1.0)**(I+J-2))/(I+J-2.0)
      CUO(I,J)=D*(I-1.0)*(T/2.0)**(I+J-2)*BETA(I,J)
      B16(J,I)=-AV3(J,I)
    8 CONTINUE
      B21(I,1)=-CUO(I,1)
      DO 9 J=2,N
      B21(I,J)=CUO(I,J)-AV1(J,I)
      B21(1,J)=-AV1(J,1)
```

```
      B14(J,I)=-B21(I,J)
    9 CONTINUE
   10 CONTINUE
      DO 13 I=1,N
      CU0(1,I)=0.0
      B16(I,1)=AV3(I,1)
      B23(1,I)=0.0
      B23(I,1)=0.0
      B14(I,1)=-AV1(I,1)
      DO 11 J=1,N
      ALFA(I,J)=(1.0-(-1.0)**(I+J-1))/(I+J-1.0)
      CV1(I,J)=(T/2.0)**(I+J-1)*D*ALFA(I,J)
      DV2(I,J)=2.0*(T/2.0)**(I+J-2)*(B1*T1**3/3.0+B2*T2**3*(-1.0)
     1**(I+J-2)/3.0)
   11 CONTINUE
      B26(I,1)=-DV2(I,1)
      B25(I,1)=-CV1(I,1)
      DO 12 J=2,N
      B26(I,J)=DV2(I,J)
      B25(I,J)=CV1(I,J)
   12 CONTINUE
   13 CONTINUE
      DO 15 I=2,N
      DO 14 J=2,N
      DELT(I,J)=(1.0-(-1.0)**(I+J-3))/(I+J-3.0)
      B23(I,J)=-2.0*B*(I-1.0)*(J-1.0)*(T/2.0)**(I+J-3)*DELT(I,J)
   14 CONTINUE
   15 CONTINUE
C     SOLVE SIMULTANEOUS EQUATIONS (A.3) AND (A.4) OF APPENDIX A
C     AA ARE THE COEFFICIENTS ON THE LHS AND GG ON THE RHS
      DO 29 I=1,M
      DO 27 J=1,M
      AA(J,I)=B12(I,J)
      GG(J,I)=B10(I,J)
   27 CONTINUE
      DO 28 J=1,N
      J1=J+M
      J2=J1+N
      AA(J1,I)=B22(I,J)
      GG(J1,I)=B21(I,J)
      AA(I,J1)=B16(J,I)
      GG(I,J1)=0.0
      GG(I,J2)=B14(J,I)
   28 CONTINUE
   29 CONTINUE
      DO 31 I=1,N
      DO 30 J=1,N
      I1=I+M
      J1=J+M
      I2=I1+N
      AA(J1,I1)=B26(I,J)
      GG(J1,I1)=B23(I,J)
      GG(J1,I2)=B25(I,J)
   30 CONTINUE
   31 CONTINUE
```

```
      CALL SIMEQ (AA,GG,MN,MN2,KO)
      IF(KO.EQ.1) GO TO 3000
C     NOW USE LINEAR CONVERSION
C     F AND G ARE THE COEFFICIENTS ON LHS AND RHS RESPECTIVELY
C     FIRST SET ALL F AND G TO ZERO
      DO 26 J=1,NW2
      DO 25 I=1,NW2
      F(I,J)=0.0
   25 CONTINUE
      G(J)=0.0
   26 CONTINUE
C     NOW DETERMINE F AND G THAT ARE NOT ZERO
      DO 50 J=1,NW
      DO 35 I=1,NW
      W(I,1)=0.0
   35 CONTINUE
      W(J,1)=1.0
C     INTEGRATE EQUATIONS (A.5),(A.6),(A.7)
      CALL INTEG (GG,W,H,M,N,MM,NW,AX,BX,CX,DX,L)
      DO 40 I=1,NW
      F(I,J)=W(I,MM)
   40 CONTINUE
      JW=J+NW
      F(J,JW)=-1.0
   50 CONTINUE
C     USE EQUATIONS (A.2)
      DO 80 J=1,M
      JW=J+NW
      DO 60 I=1,M
      I2=I+2*M
      F(JW,I)=-B10(I,J)
      F(JW,I2)=B12(I,J)
   60 CONTINUE
      DO 70 I=1,N
      I4=I+3*M+N
      I6=I4+2*N
      F(JW,I4)=-B14(I,J)
      F(JW,I6)=B16(I,J)
   70 CONTINUE
   80 CONTINUE
C     NOW USE THE BOUNDARY CONDITIONS
      DO 400 I=1,M
      I1=I+M
      I2=I1+M
      I7=I+NW
      I8=I1+NW
      I9=I2+NW
      DO 90 J=2,M
      JW1=J+NW+M
      F(JW1,I1)=AU2(I,J)
      G(JW1)=P*(-T/2.0)**(J-1)
   90 CONTINUE
      DO 100 J=1,M
      JW2=J+NW+2*M
      F(JW2,I8)=AU2(I,J)
```

```
      G(JW2)=P*(T/2.0)**(J-1)
  100 CONTINUE
      DO 200 J=2,N
      JW3=J+NW+3*M
      JW4=JW3+N
      F(JW3,I)=CU0(I,J)
      F(JW3,I2)=-DU1(I,J)
      G(JW3)=V*(-T/2.0)**(J-1)
      F(JW4,I1)=DU1(I,J)
      G(JW4)=(-T/2.0)**(J-1)*(P*T2/2.0+C2)
  200 CONTINUE
      DO 300 J=1,N
      JW5=J+NW+2*N+3*M
      JW6=JW5+N
      F(JW5,I7)=CU0(I,J)
      F(JW5,I9)=-DU1(I,J)
      G(JW5)=V*(T/2.0)**(J-1)
      F(JW6,I8)=DU1(I,J)
      G(JW6)=-(T/2.0)**(J-1)*(P*T1/2.0-C1)
  300 CONTINUE
  400 CONTINUE
      DO 900 I=1,N
      I3=I+3*M
      I4=I3+N
      I5=I4+N
      I6=I5+N
      I10=I3+NW
      I11=I4+NW
      I12=I5+NW
      I13=I6+NW
      DO 500 J=2,M
      JW1=J+NW+M
      F(JW1,I3)=AV1(I,J)
      F(JW1,I5)=AV3(I,J)
  500 CONTINUE
      DO 600 J=1,M
      JW2= J+NW+2*M
      F(JW2,I10)=AV1(I,J)
      F(JW2,I12)=AV3(I,J)
  600 CONTINUE
      DO 700 J=2,N
      JW3=J+NW+3*M
      JW4=JW3+N
      F(JW3,I4)=CV1(I,J)
      F(JW3,I6)=-DV2(I,J)
      F(JW4,I5)=DV2(I,J)
  700 CONTINUE
      DO 800 J=1,N
      JW5=J+NW+2*N+3*M
      JW6=JW5+N
      F(JW5,I11)=CV1(I,J)
      F(JW5,I13)=-DV2(I,J)
      F(JW6,I12)=DV2(I,J)
  800 CONTINUE
  900 CONTINUE
```

```
      J0=NW+M+1
      J10=J0+2*M
      J20=J10+N
      I30=3*M+1
      I40=I30+N
      F(J0,1)=1.0
      F(J10,I30)=1.0
      F(J20,I40)=1.0
      DO 950 I=1,NW2
      GX(I,1)=G(I)
  950 CONTINUE
C     SOLVE FOR INITIAL AND FINAL VALUES OF W
      CALL SIMEQ (F,GX,NW2,1,KO)
      IF(KO.EQ.1) GO TO 3000
      DO 1000 I=1,NW
      W(I,1)=GX(I,1)
 1000 CONTINUE
C     FINAL INTEGRATION
      CALL INTEG (GG,W,H,M,N,MM,NW,AX,BX,CX,DX,L)
C     INTEGRATION DESTROYS W(I,1), RESTORE W(I,1)
      DO 1020 I=1,NW
      W(I,1)=GX(I,1)
C     CHECK IF THE INTEGRATION IS ACCURATE
      IW=I+NW
 1020 AX(I)=1.0-W(I,MM)/GX(IW,1)
C     AX SHOULD ME MUCH LESS THAN 1
C     IF THE ABOVE CHECK IS UNSUCCESSFUL, THE STEP SIZE H NEEDS
C     TO BE DECREASED
C     DETERMINE STRAINS AND STRESSES
      DO 1500 J=1,NN
      Y=T*(J-1.0)/(NN-1.0)-T/2.0
      DO 1400 I =1,MM
      EX=W((M+1),I)+Y*W((M+2),I)
      EY=W((3*M+2),I)
      EXY=W(2,I)+W((3*M+N+1),I)+Y*W((3*M+N+2),I)
      IF(M.LT.3) GO TO 1210
      DO 1200 II=3,M
      III=II+M
      EX=EX+Y**(II-1)*W(III,I)
      EXY=EXY+(II-1.0)*Y**(II-2)*W(II,I)
 1200 CONTINUE
 1210 IF(N.LT.3) GO TO 1310
      DO 1300 JJ=3,N
      JJ3=3*M+JJ
      JJ4=3*M+N+JJ
      EY=EY+(JJ-1.0)*Y**(JJ-2)*W(JJ3,I)
      EXY=EXY+Y**(JJ-1)*W(JJ4,I)
 1300 CONTINUE
 1310 SX=2.0*B*EX+BB*EY
      SY=2.0*B*EY+BB*EX
      SXY=D*EXY
      SHEAR=DSQRT((SX-SY)**2/4.0+SXY**2)
      SIGMAX(I,J)=SX
      SIGMAY(I,J)=SY
      TAUXY(I,J)=SXY
```

```
      TAUMAX(I,J)=SHEAR
 1400 CONTINUE
 1500 CONTINUE
 3000 STOP
      END

      SUBROUTINE INTEG (GG,W,H,M,N,MM,NW,A,B,C,D,MM1)
      IMPLICIT REAL*8(A-H,O-Z)
      DIMENSION GG(MN,MN2),W(NW,MM),A(NW),B(NW),C(NW),D(NW)
      MX=1
      DO 2000 KX=2,MM
      DO 1000 MMX=1,MM1
      DO 10 I=1,NW
      C(I)=0.0
   10 CONTINUE
      K=-1
  100 K=K+1
      DO 200 I=1,M
      I1=I+M
      I2=I1+M
      D(I)=H*(W(I1,MX)+C(I1))
      D(I1)=H*(W(I2,MX)+C(I2))
      D(I2)=0.0
      DO 120 JJ=1,M
      JJ1=JJ+M
      D(I2)=D(I2)+H*GG(I,JJ)*(W(JJ1,MX)+C(JJ1))
  120 CONTINUE
      DO 150  JJ=1,N
      JJ1=JJ+M
      JJ2=JJ1+N
      JJ3=JJ+3*M
      JJ5=JJ3+2*N
      D(I2)=D(I2)+H*GG(I,JJ1)*(W(JJ3,MX)+C(JJ3))+H*GG(I,JJ2)*(W(JJ5,MX)
     1+C(JJ5))
  150 CONTINUE
  200 CONTINUE
      DO 300 I=1,N
      I1=I+M
      I3=I+3*M
      I4=I3+N
      I5=I4+N
      I6=I5+N
      D(I3)=H*(W(I4,MX)+C(I4))
      D(I4)=H*(W(I5,MX)+C(I5))
      D(I5)=H*(W(I6,MX)+C(I6))
      D(I6)=0.0
      DO 220 JJ=1,M
      JJ1=JJ+M
      D(I6)=D(I6)+H*GG(I1,JJ)*(W(JJ1,MX)+C(JJ1))
  220 CONTINUE
      DO 250 JJ=1,N
      JJ1=JJ+M
      JJ2=JJ1+N
      JJ3=JJ+3*M
      JJ5=JJ3+2*N
```

```
      D(I6)=D(I6)+H*GG(II,JJ1)*(W(JJ3,MX)+C(JJ3))+H*GG(II,JJ2)*
     1(W(JJ5,MX)+C(JJ5))
  250 CONTINUE
  300 CONTINUE
      IF(K.EQ.1) GO TO 400
      IF(K.EQ.2) GO TO 500
      IF(K.EQ.3) GO TO 600
      DO 350 I=1,NW
      A(I)=D(I)
      C(I)=D(I)/2.0
  350 CONTINUE
      GO TO 100
  400 DO 450 I=1,NW
      B(I)=D(I)
      C(I)=D(I)/2.0
  450 CONTINUE
      GO TO 100
  500 DO 550 I=1,NW
      C(I)=D(I)
  550 CONTINUE
      GO TO 100
  600 DO 700 I=1,NW
      W(I,1)=W(I,1)+(A(I)+2.0*B(I)+2.0*C(I)+D(I))/6.0
  700 CONTINUE
 1000 CONTINUE
      DO 1100 I=1,NW
 1100 W(I,KX)=W(I,1)
 2000 CONTINUE
      RETURN
      END
C
      SUBROUTINE SIMEQ (A,B,NROW,NRHS,KO)
C     THIS SUBROUTINE SOLVES SIMULTANEOUS EQUATIONS WITH REAL
C     COEFFICIENTS
      IMPLICIT REAL*8 (A-H,O-Z)
  100 FORMAT(/' SINGULAR MATRIX'/)
      DIMENSION A(NROW,NROW),B(NROW,NRHS),C(NW2),II(NW2),JJ(NW2,2
      DO 1 I=1,NROW
    1 II(I)=0
      DO 17 I=1,NROW
      D=0.DO
      DO 6 J=1,NROW
      IF(II(J)-1) 2,6,2
    2 DO 5 K=1,NROW
      IF(II(K)-1) 3,5,21
    3 IF(DABS(D)-DABS(A(J,K))) 4,4,5
    4 IR=J
      IC=K
      D=A(J,K)
    5 CONTINUE
    6 CONTINUE
      II(IC)=II(IC)+1
      IF(IR-IC) 7,10,7
    7 DO 8 J=1,NROW
      D=A(IR,J)
```

```
      A(IR,J)=A(IC,J)
    8 A(IC,J)=D
      DO 9 J=1,NRHS
      D=B(IR,J)
      B(IR,J)=B(IC,J)
    9 B(IC,J)=D
   10 JJ(I,1)=IR
      JJ(I,2)=IC
      C(I)=A(IC,IC)
      IF(C(I)) 11,21,11
   11 A(IC,IC)=1.DO
      DO 12 J=1,NROW
   12 A(IC,J)=A(IC,J)/C(I)
      DO 13 J=1,NRHS
   13 B(IC,J)=B(IC,J)/C(I)
      DO 17 J=1,NROW
      IF(J-IC) 14,17,14
   14 D=A(J,IC)
      A(J,IC)=0.DO
      DO 15 K=1,NROW
   15 A(J,K)=A(J,K)-A(IC,K)*D
      DO 16 K=1,NRHS
   16 B(J,K)=B(J,K)-B(IC,K)*D
   17 CONTINUE
      DO 20 I=1,NROW
      J=NROW+1-I
      IF(JJ(J,1)-JJ(J,2)) 18,20,18
   18 IR=JJ(J,1)
      IC=JJ(J,2)
      DO 19 J=1,NROW
      D=A(J,IR)
      A(J,IR)=A(J,IC)
   19 A(J,IC)=D
   20 CONTINUE
      KO=0
      RETURN
   21 WRITE(6,100)
      KO=1
      RETURN
      END
```

APPENDIX C

FORTRAN PROGRAM BASED ON IBM SYSTEM 360/75 FOR THE IDENTICAL ADHEREND CASE

Notation:

E,E1 = E, E_1 respectively

D,D1 = G, G_1 respectively

H,H1 = λ, λ_1 respectively

B,B1 = $Q/2$, $Q_1/2$ respectively

A = Overlap Length, a

P,V,C1,C2 = P, V, M_1, M_2 respectively

MM= Number of data points along x-axis, (MM-1) Δx = a

NN= Number of data points along y-axis, (NN-1) Δy = t

```
C     THE PURPOSE OF THIS PROGRAM IS TO DETERMINE STRESSES IN THE
C     ADHESIVE LAYER OF A LAP JOINT WITH IDENTICAL ADHERENDS
C     AND GIVEN LOADING.
C
C     INPUT = E,E1,D,D1,B,B1,T,T1,P,V,M1,A,MM,NN
C
C     OUTPUT = SIGMAX, SIGMAY, TAUXY, TAUMAX
C
      IMPLICIT REAL*8(A-E,H,O-Y), COMPLEX*16(F,G,Z)
      COMPLEX*16 CDEXP, DCMPLX, CDSQRT
      DIMENSION SIGMAX(MM,NN),SIGMAY(MM,NN),TAUXY(MM,NN),TAUMAX(MM,NN)
      DIMENSION UU12(MM),UU13(MM),VV01(MM),VV02(MM),VV03(MM),VV04(MM)
      DIMENSION UU0(MM),UU01(MM),UU02(MM),UU03(MM),UU1(MM),UU11(MM)
      DIMENSION VV1(MM),VV11(MM),VV12(MM),VV13(MM),VV14(MM)
      DIMENSION F(5,5),G(5,1)
      DIMENSION ZX(4),ZY(2),Z(11)
      C2= C1+V*A-P*(T1+T)
      BT=B*T+2.0*B1*T1
      CT=B*T/3.0+2.0*B1*T1
      AA1=B1*T1**2*T/(2.0*BT)
      AA2=-H*T/(2.0*BT)
      AA3=B1*T1**2*(4.0/3.0*T1+T)/(T*(B1*T1**2+CT*T/2.0))
      CV=T*CT*AA3-2.0*B1*T1**2
```

```
      CCC=B1*T1**3*T*(2.0*B*T+B1*T1)
      CC=-6.0*H*BT/CCC
      CC0=3.0*H*(2.0*BT-H*T)/CCC+12.0*BT*D/CCC
      CC2=6.0*H*T*B1*T1**2/CCC+D*T*T/12.0*CC/H
      CCD=B1*T1**2-CT*T/2.0*AA3
      CC1=D*(AA3+1.0)/CCD
      Q2=-D/(6.0*CCD)
      Q1=3.0*Q2
      Q0=6.0*Q2
      Q3=(CT*T/2.0)/CCD
      Z(5)=P/(2.0*BT)
      FF=-CC1
      ZZ=(CC2/2.0)**2-CC0
      DO 100 N=1,2
      ZX(N)=CDSQRT(-CC2/2.0+(-1)**N*CDSQRT(ZZ))
      ZX(N+2)=-ZX(N)
      ZY(N)=(-1)**N*CDSQRT(FF)
  100 CONTINUE
      DO 200 J=1,4
      F(1,J)=(D*T*T/6.0+2.0*AA2*B1*T1**2)*ZX(J)+2.0*B1*T1**2*(AA1-
     1T1*T/3.0)*ZX(J)**3
      F(2,J)=F(1,J)*CDEXP(ZX(J)*A)
      F(3,J)=B1*T1**2*((T1*T/3.0-AA1)*ZX(J)**2-AA2)
      F(4,J)=F(3,J)*CDEXP(ZX(J)*A)
  200 CONTINUE
      G(1,1)=-V
      G(2,1)=V
      G(3,1)=-(C2-V*A1+P*T1/2.0)/2.0+(1.0+AA2*CC/CC0)*B1*T1**2*Z(5)
      G(4,1)=(C1+V*A1)/2.0-P*T1/4.0+(1.0+AA2*CC/CC0)*B1*T1**2*Z(5)
      CALL SIMEQ (F,G,4,1,KO)
      DO 300 N=1,4
      Z(N)=G(N,1)
  300 CONTINUE
      DO 400 J=1,2
      F(1,J)=CV*ZY(J)**2
      F(2,J)=F(1,J)*CDEXP(ZY(J)*A)
      F(3,J)=(D*T*(AA3+1.0)*ZY(J)+B1*T1**2*(AA3*T-4.0/3.0*T1)*ZY(J)
     1**3)*CDEXP(ZY(J)*A)
      F(4,J)=(4.0/3.0*T1-AA3*T)*ZY(J)**2*CDEXP(ZY(J)*A)
      F(5,J)=ZY(J)
  400 CONTINUE
      F(1,3)=0.0
      F(2,3)=6.0*CV*Q2*A/CC1+CT*T*A
      F(3,3)=D*T*(AA3+1.0)/CC1*(3.0*Q2*A*A-6.0*Q2/CC1+Q3)+A*A/2.0*D*T
     1+B1*T1**2*((AA3*T-4.0/3.0*T1)*6.0*Q2/CC1+T)
      F(4,3)=A*((8.0*T1-6.0*AA3*T)/CC1*Q2-T)
      F(5,3)=(Q3-6.0*Q2/CC1)/CC1
      F(1,4)=2.0*CV*Q1/CC1+CT*T
      F(2,4)=F(1,4)
      F(3,4)=D*T*A*((AA3+1.0)*2.0*Q1/CC1+1.0)
      F(4,4)=2.0*Q1*(4.0/3.0*T1-AA3*T)/CC1-T
      F(5,4)=0.0
      F(1,5)=0.0
      F(2,5)=0.0
      F(3,5)=D*T*(1.0+Q0*(AA3+1.0)/CC1)
```

```
      F(4,5)=0.0
      F(5,5)=Q0/CC1
      G(1,1)=-P
      G(2,1)=P
      G(3,1)=V
      G(4,1)=(C1+V*A1-P*T1/2.0)/(B1*T1**2)
      G(5,1)=0.0
      CALL SIMEQ (F,G,5,1,KO)
      DO 500 N=6,10
      Z(N)=G((N-5),1)
  500 CONTINUE
      DO 800 N=1,NN
      Y=T*(N-1.0)/(NN-1.0)-T/2.0
      DO 700 M=1,MM
      X=(M-1.0)*A/(MM-1.0)
      V01=Z(6)*ZY(1)*CDEXP(ZY(1)*X)+Z(7)*ZY(2)*CDEXP(ZY(2)*X)+3.0*
     1Z(8)*X*X*Q2/CC1+(2.*Q1*Z(9)*X+Q0*Z(10)+Q3*Z(8)-6.*Q2*Z(8)/CC1
     2)/CC1
      V02=Z(6)*ZY(1)**2*CDEXP(ZY(1)*X)+Z(7)*ZY(2)**2*CDEXP(ZY(2)*X)+
     16.0*Q2/CC1*Z(8)*X+2.0*Q1/CC1*Z(9)
      V03=Z(6)*ZY(1)**3*CDEXP(ZY(1)*X)+Z(7)*ZY(2)**3*CDEXP(ZY(2)*X)+
     16.0*Q2/CC1*Z(8)
      V04=Z(6)*ZY(1)**4*CDEXP(ZY(1)*X)+Z(7)*ZY(2)**4*CDEXP(ZY(2)*X)
      VV01(M)=V01
      VV02(M)=V02
      VV03(M)=V03
      VV04(M)=V04
      U1=AA3*V01+Z(8)*X*X/2.0+Z(9)*X+Z(10)
      U11=AA3*V02+Z(8)*X+Z(9)
      UU12(M)=AA3*V03+Z(8)
      UU13(M)=AA3*V04
      UU1(M)=U1
      UU11(M)=U11
      FV1=CC*Z(5)/CC0
      FV11=0.0
      FV12=0.0
      FV13=0.0
      FV14=0.0
      DO 600 K=1,4
      FV1=FV1+Z(K)*CDEXP(ZX(K)*X)
      FV11=FV11+Z(K)*ZX(K)*CDEXP(ZX(K)*X)
      FV12=FV12+Z(K)*ZX(K)**2*CDEXP(ZX(K)*X)
      FV13=FV13+Z(K)*ZX(K)**3*CDEXP(ZX(K)*X)
      FV14=FV14+Z(K)*ZX(K)**4*CDEXP(ZX(K)*X)
  600 CONTINUE
      V1=FV1
      V11=FV11
      V12=FV12
      VV1(M)=V1
      VV11(M)=V11
      VV12(M)=V12
      VV13(M)=FV13
      VV14(M)=FV14
      U01=AA1*V12+AA2*V1+Z(5)
      UU01(M)=U01
```

```
      UU02(M)=AA1*VV13(M)+AA2*V11
      UU03(M)=AA1*VV14(M)+AA2*V12
      SX=2.0*B*(U01+Y*U11)+H*V1
      SY=H*(U01+Y*U11)+2.0*B*V1
      SXY=D*(V01+Y*V11+U1)
      SHEAR=DSQRT((SX-SY)**2/4.0+SXY**2)
      SIGMAX(M,N)=SX
      SIGMAY(M,N)=SY
      TAUXY(M,N)=SXY
      TAUMAX(M,N)=SHEAR
      STOP
      END
C
      SUBROUTINE SIMEQ (F,G,NROW,NRHS,KO)
C     THIS SUBROUTINE SOLVES SIMULTANEOUS EQUATIONS WITH COMPLEX
C     COEFFICIENTS
      IMPLICIT COMPLEX*16 (A-H,O-Z)
      REAL*8CDABS
      DIMENSION F(5,5),G(5,1),C(5),II(5),JJ(5,2)
  100 FORMAT(/' SINGULAR MATRIX'/)
      DO 1 I=1,NROW
    1 II(I)=0
      DO 17 I=1,NROW
      D=(0.D0,0.D0)
      DO 6 J=1,NROW
      IF(II(J)-1) 2,6,2
    2 DO 5 K=1,NROW
      IF(II(K)-1) 3,5,21
    3 IF(CDABS(D)-CDABS(F(J,K))) 4,4,5
    4 IR=J
      IC=K
      D=F(J,K)
    5 CONTINUE
    6 CONTINUE
      II(IC)=II(IC)+1
      IF(IR-IC) 7,10,7
    7 DO 8 J=1,NROW
      D=F(IR,J)
      F(IR,J)=F(IC,J)
    8 F(IC,J)=D
      DO 9 J=1,NRHS
      D=G(IR,J)
      G(IR,J)=G(IC,J)
    9 G(IC,J)=D
   10 JJ(I,1)=IR
      JJ(I,2)=IC
      C(I)=F(IC,IC)
      IF(CDABS(C(I))) 11,21,11
   11 F(IC,IC)=(1.D0,0.D0)
      DO 12 J=1,NROW
   12 F(IC,J)=F(IC,J)/C(I)
      DO 13 J=1,NRHS
   13 G(IC,J)=G(IC,J)/C(I)
      DO 17 J=1,NROW
      IF(J-IC) 14,17,14
```

```
14 D=F(J,IC)
   F(J,IC)=(0.D0,0.D0)
   DO 15 K=1,NROW
15 F(J,K)=F(J,K)-F(IC,K)*D
   DO 16 K=1,NRHS
16 G(J,K)=G(J,K)-G(IC,K)*D
17 CONTINUE
   DO 20 I=1,NROW
   J=NROW+1-I
   IF(JJ(J,1)-JJ(J,2)) 18,20,18
18 IR=JJ(J,1)
   IC=JJ(J,2)
   DO 19 J=1,NROW
   D=F(J,IR)
   F(J,IR)=F(J,IC)
19 F(J,IC)=D
20 CONTINUE
   KO=0
   RETURN
21 WRITE(6,100)
   KO=1
   RETURN
   END
```

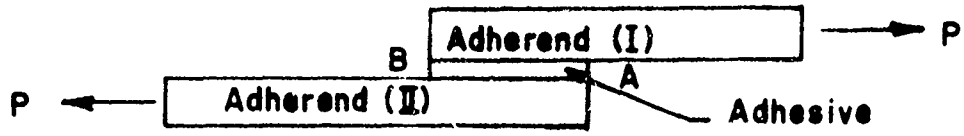

(a)

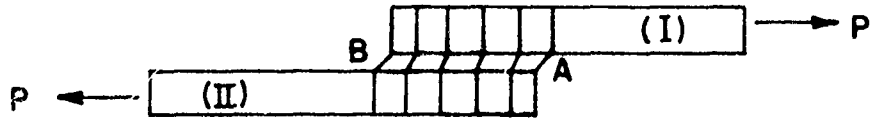

(b)

FIG. 1 Stress due to Stretching of Adherends

(a) Joint Prior to Stretching, (b) Joint after Stretching

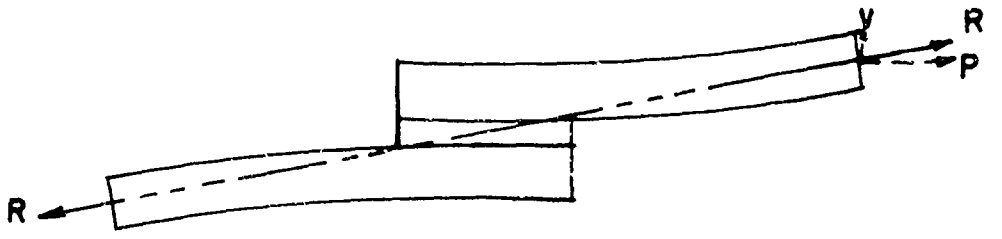

(a)

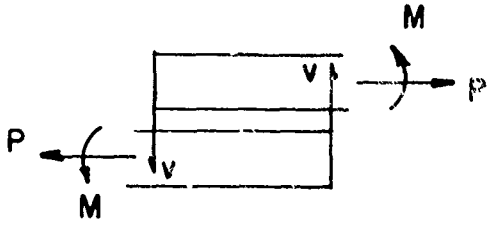

(b)

FIG.2 System Considered by Goland and Reissner

(a) Forces Acting on Adherends, (b) Forces at Joint Edges

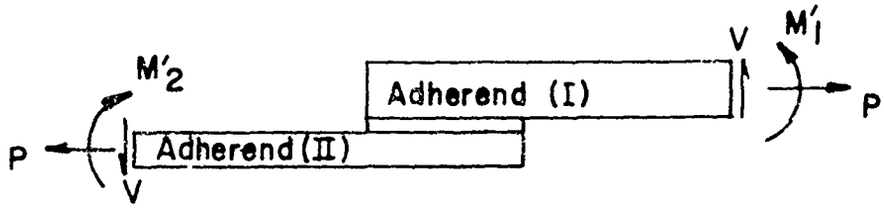

(a)

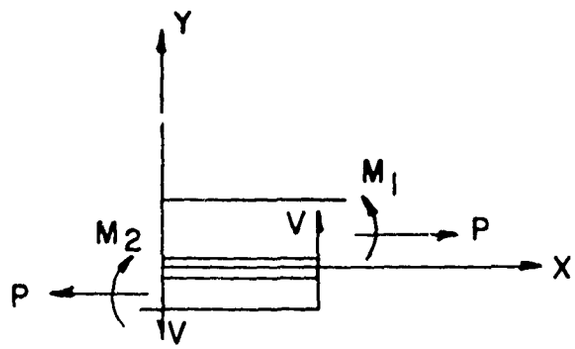

(b)

FIG. 3 Lap Joint Under a General loading
(a) Forces Acting on Adherends, (b) Forces at Joint Edges

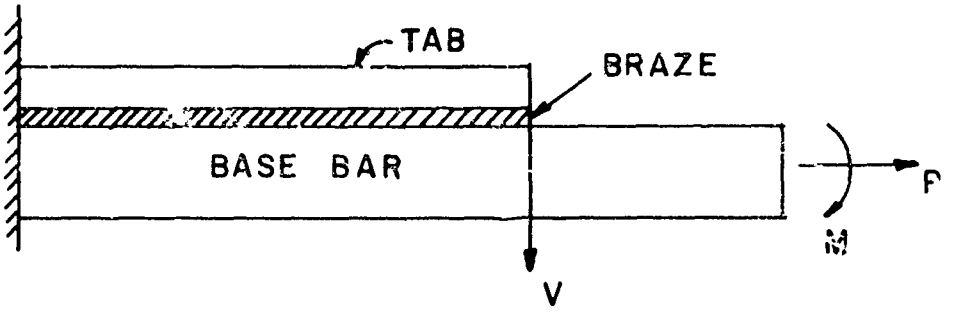

FIG. 4 Joint Considered by Cornell

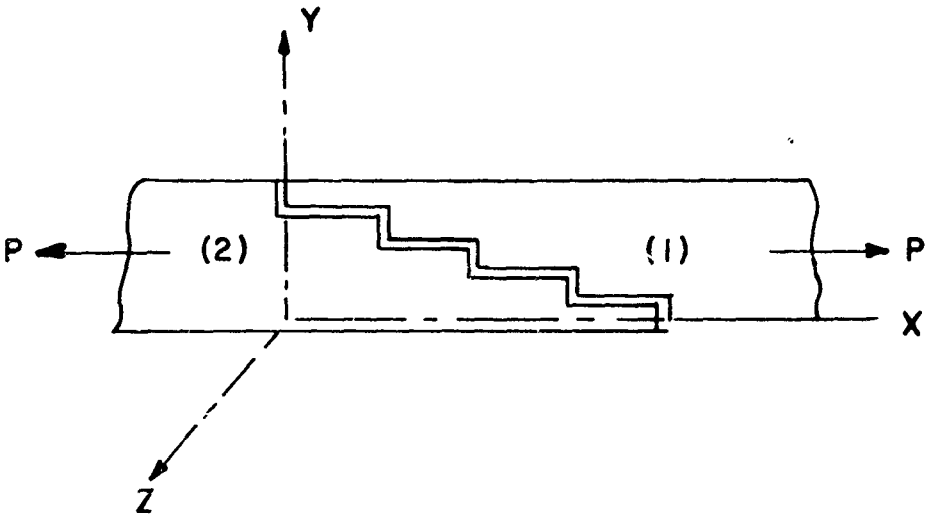

(a)

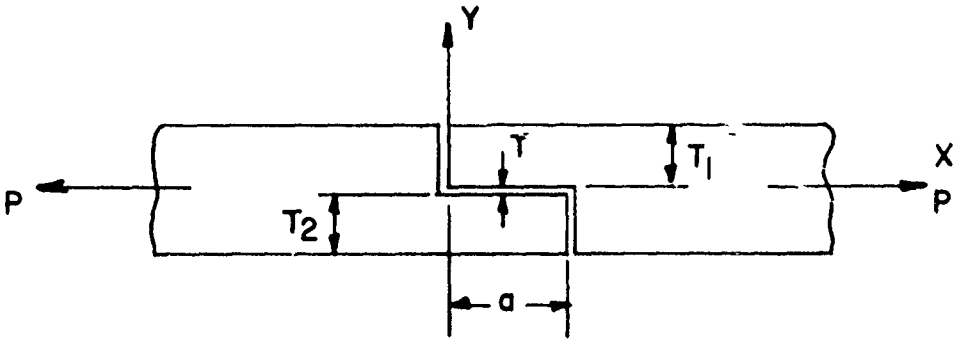

(b)

FIG. 5 Step Joint of Erdogan and Ratwani
(a) Multiple Step Joint, (b) Single Step Joint

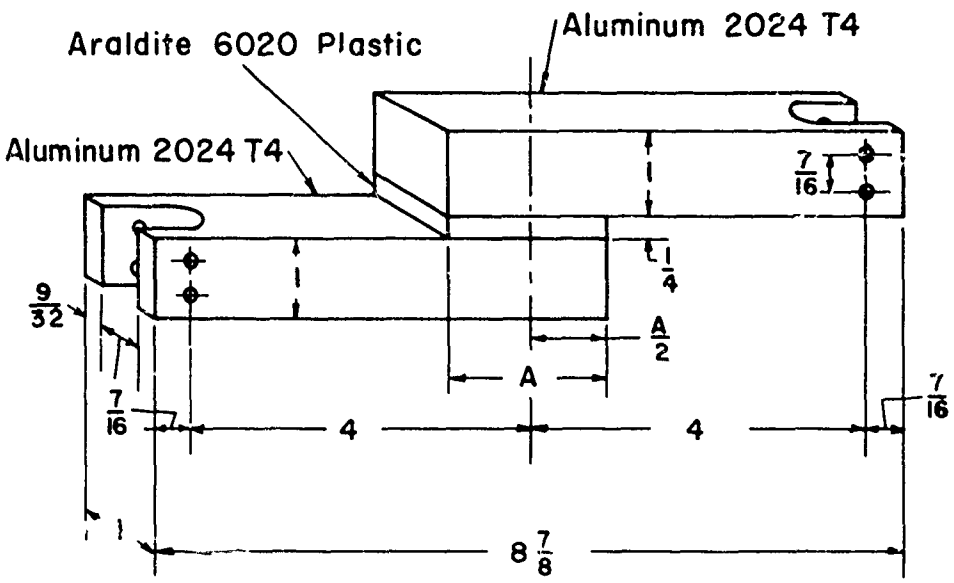

A = 2" for Specimen 1
A = 3" for Specimen 2

Fig. 6 Dimensions of Test Models

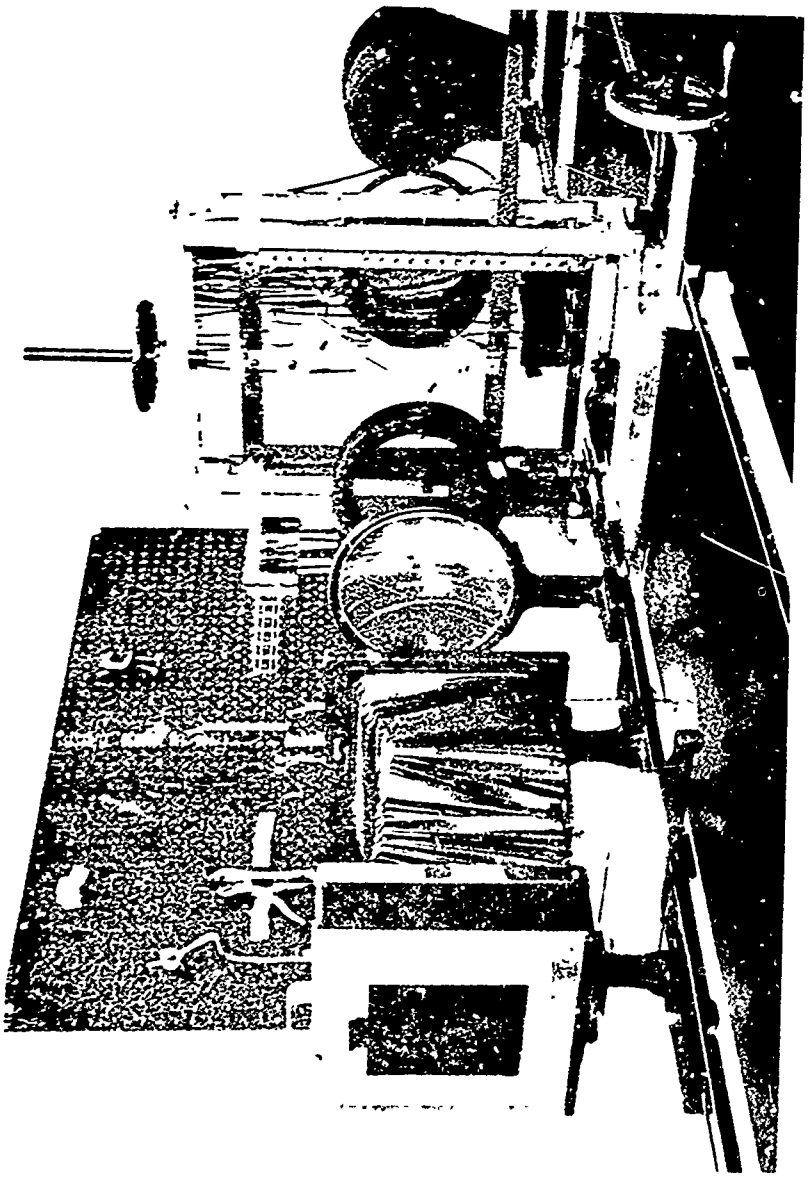

Fig. 7 Photoelastic Test Bench

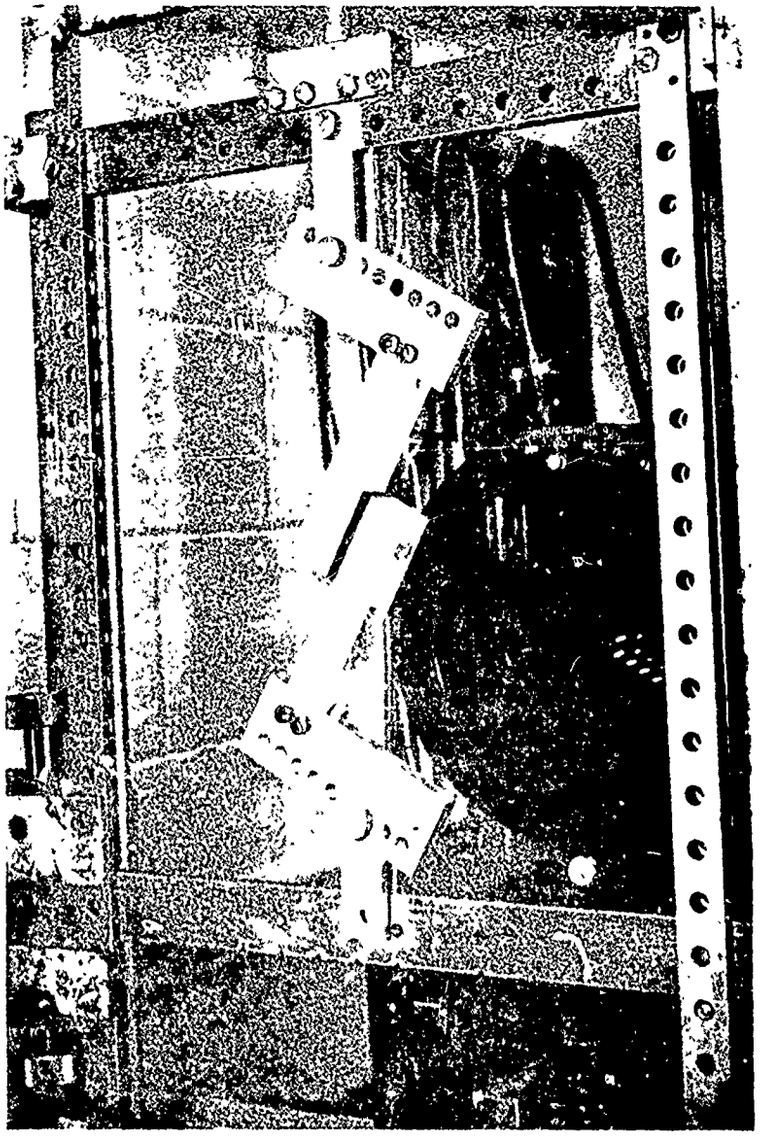

Fig. 8 Loading the Specimen at an Angle

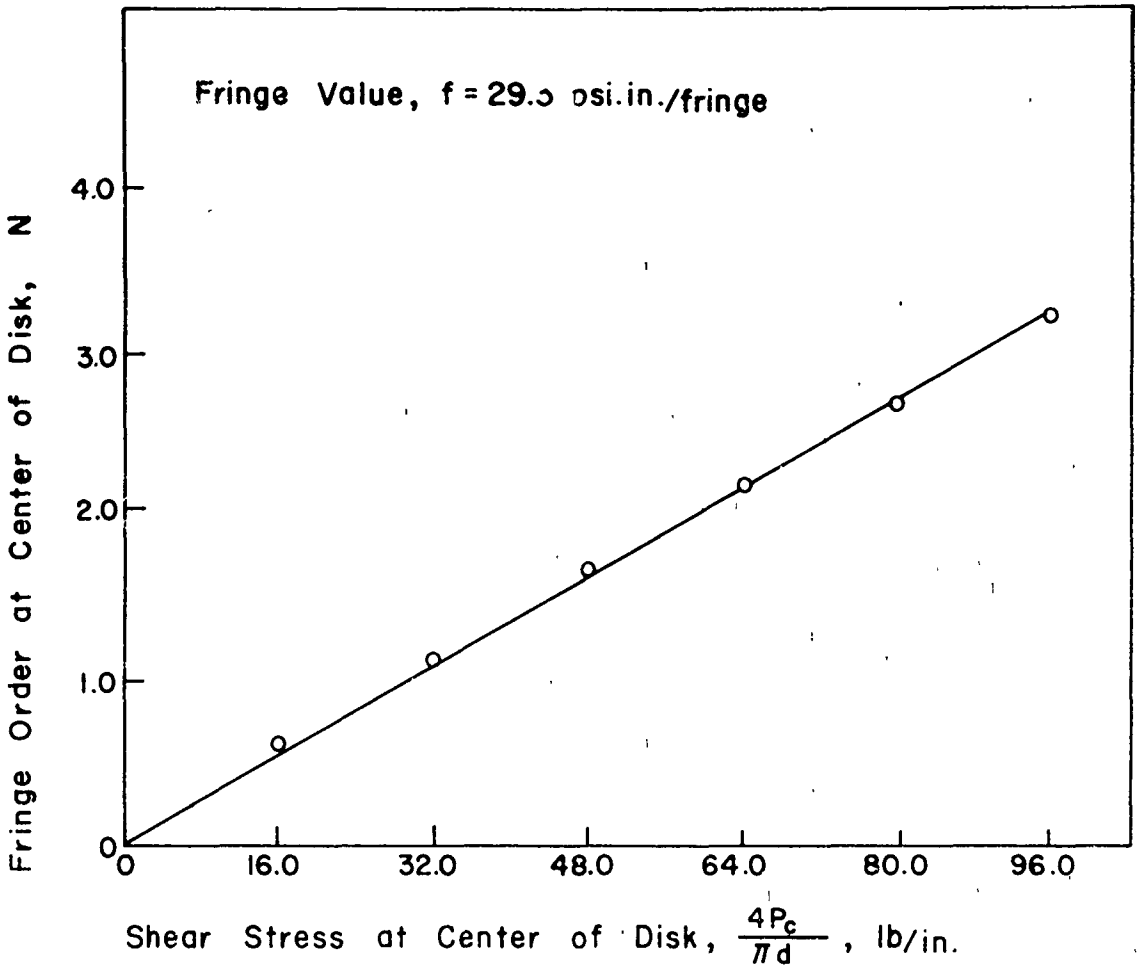

Fig. 9 Calibration of Araldite 6020 Epoxy to Determine Fringe Value

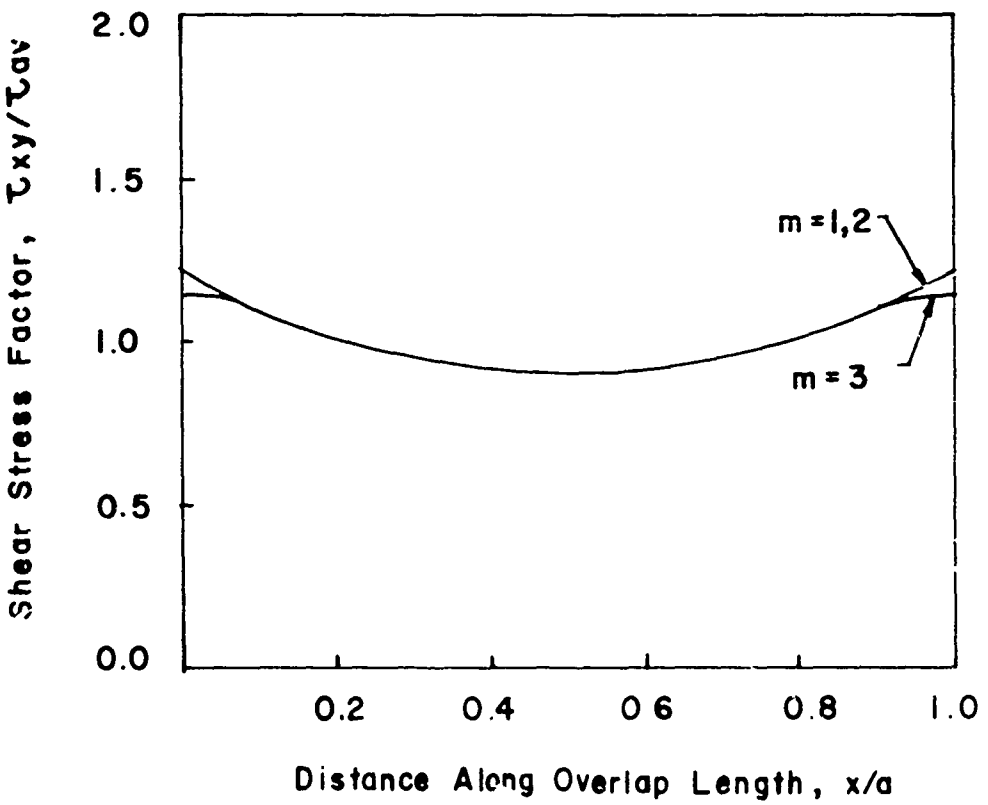

Fig. 10 Theoretical Distribution of τ_{xy} at Mid-plane for Different Values of m
($E_1/E = 20$, $t_1/t = 4$, $t_1/a = .5$, $V = 0$, $n = 1$)

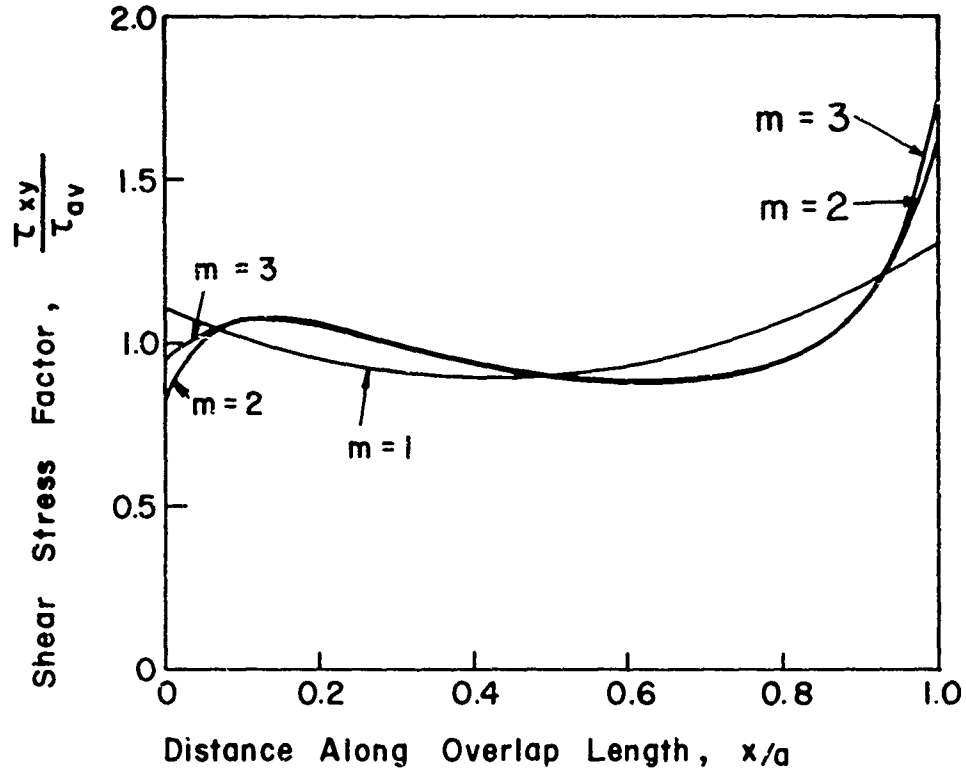

Fig. 11 Theoretical Distribution of τ_{xy} at Interfacial Plane for Different Values of m
($E_1/E = 20$, $t_1/t = 4$, $t_1/a = .5$, $V = 0$, $n = 1$)

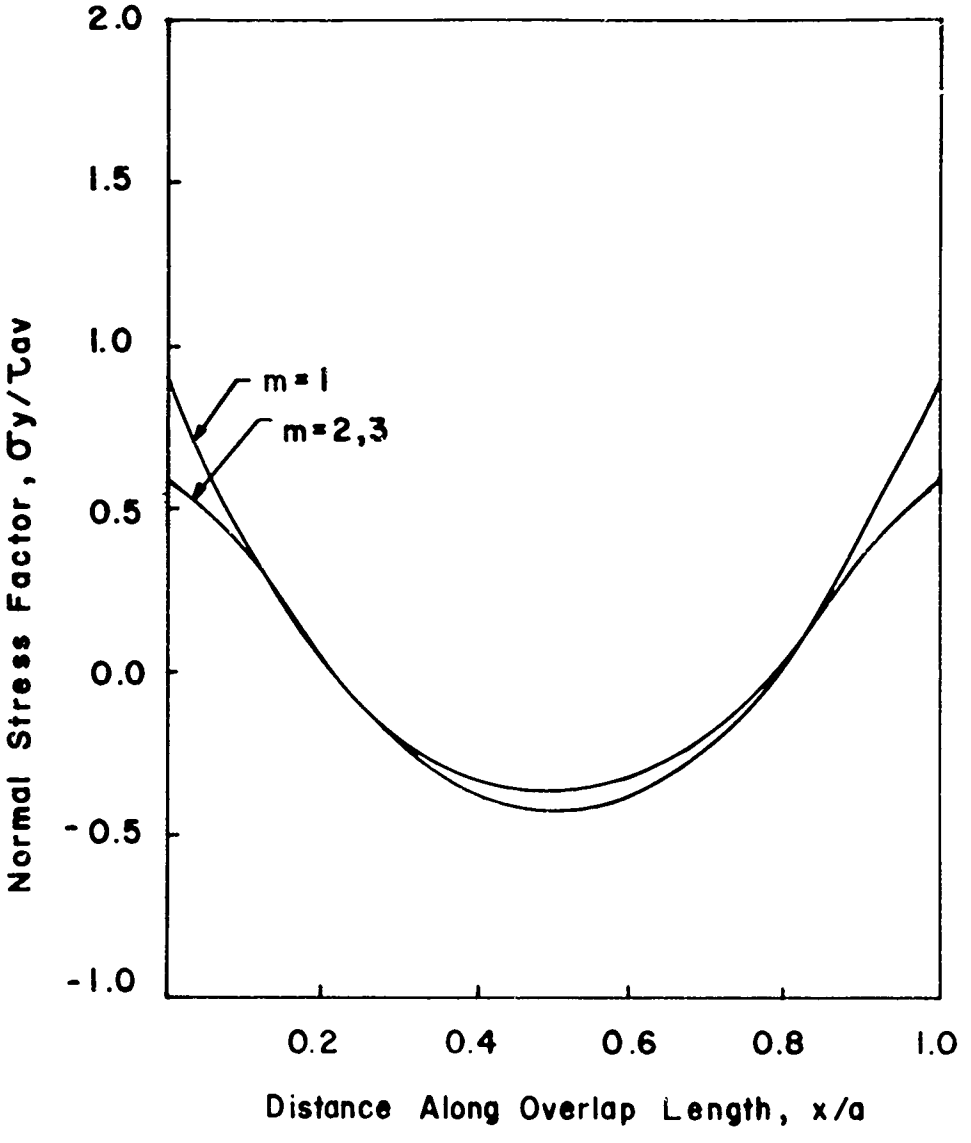

Fig. 12 Theoretical Distribution of σ_y at Mid-plane for Different Values of m

($E_i/E = 20$, $t_i/t = 4$, $t_i/a = .5$, $V = 0$, $n = 1$)

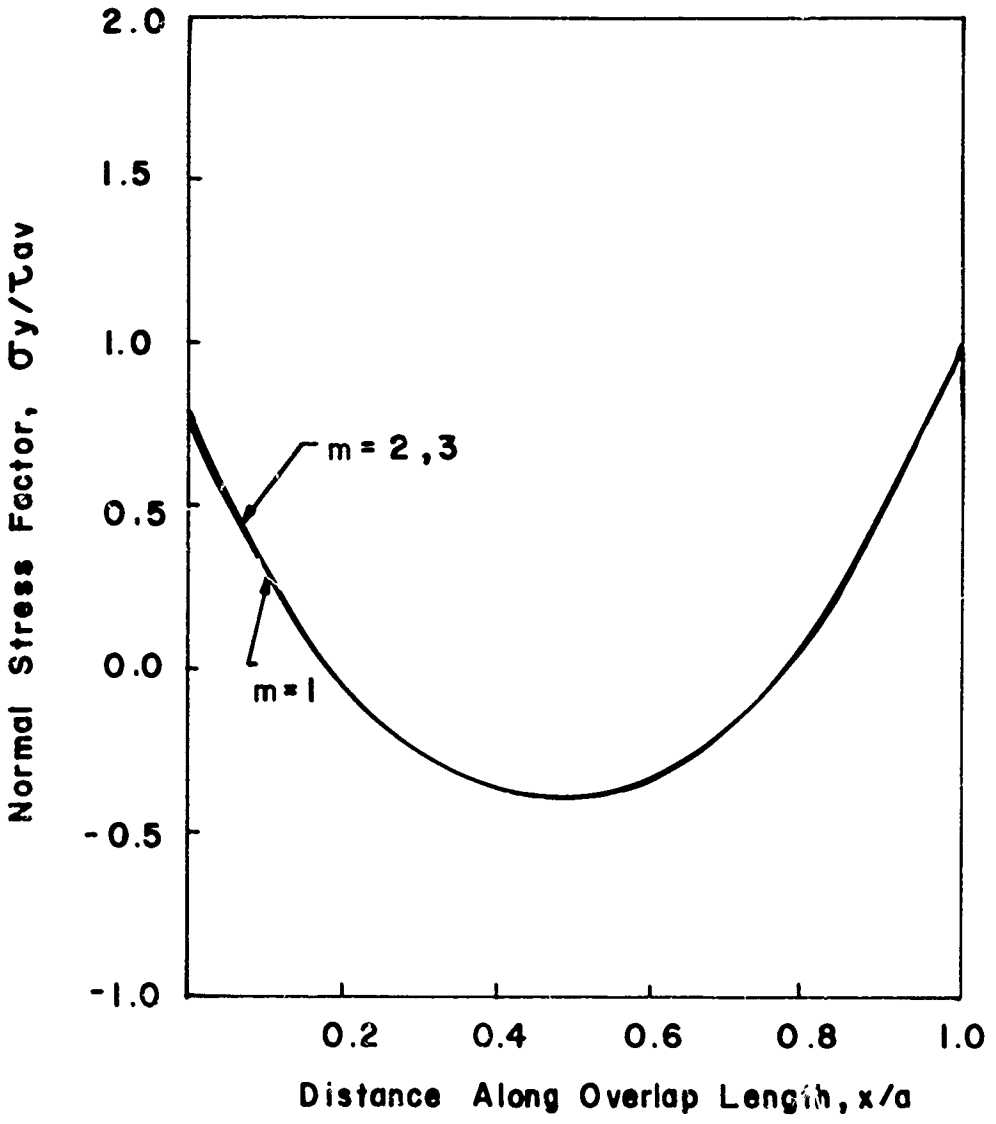

Fig. 13 Theoretical Distribution of σ_y at Interfacial plane for Different Values of m
($E_1/E = 20$, $t_1/t = 4$, $t_1/a = .5$, $V = 0$, $n = 1$)

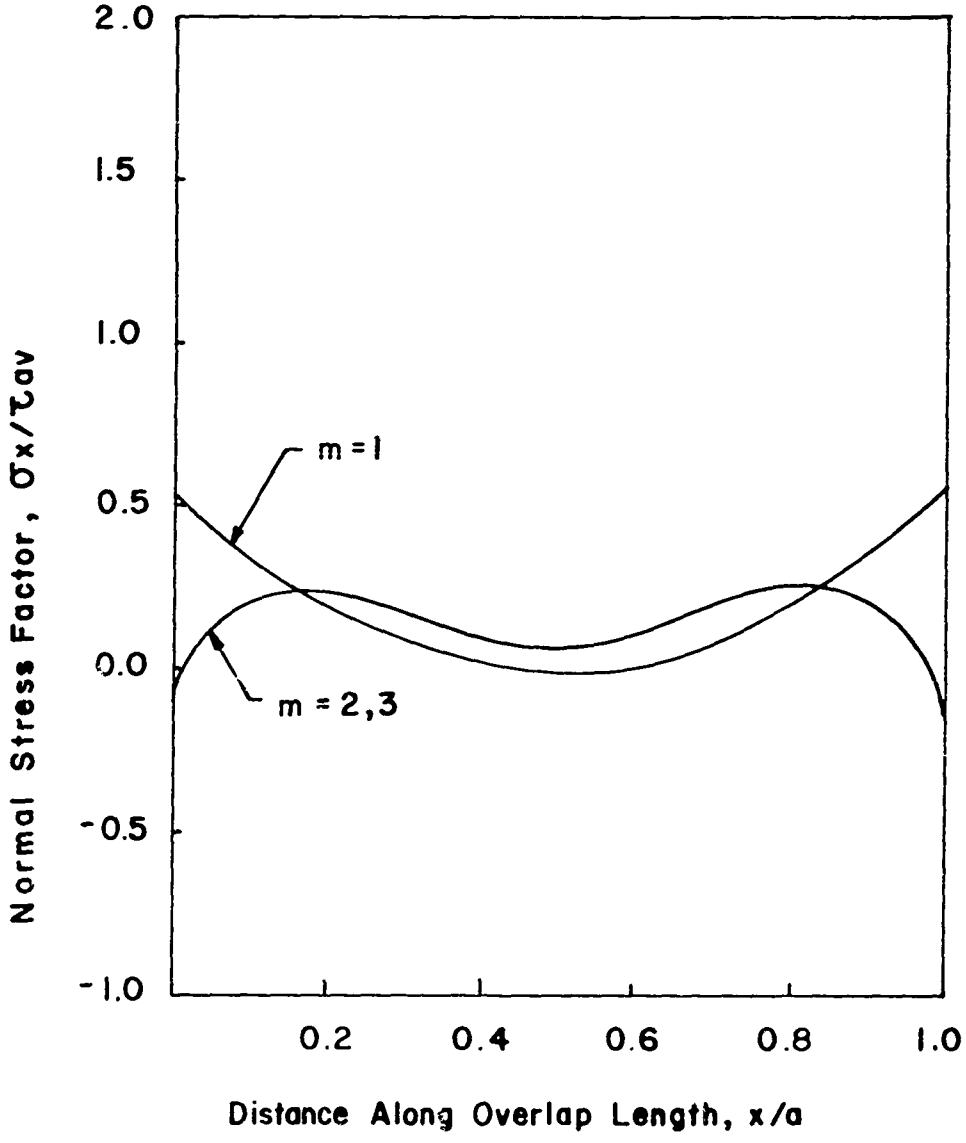

Fig. 14 Theoretical Distribution of σx at Mid-plane for Different Values of m

($E_1/E = 20$, $t_1/t = 4$, $t_1/a = .5$, $V = 0$, $n = 1$)

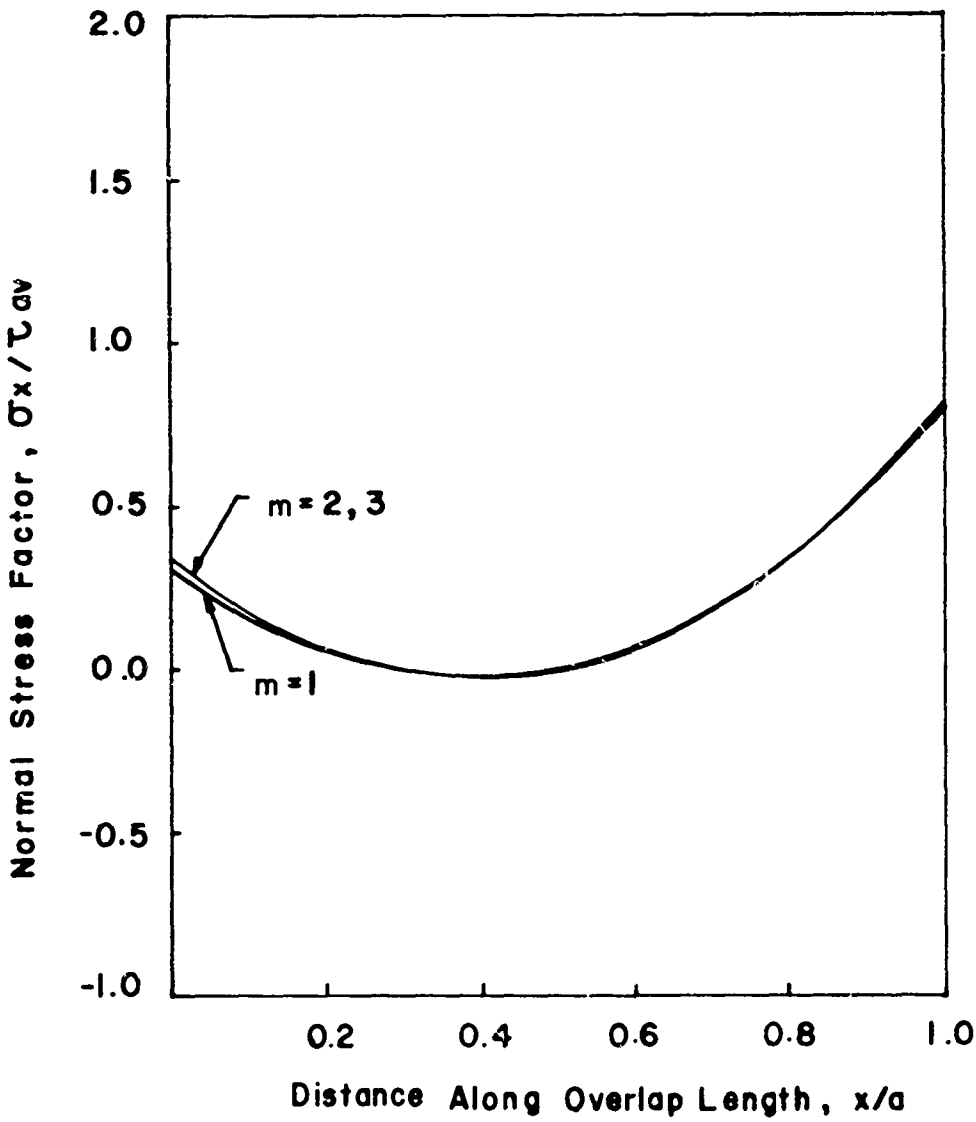

Fig.15 Theoretical Distribution of σx at Interfacial Plane for Different Values of m

($E_1/E = 20$, $t_1/t = 4$, $t_1/a = .5$, $V = 0$, $n = 1$)

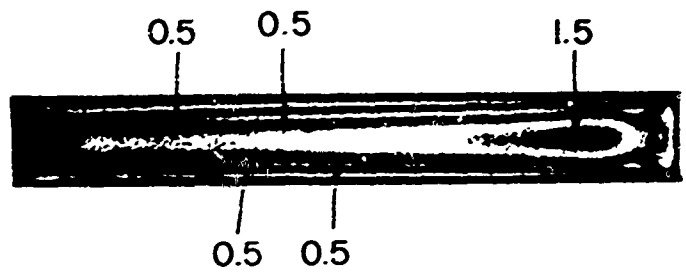

(a)

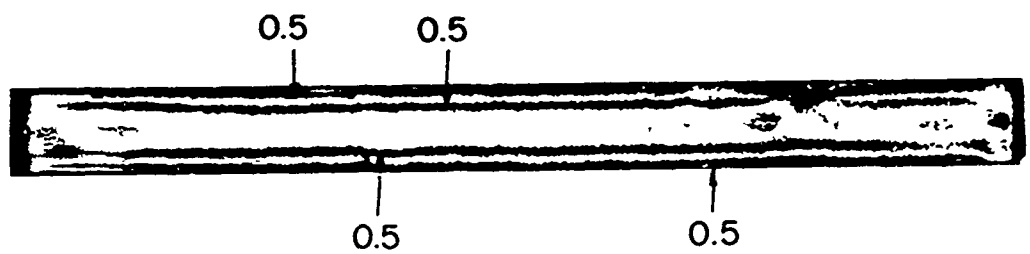

(b)

Fig. 16 Fringe Pattern at No Load
(a) 2 in. Overlap Specimen
(b) 3 in. Overlap Specimen

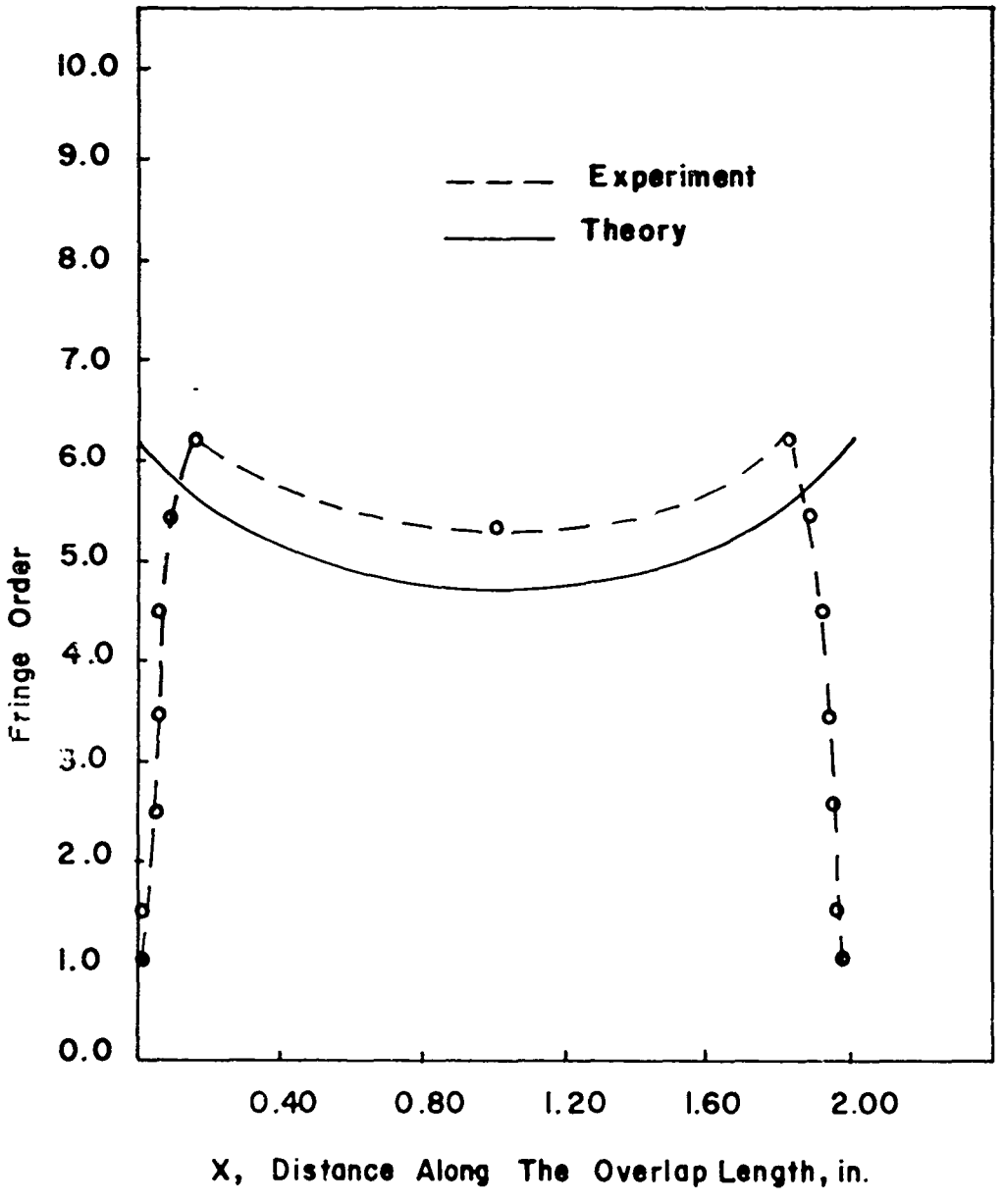

Fig. 17 Comparison of Theory and Experiment (y = 0 plane)
a = 2in., V/P = 0

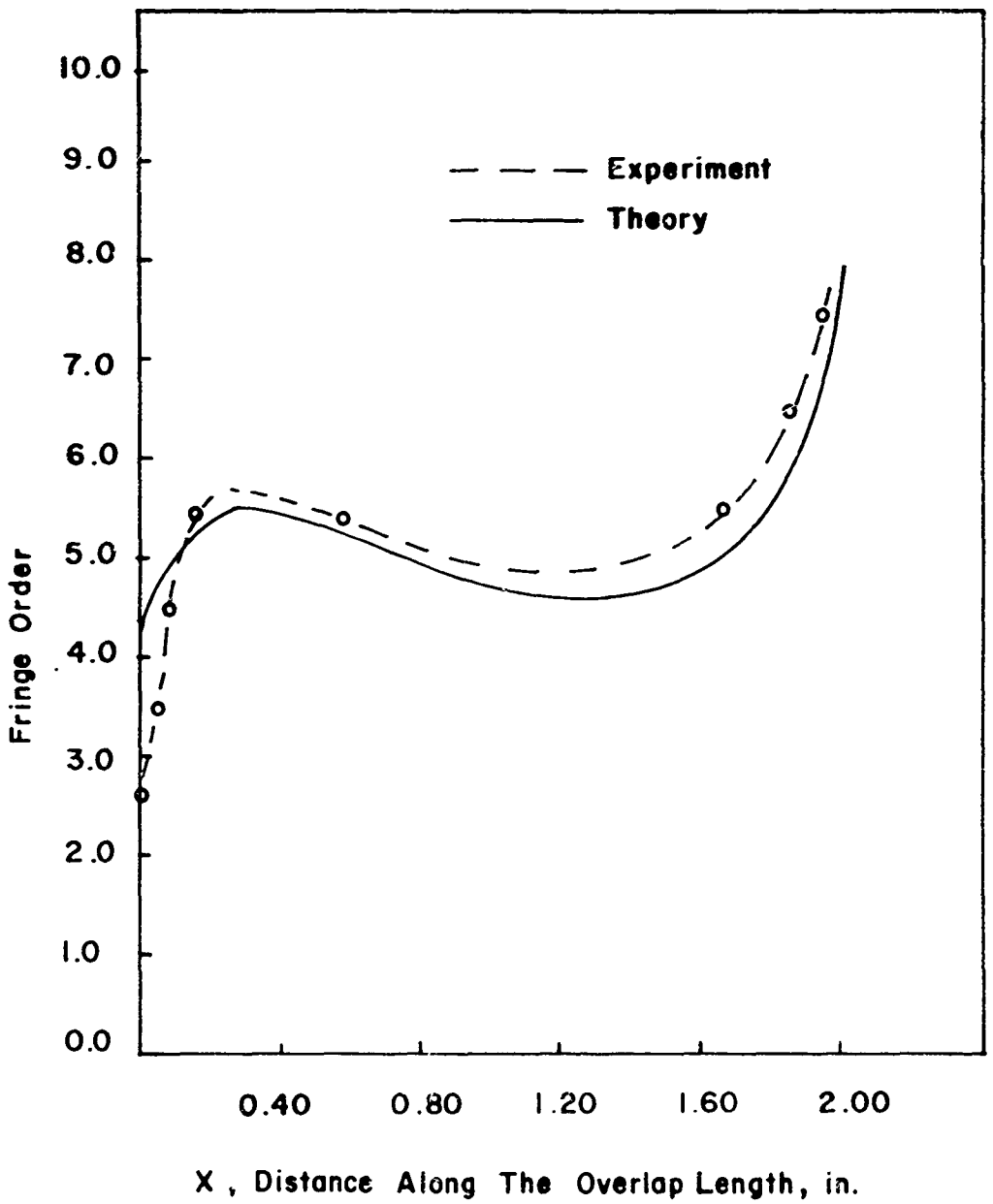

Fig. 18 Comparison of Theory and Experiment (y = t/2 plane)
a = 2 in., V/P = 0

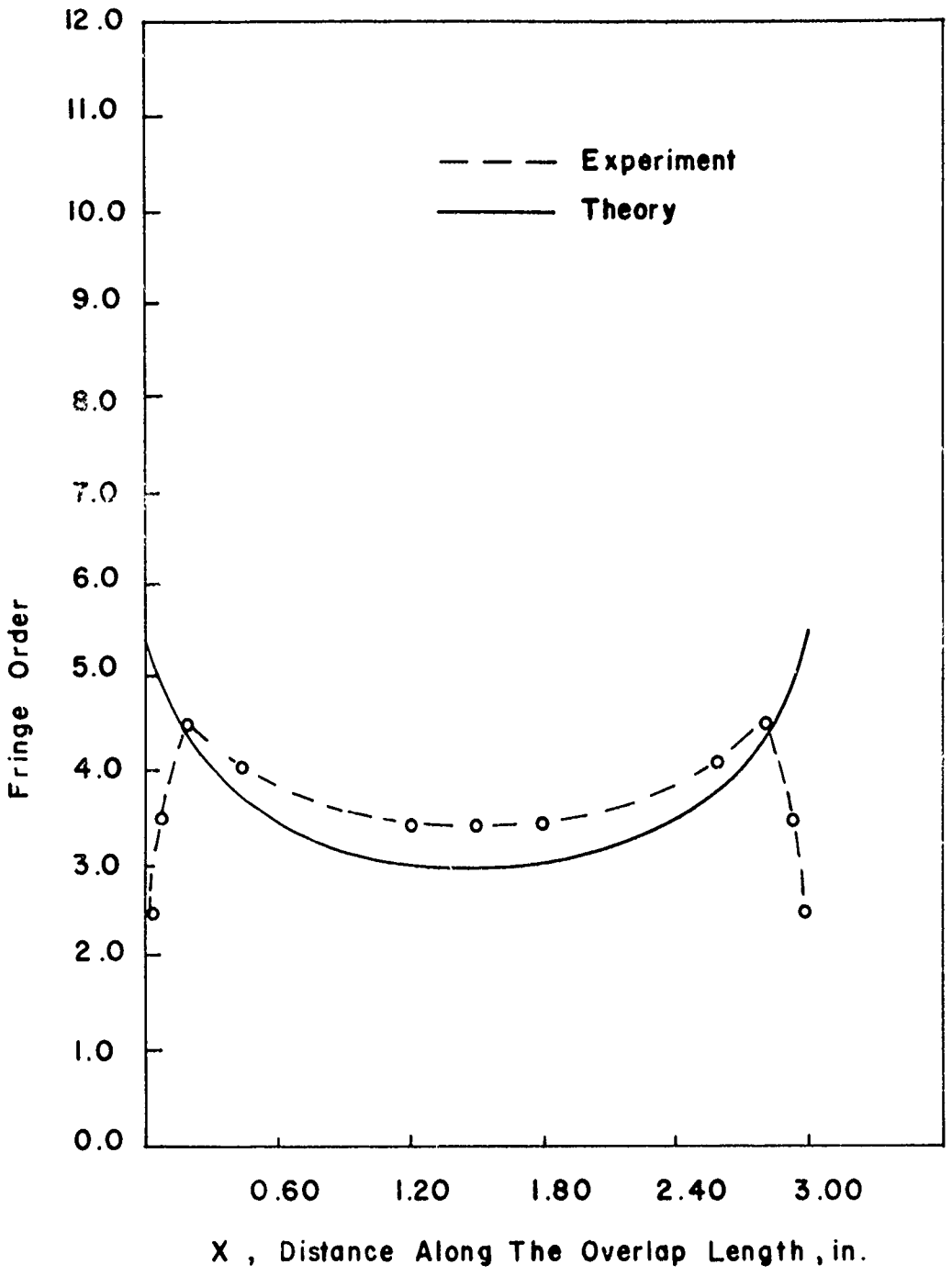

Fig. 19 Comparison of Theory and Experiment (y = 0 plane)
a = 3 in., V/P = 0

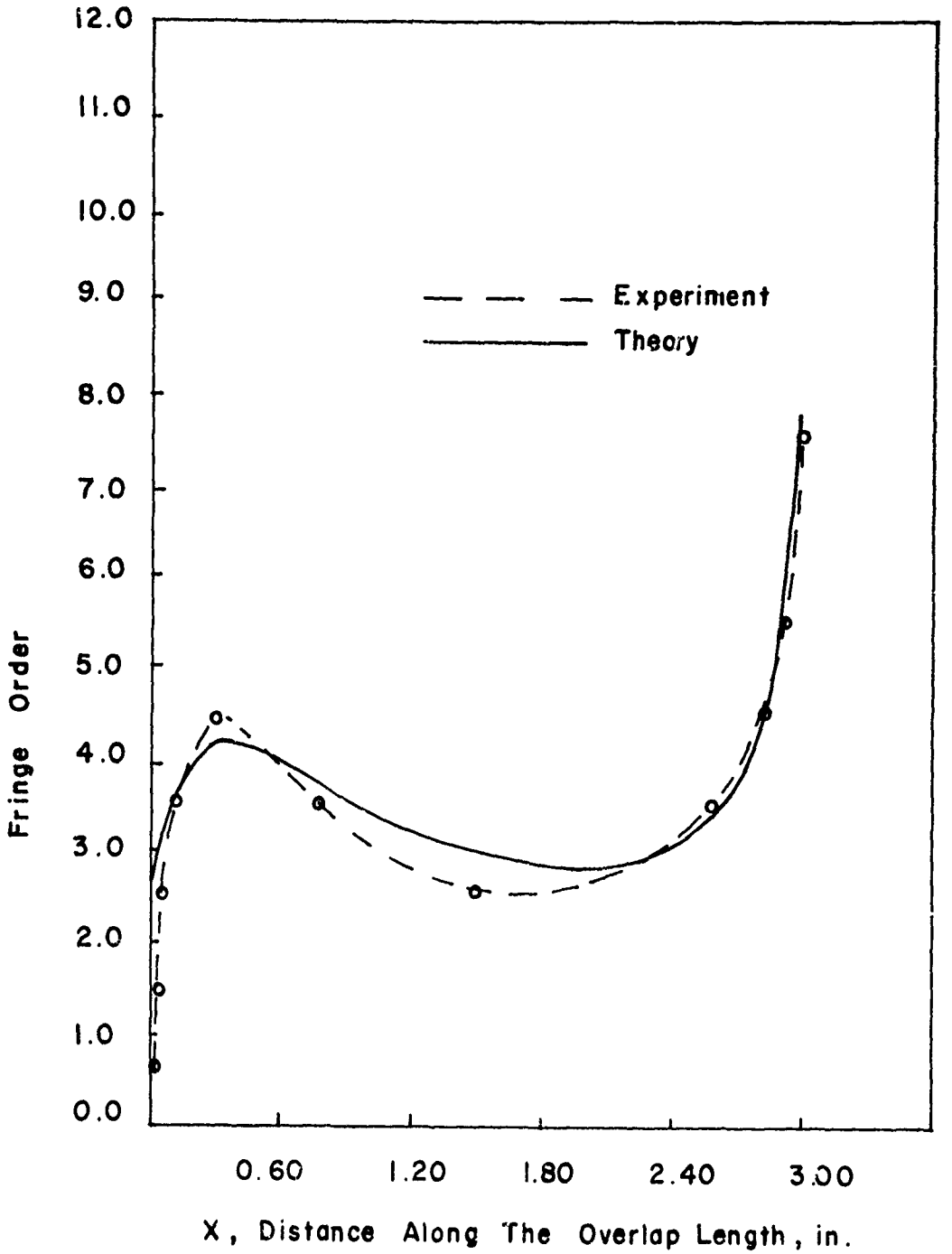

Fig. 20 Comparison of Theory and Experiment (y = t/2 plane)
a = 3in., V/P = 0

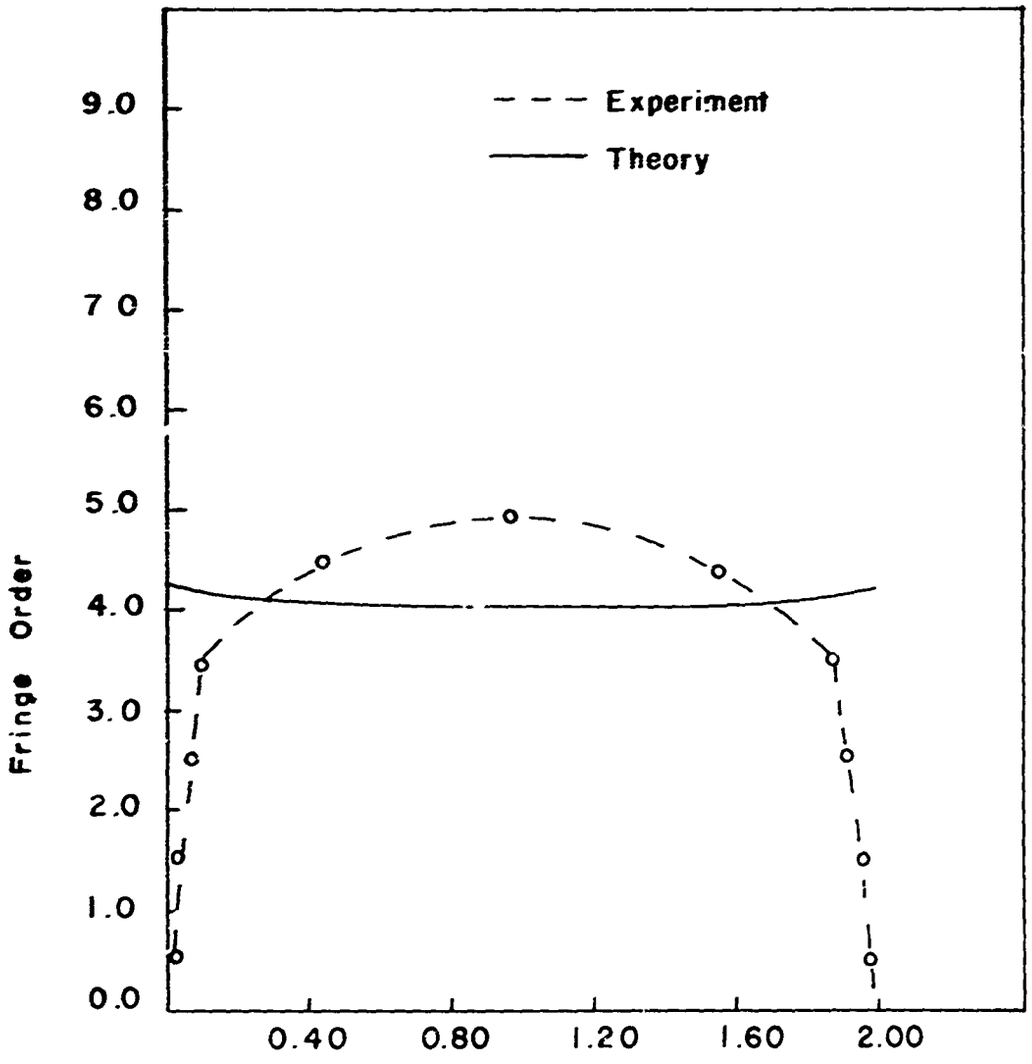

Fig. 21 Comparison of Theory and Experiment (y=0 plane)
a = 2 in., V/P = 0.8

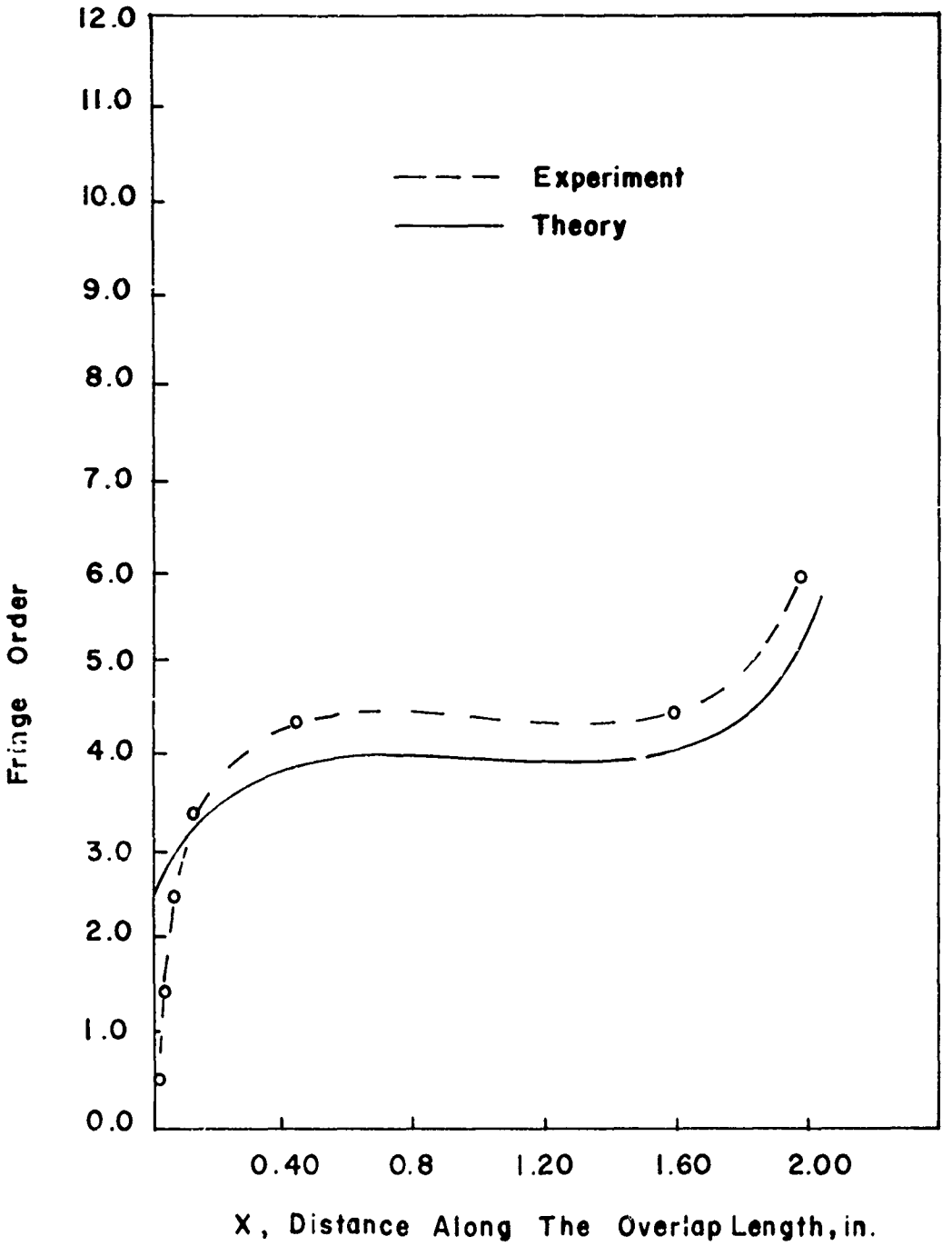

Fig. 22 Comparison of Theory and Experiment (y = t/2 plane)
a = 2 in., V/P = 0.8

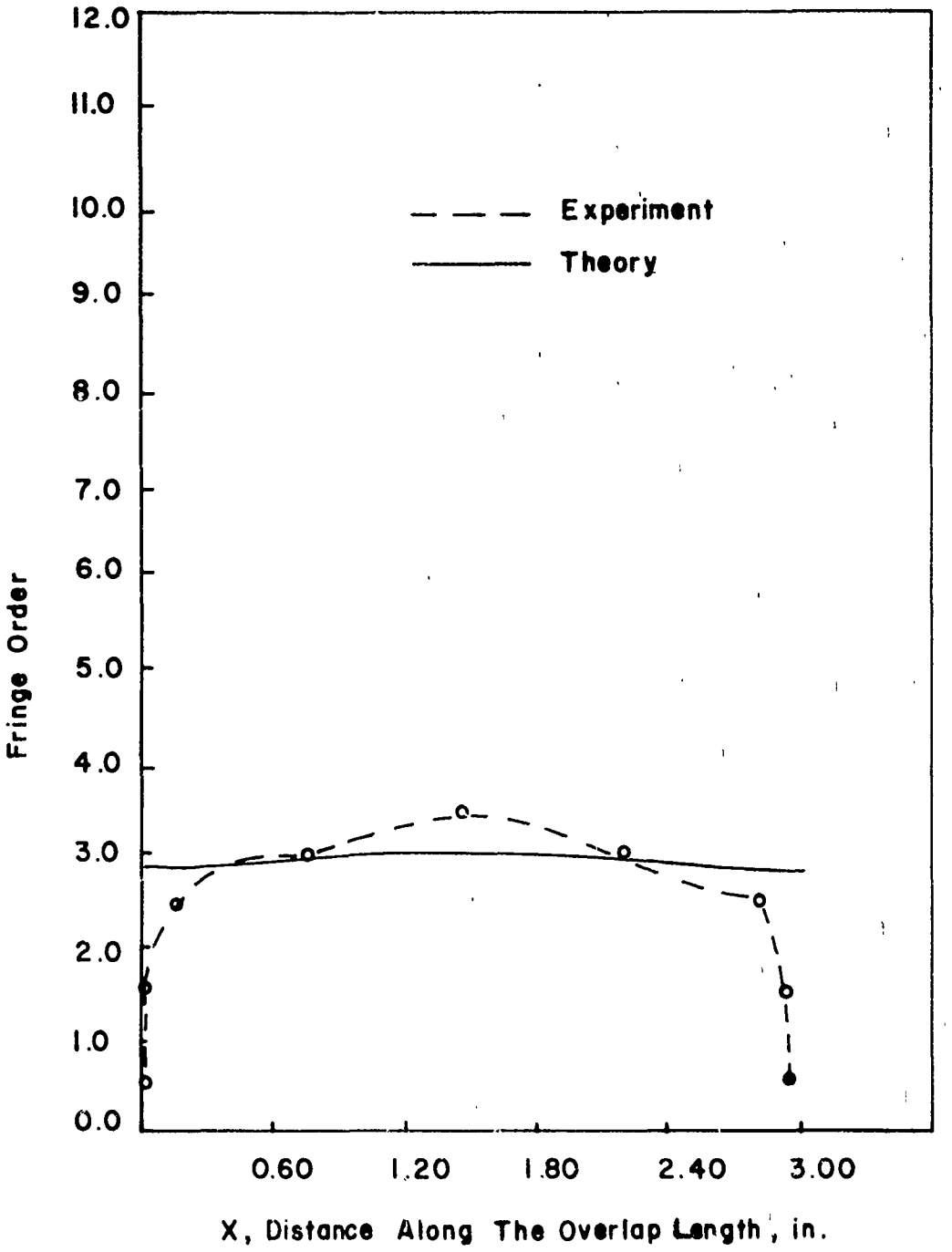

Fig. 23 Comparison of Theory and Experiment (y = 0 plane)
a = 3in., V/P = 0.6

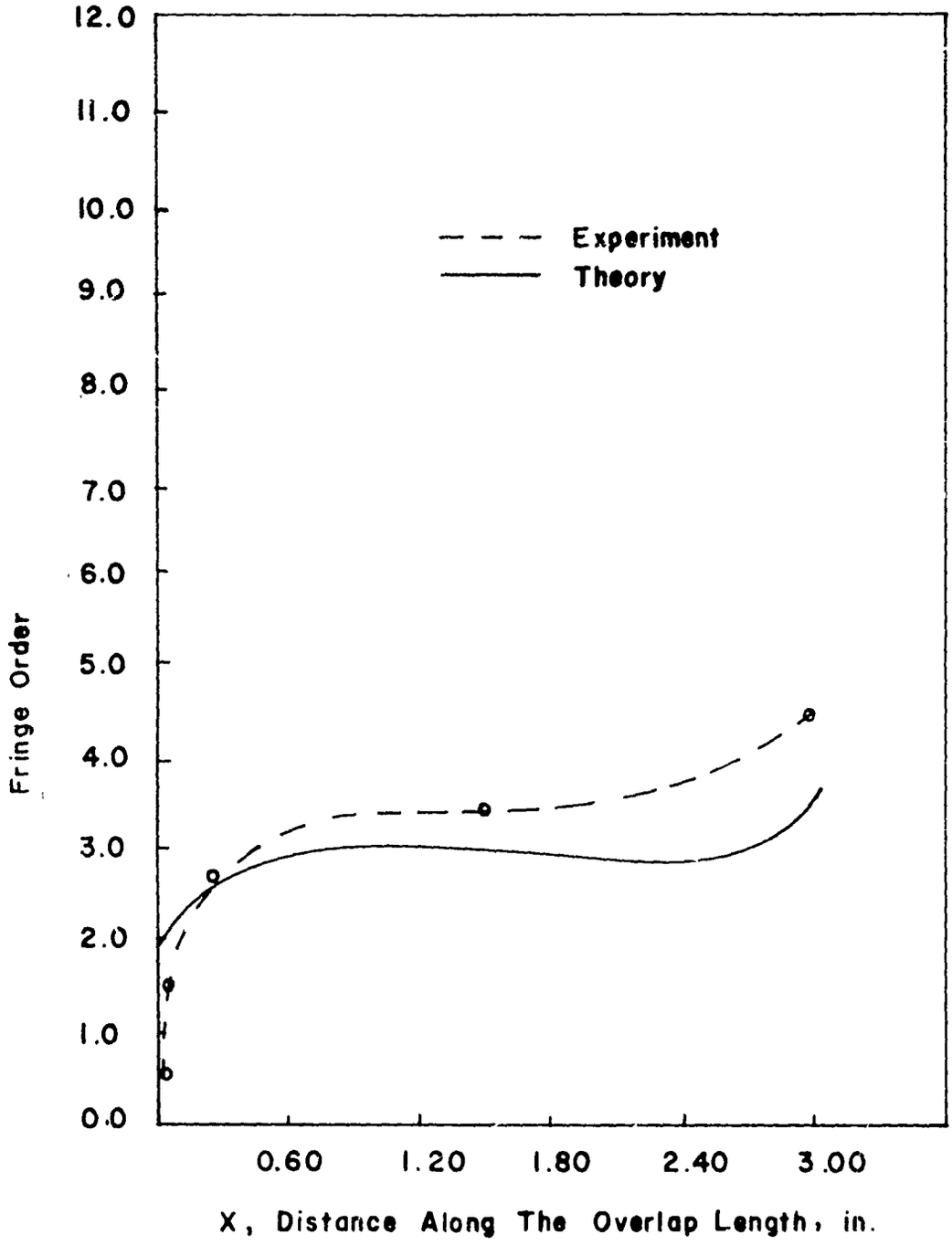

Fig. 24 Comparison of Theory and Experiment (y=t/2 plane)
a=3in, V/P = 0.6

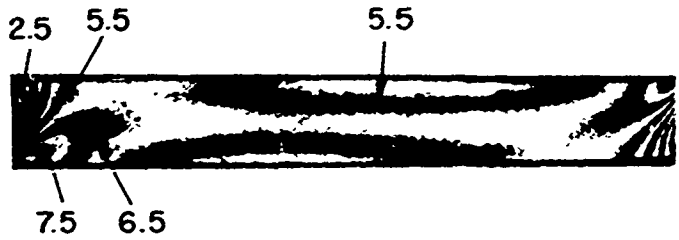

Experiment (V/P = 0.0)

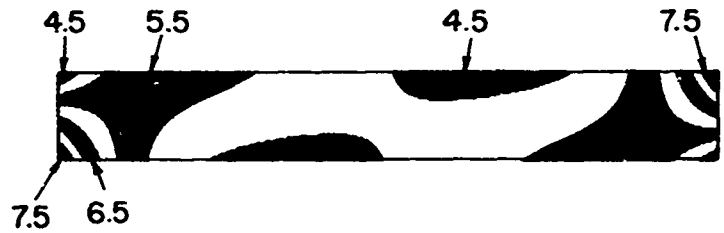

Theory (V/P = 0.0)

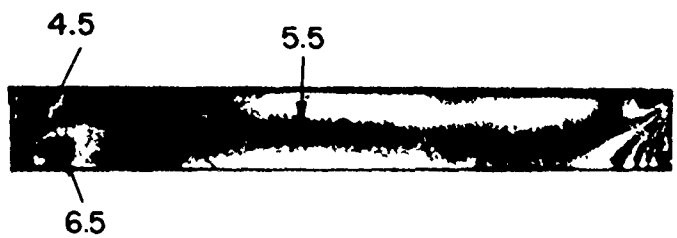

Experiment (V/P = 0.4)

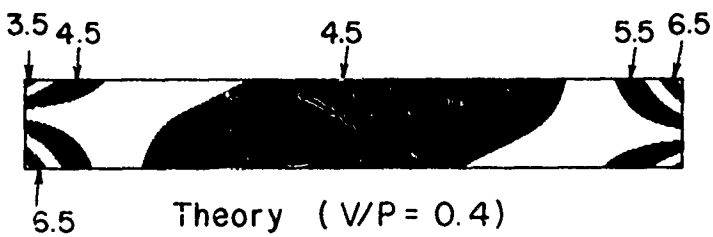

Theory (V/P = 0.4)

Fig. 25 Comparison of Experimental and Theoretical Fringe Patterns (a = 2 in., V/P = 0.0, 0.4)

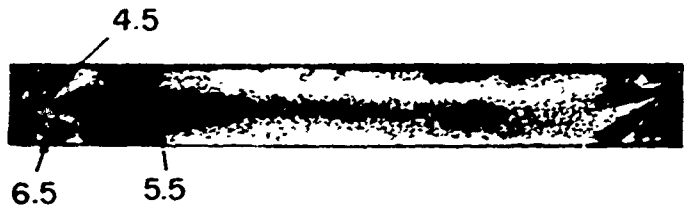

Experiment (V/P = 0.5)

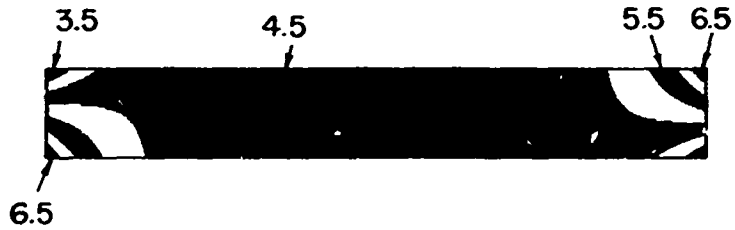

Theory (V/P = 0.5)

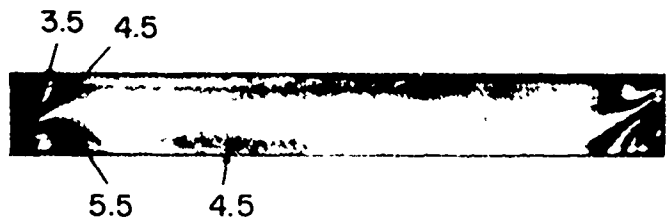

Experiment (V/P = 0.6)

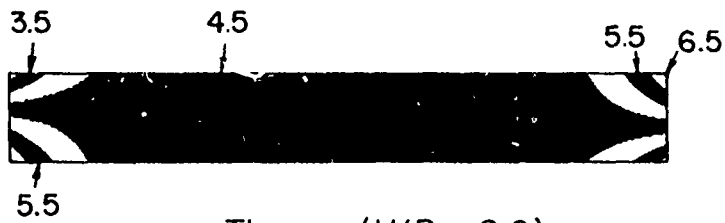

Theory (V/P = 0.6)

Fig. 26 Comparison of Experimental and Theoretical Fringe Patterns (a = 2 in., V/P = 0.5, 0.6)

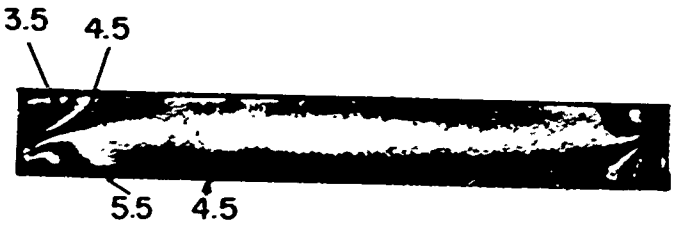

Experiment (V/P = 0.7)

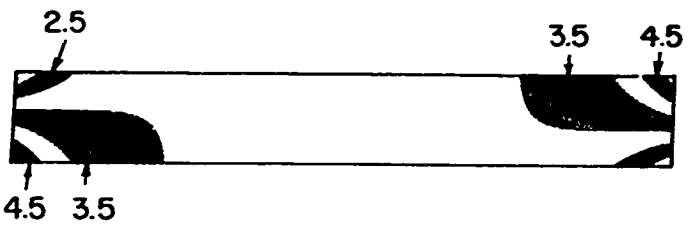

Theory (V/P = 0.7)

Experiment (V/P = 0.8)

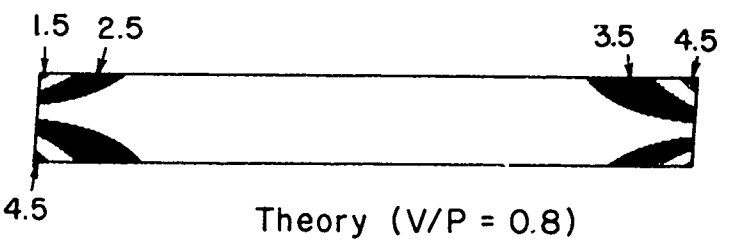

Theory (V/P = 0.8)

Fig. 27 Comparison of Experimental and Theoretical Fringe Patterns (a = 2 in., V/P = 0.7, 0.8)

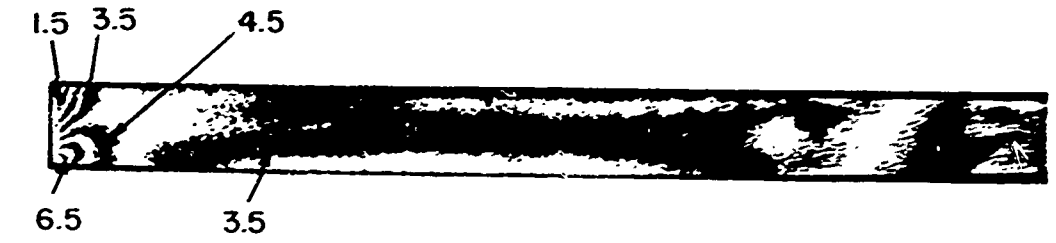

Experiment (V/P = 0)

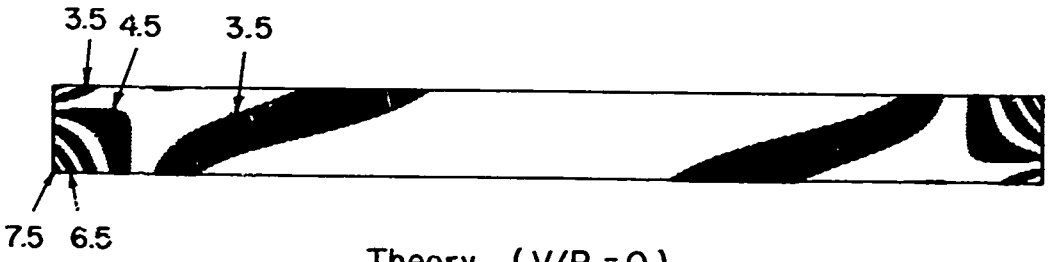

Theory (V/P = 0)

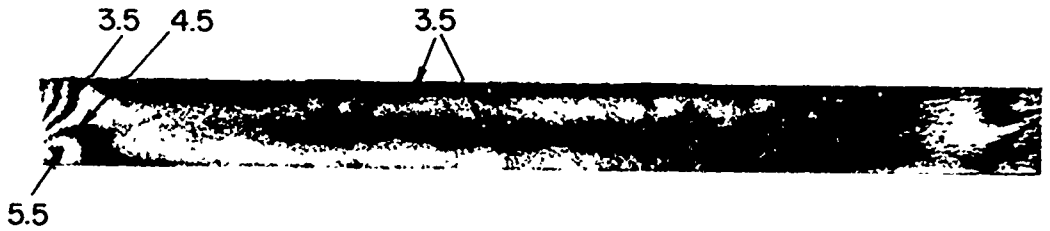

Experiment (V/P = 0.4)

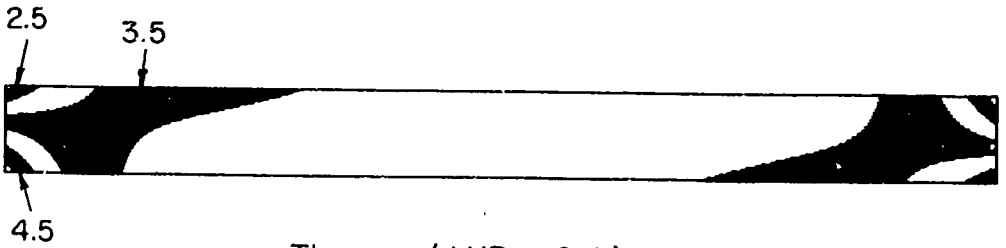

Theory (V/P = 0.4)

Fig. 28 Comparison of Experimental and Theoretical Fringe Patterns (a = 3 in., V/P = 0.0, 0.4)

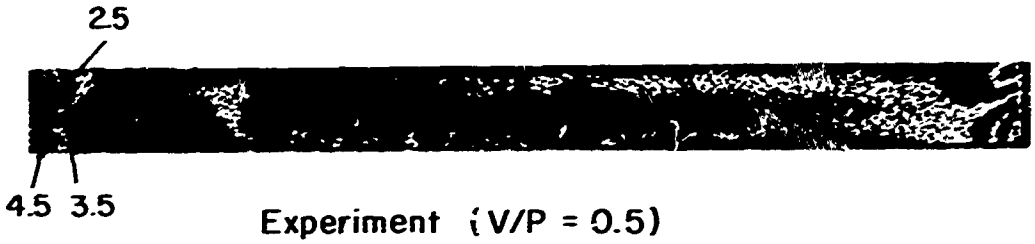

Experiment (V/P = 0.5)

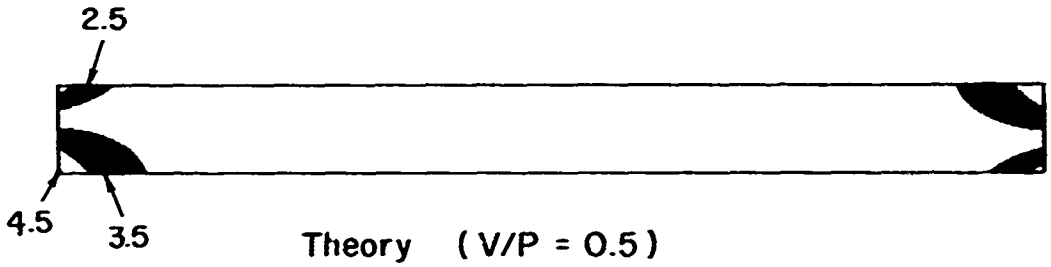

Theory (V/P = 0.5)

Experiment (V/P = 0.6)

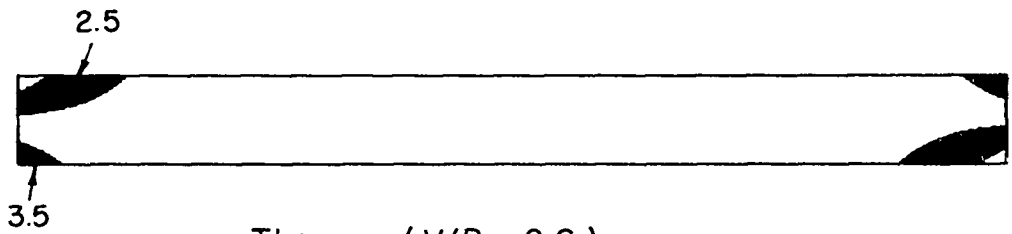

Theory (V/P = 0.6)

Fig. 29 Comparison of Experimental and Theoretical Fringe Patterns (a = 3 in., V/P = 0.5, 0.6)

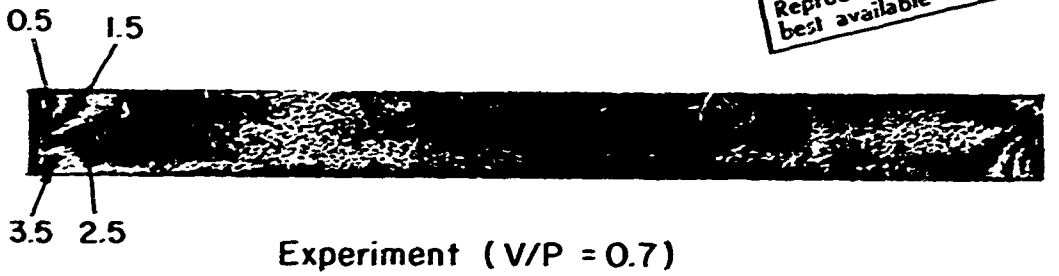

Experiment (V/P = 0.7)

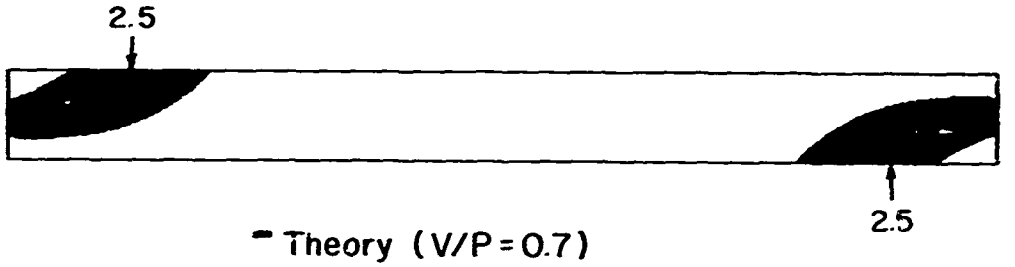

Theory (V/P = 0.7)

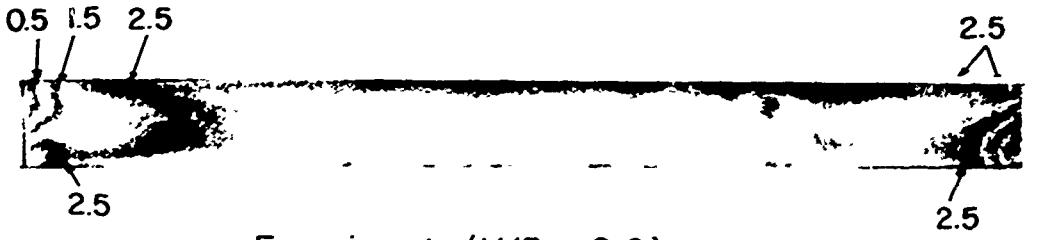

Experiment (V/P = 0.8)

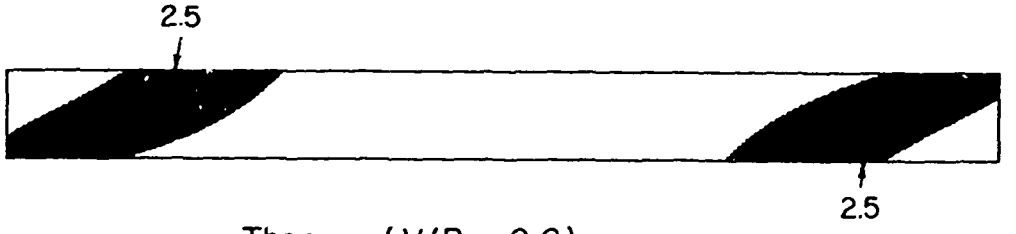

Theory (V/P = 0.8)

Fig. 30 Comparison of Experimental and Theoretical Fringe Patterns (a = 3in., V/P = 0.7, 0.8)

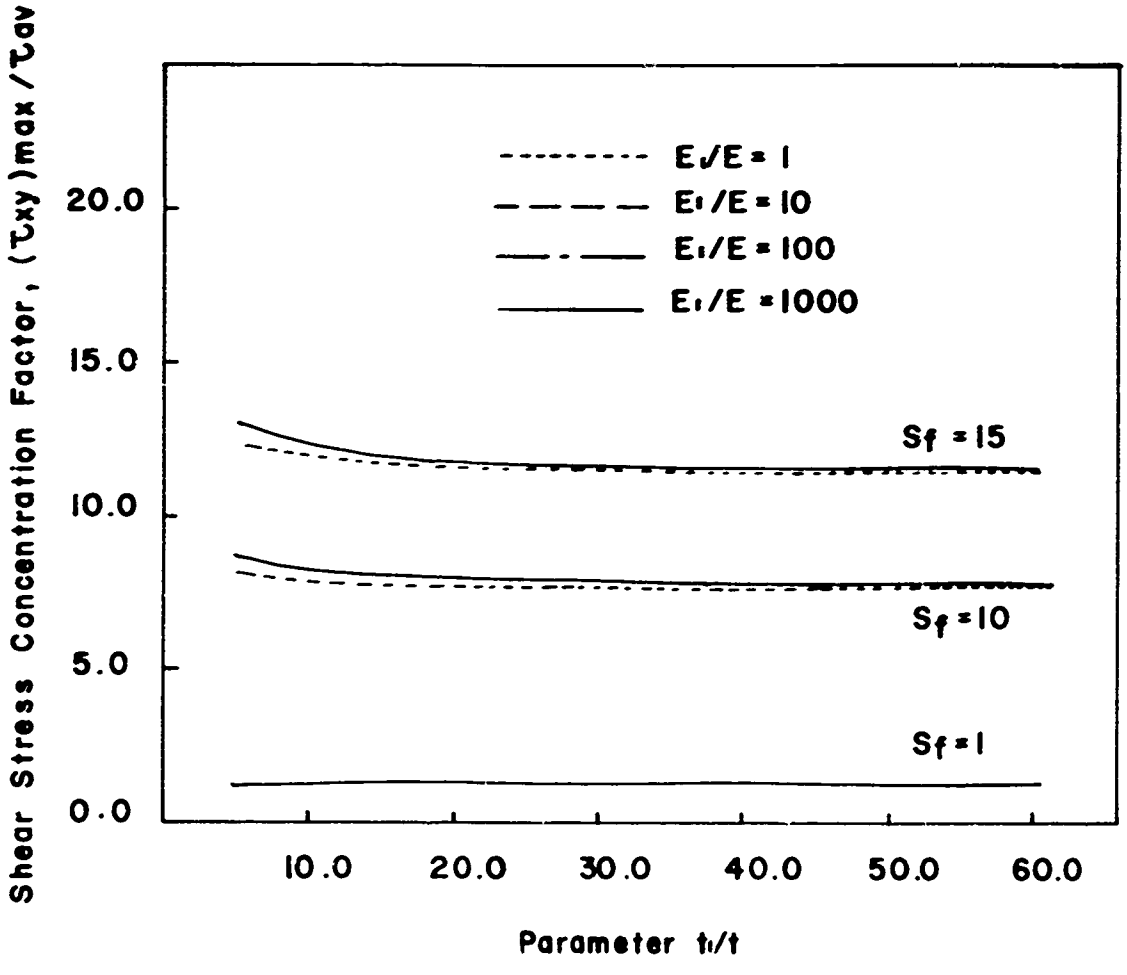

Fig.31 Shear Stress Concentration Factor at the Mid-plane of Adhesive Layer as a Function of t_1/t, E_1/E, and S_f, for $V_f = 0$

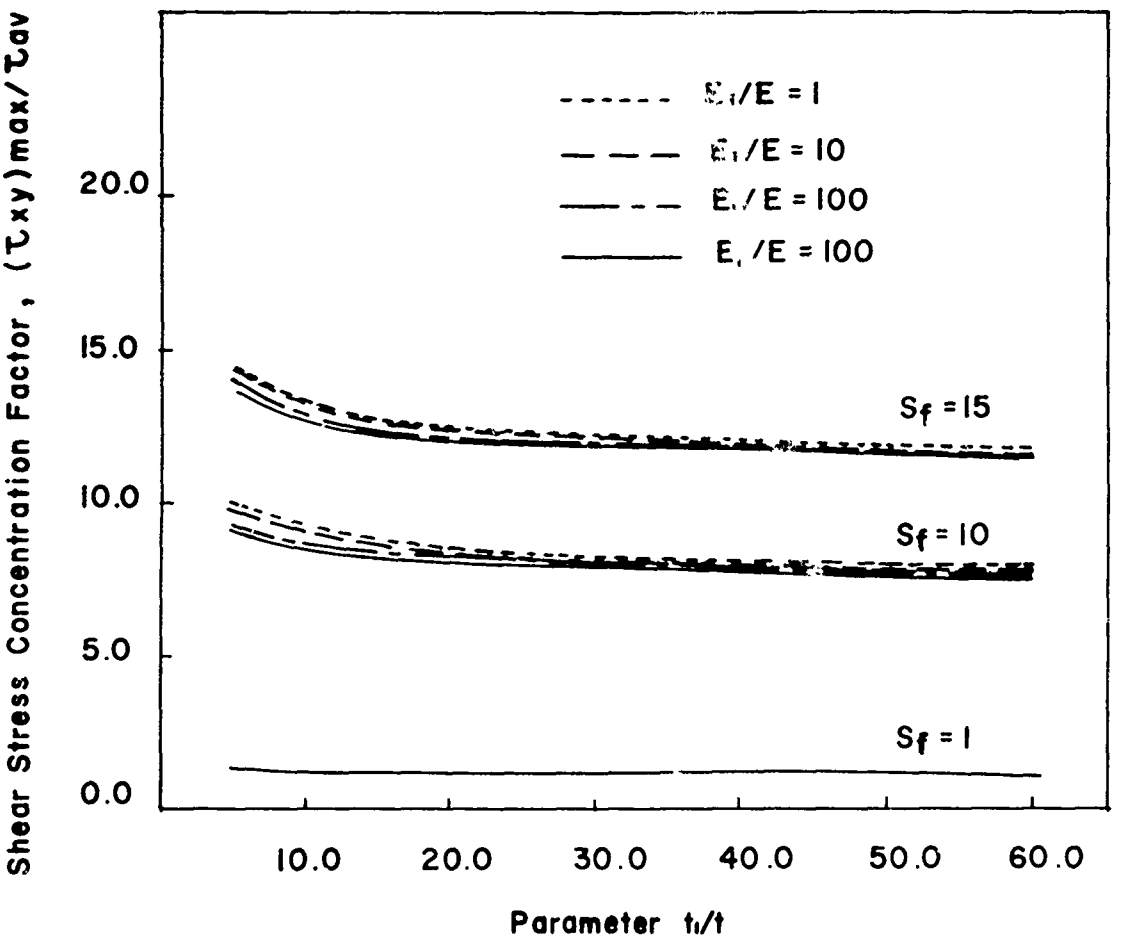

Fig.32 Shear Stress Concentration Factor at the Interfacial Plane as a Function of t_1/t, E_1/E, and S_f, for $V_f = 0$

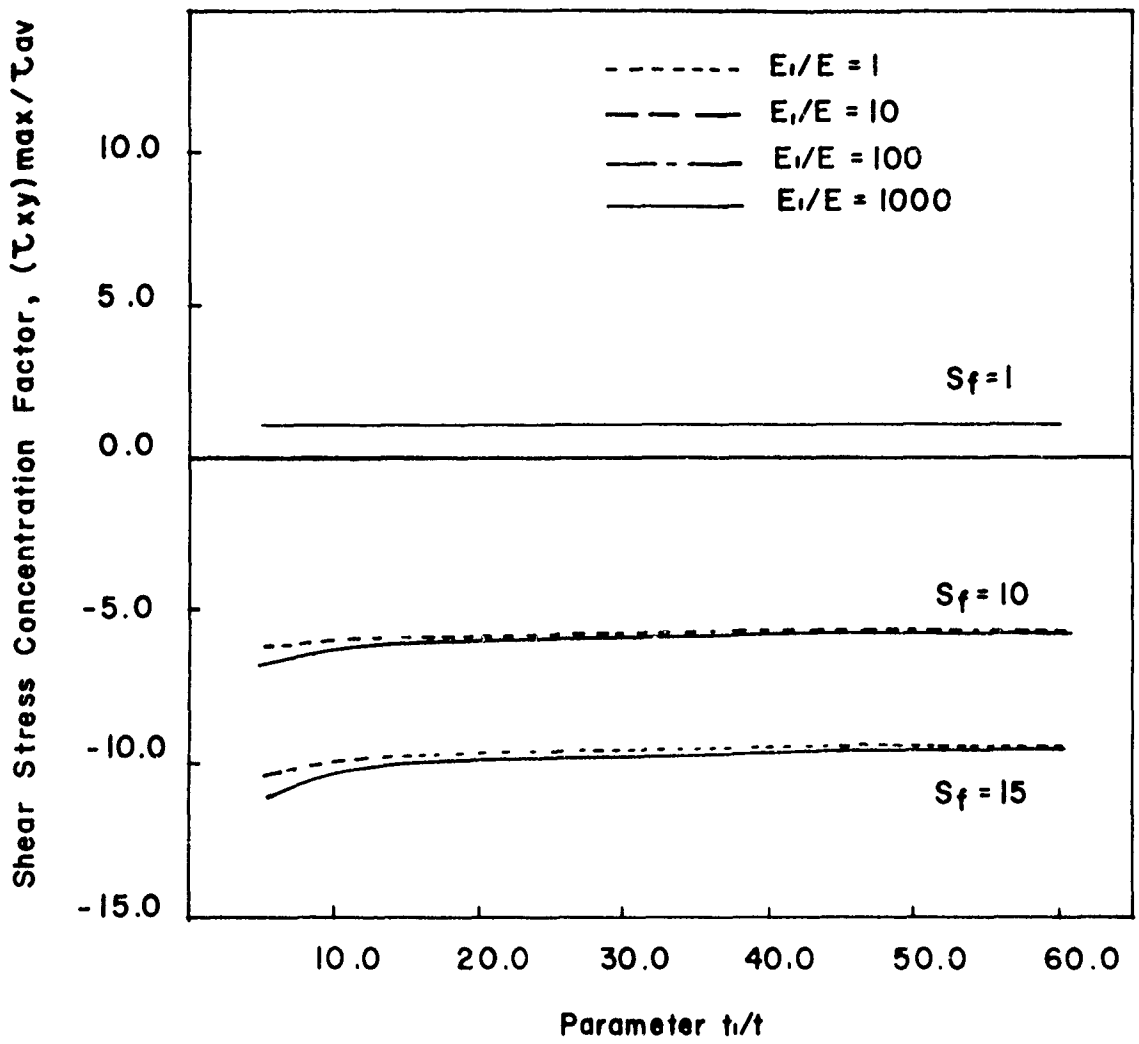

Fig. 33 Shear Stress Concentration Factor at the Mid-plane of the Adhesive Layer as Function of t_1/t, E_1/E, and S_f, for $V_f = 2$

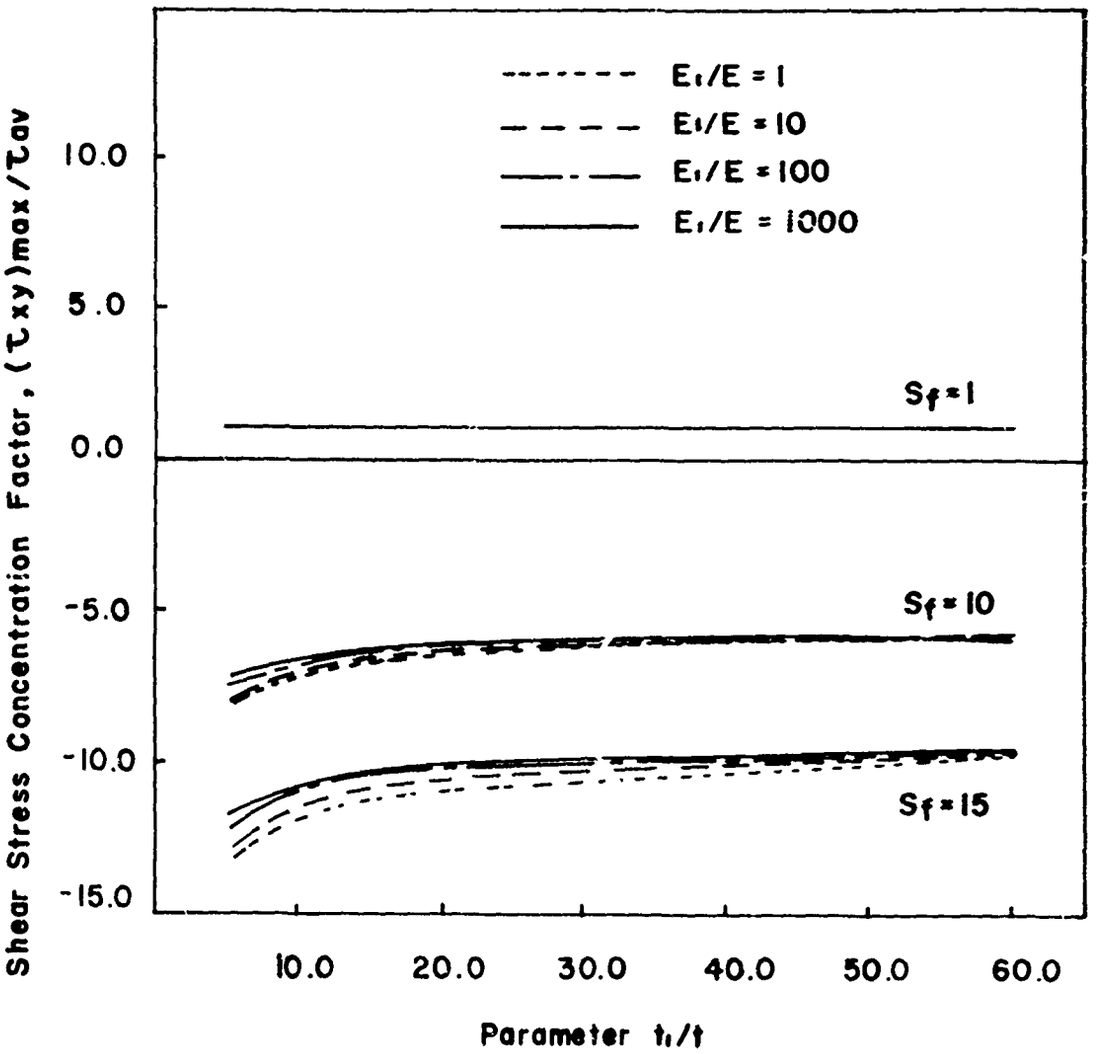

Fig. 34 Shear Stress Concentration Factor at the Interfacial Plane as a Function of t_1/t, E_1/E, and S_f, for $V_f = 2$

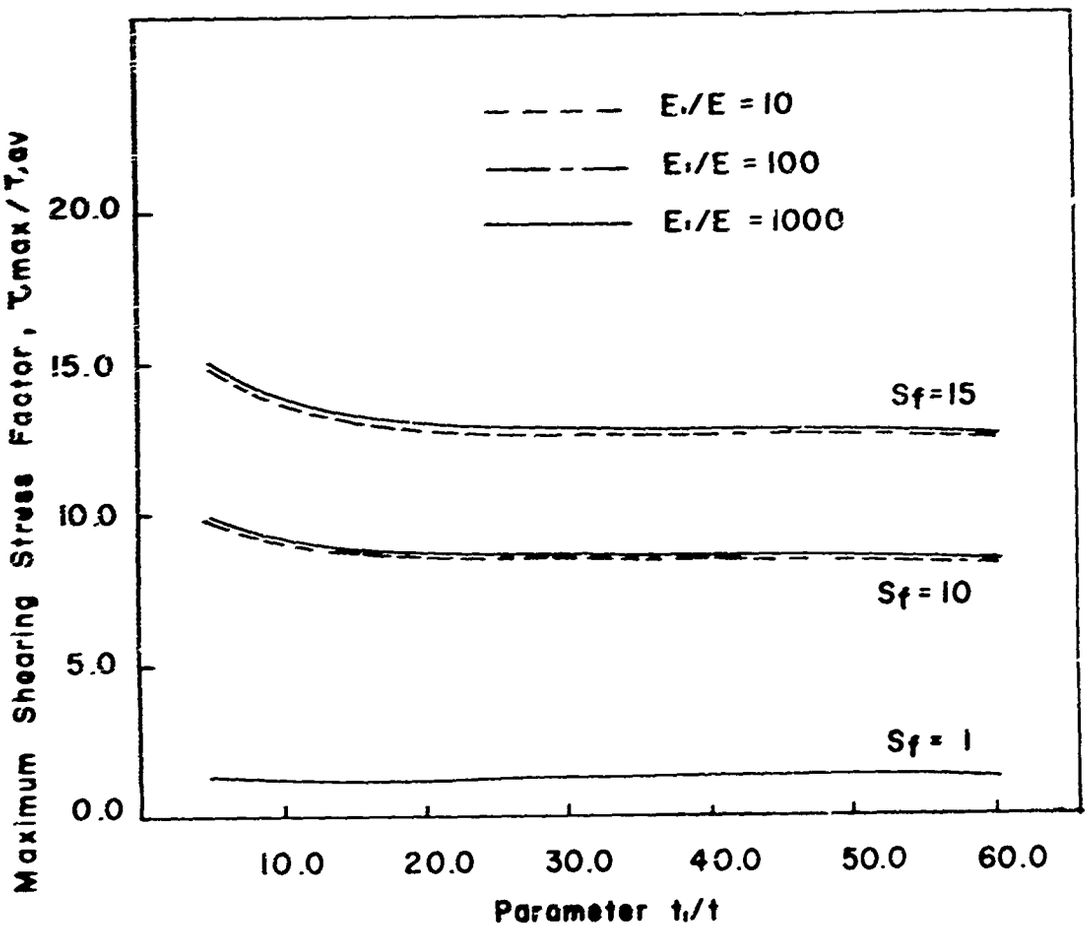

Fig. 35 Maximum Shearing Stress Factor as a Function of t_1/t, E_1/E, and S_f, for $V_f = 0$

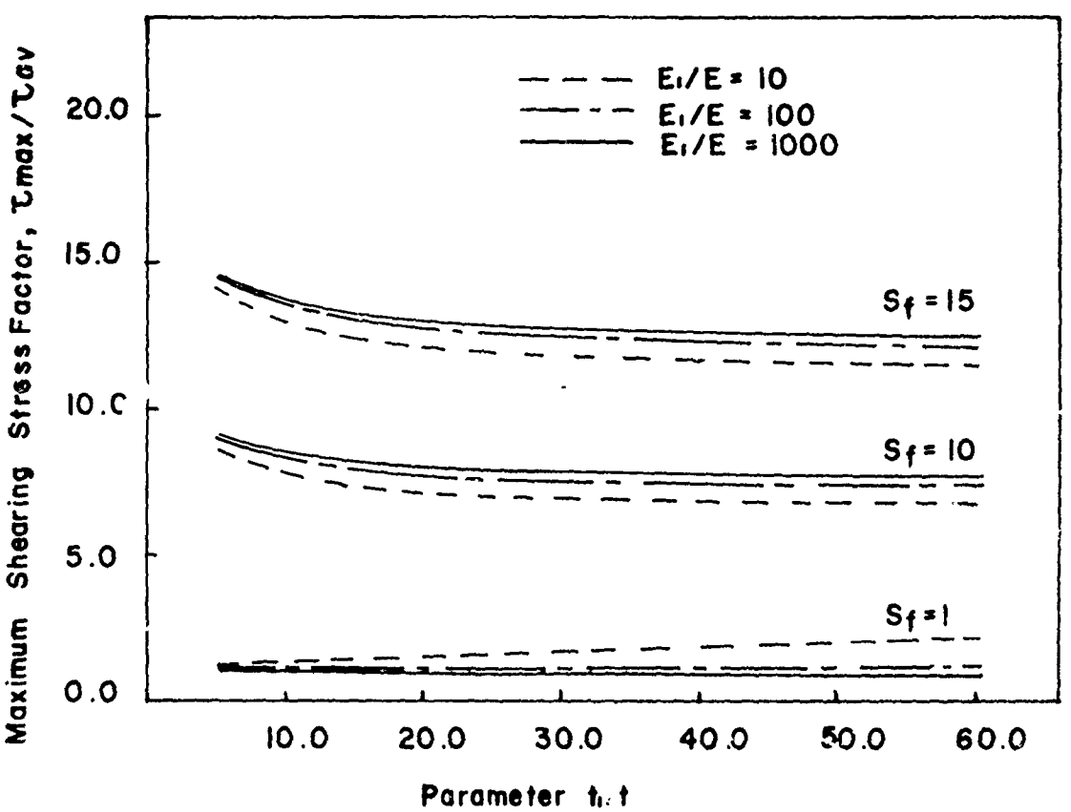

Fig. 36 Maximum Shearing Stress Factor as a Function of t_1/t, E_1/E, and S_f, for $V_f = 2$

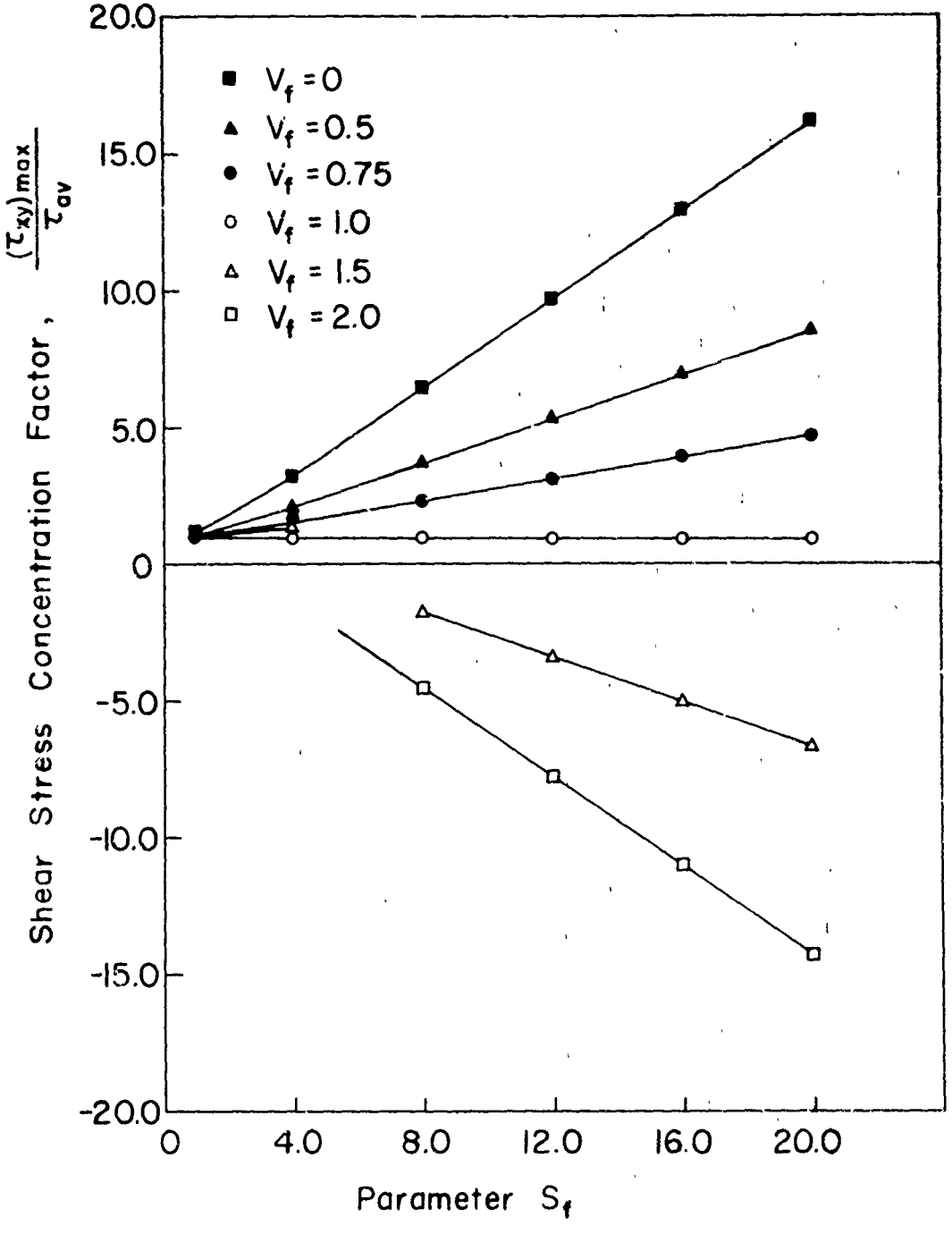

Fig. 37 Shear Stress Concentration Factor at the Midplane As a Function of S_f and V_f

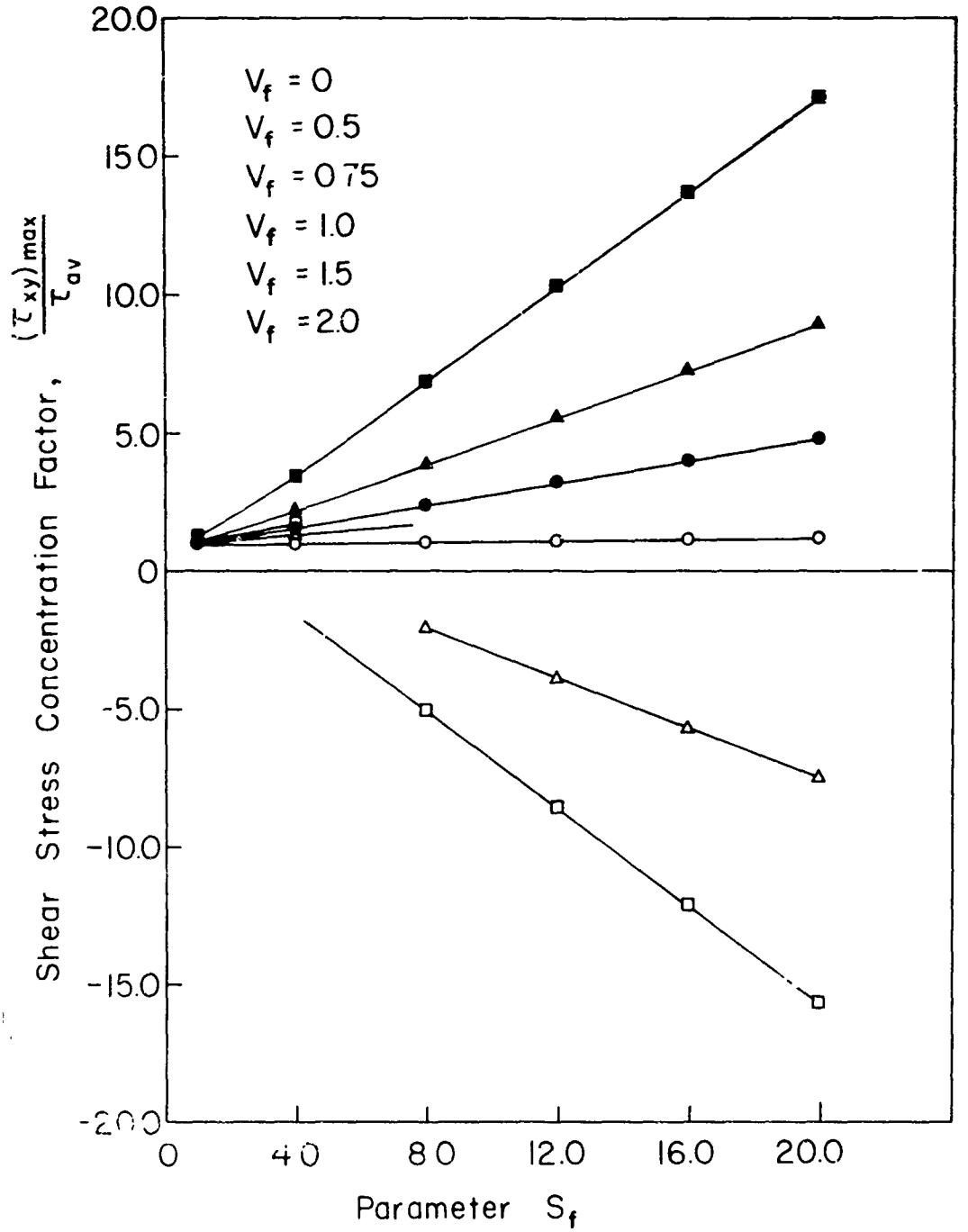

Fig 38 Shear Stress Concentration Factor at the Interfacial Plane As a Function of S_f and V_f

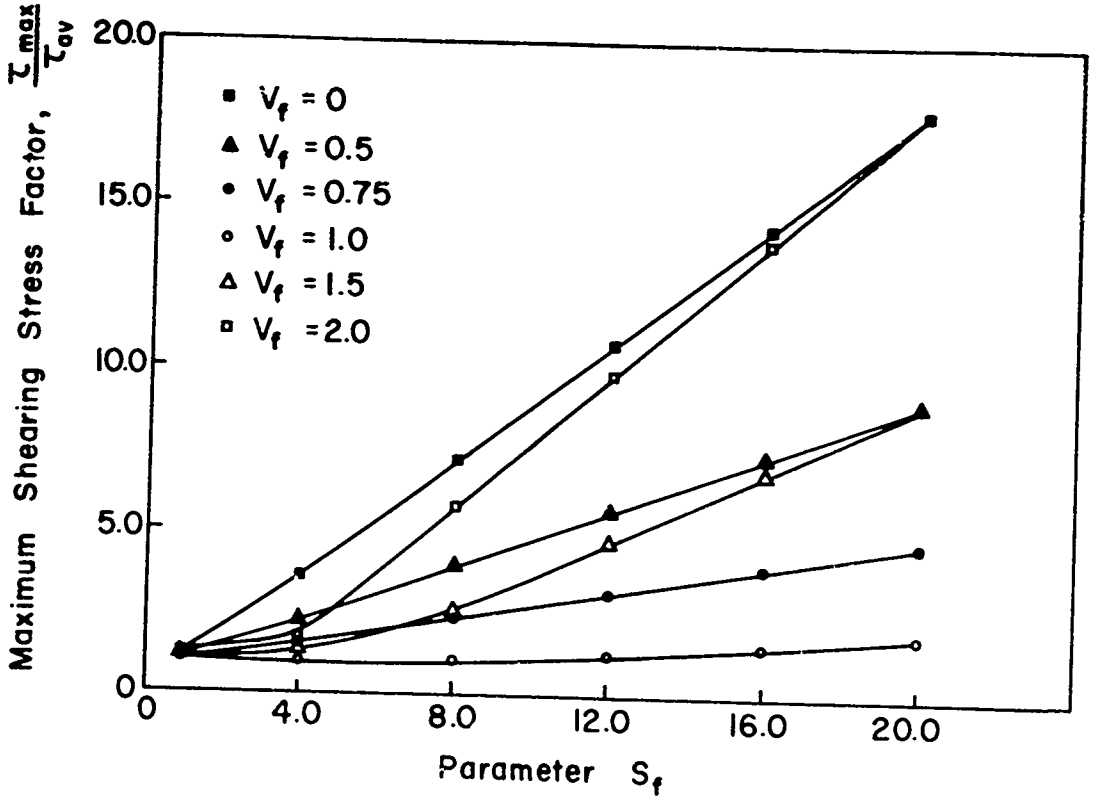

Fig. 39 Maximum Shearing Stress Factor As a Function of S_f and V_f

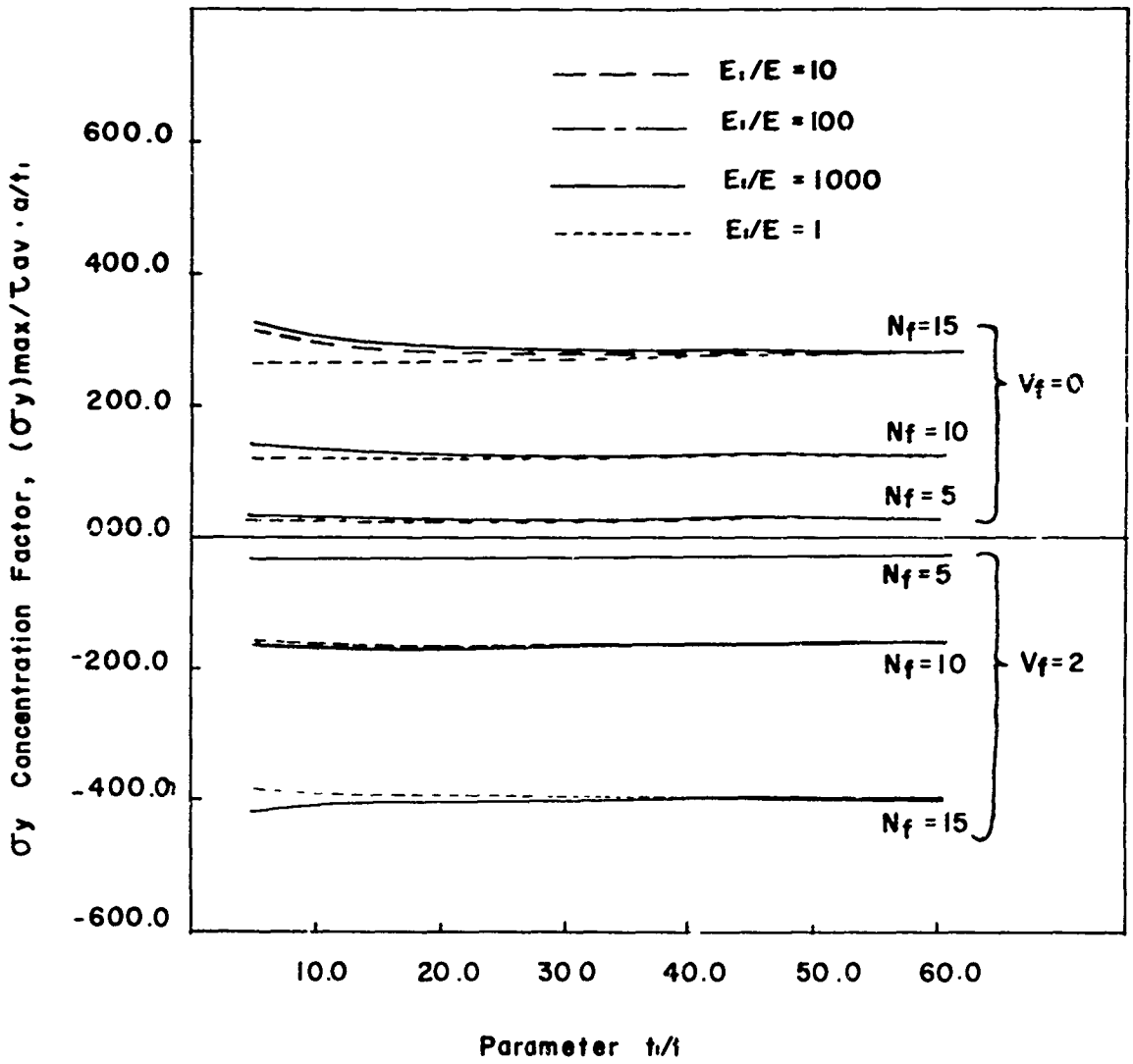

Fig. 40 σ_y Concentration Factor at the Mid-plane as a Function of t_1/t, E_1/E, N_f, and V_f

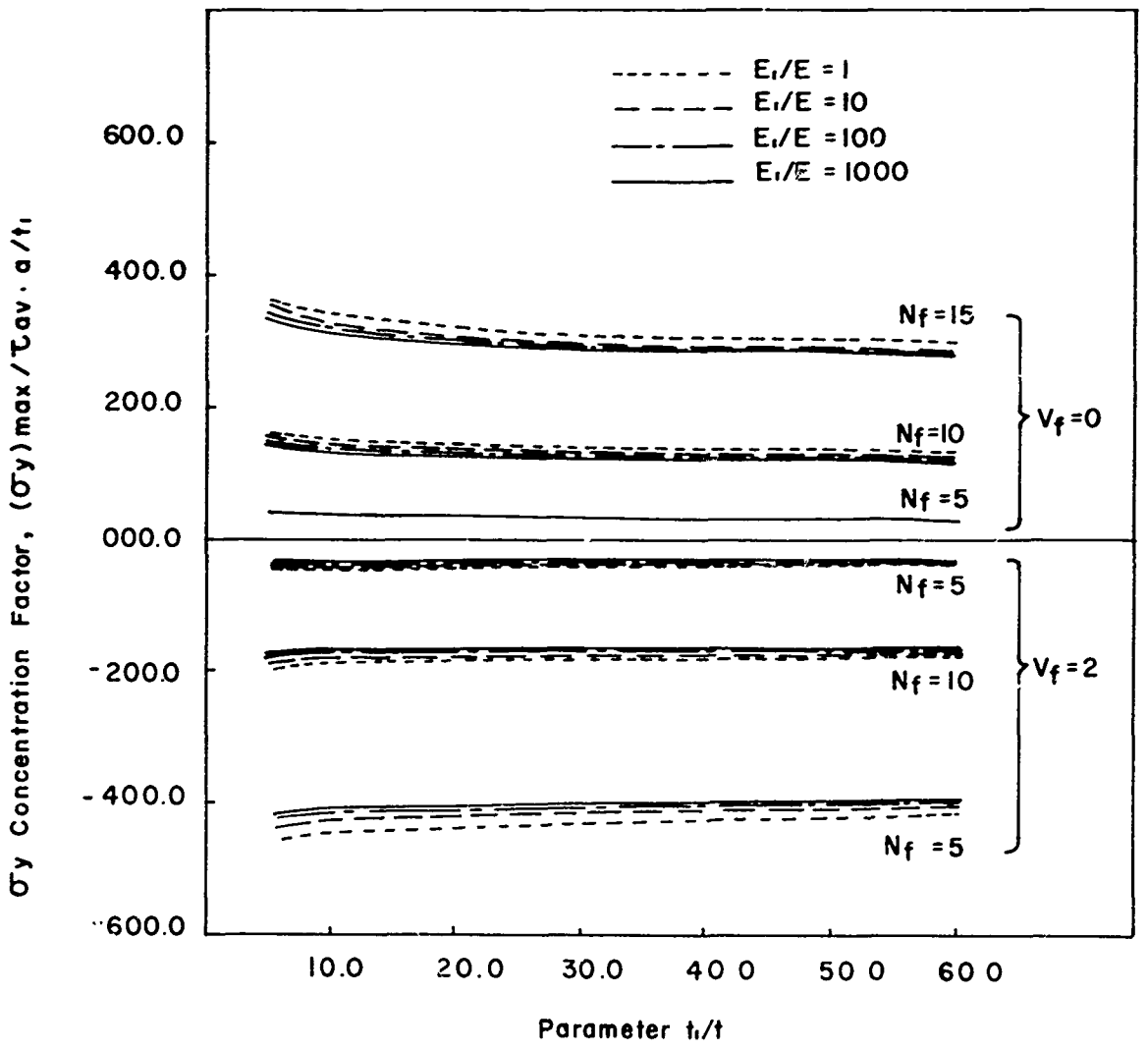

Fig. 41 σy Concentration Factor at the Interfacial plane as a Function of t_1/t, E_1/E, N_f, and V_f

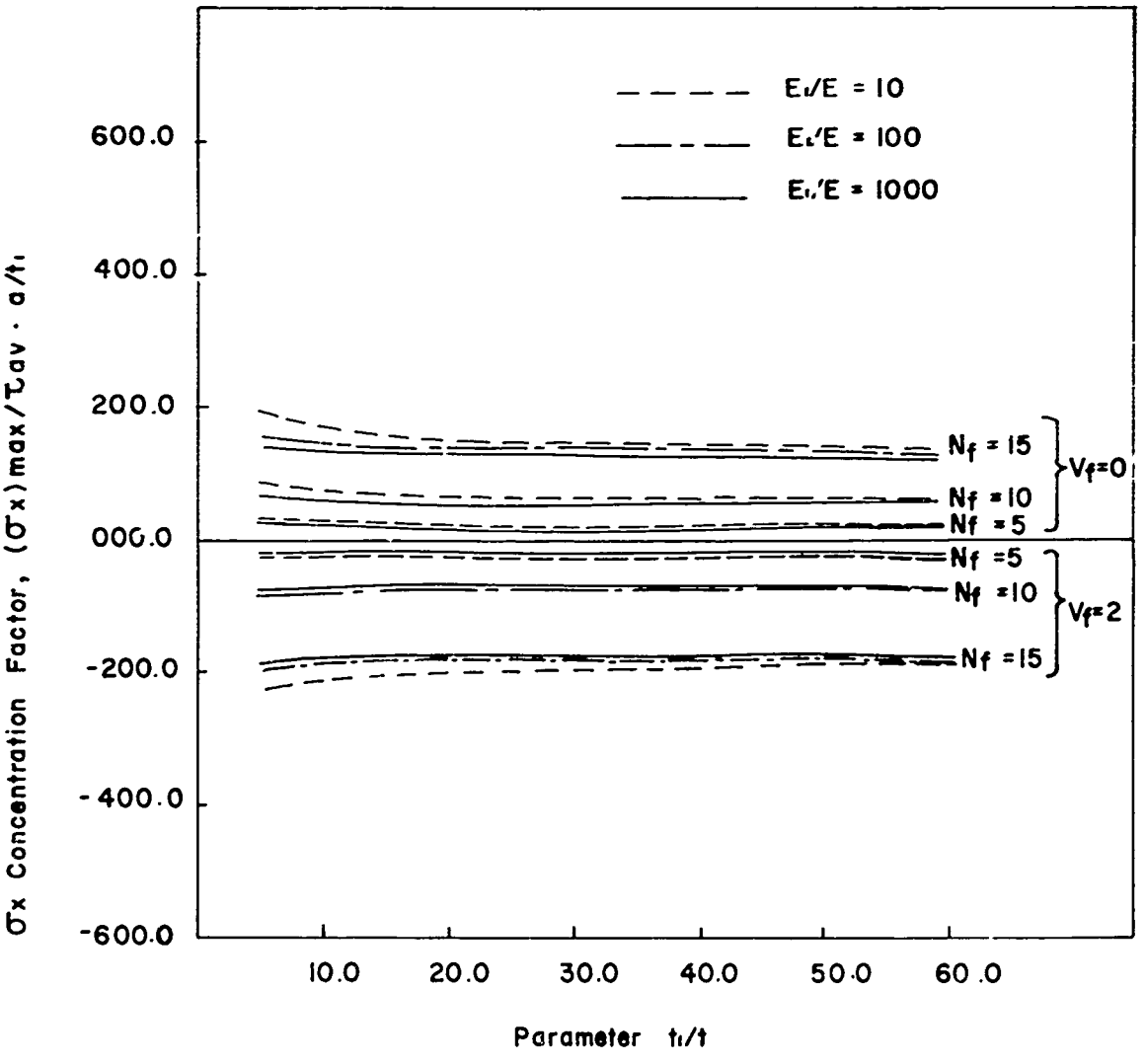

Fig.42 σx Concentration Factor at the Mid-plane as a Function of t_i/t, E_i/E, N_f, and V_f

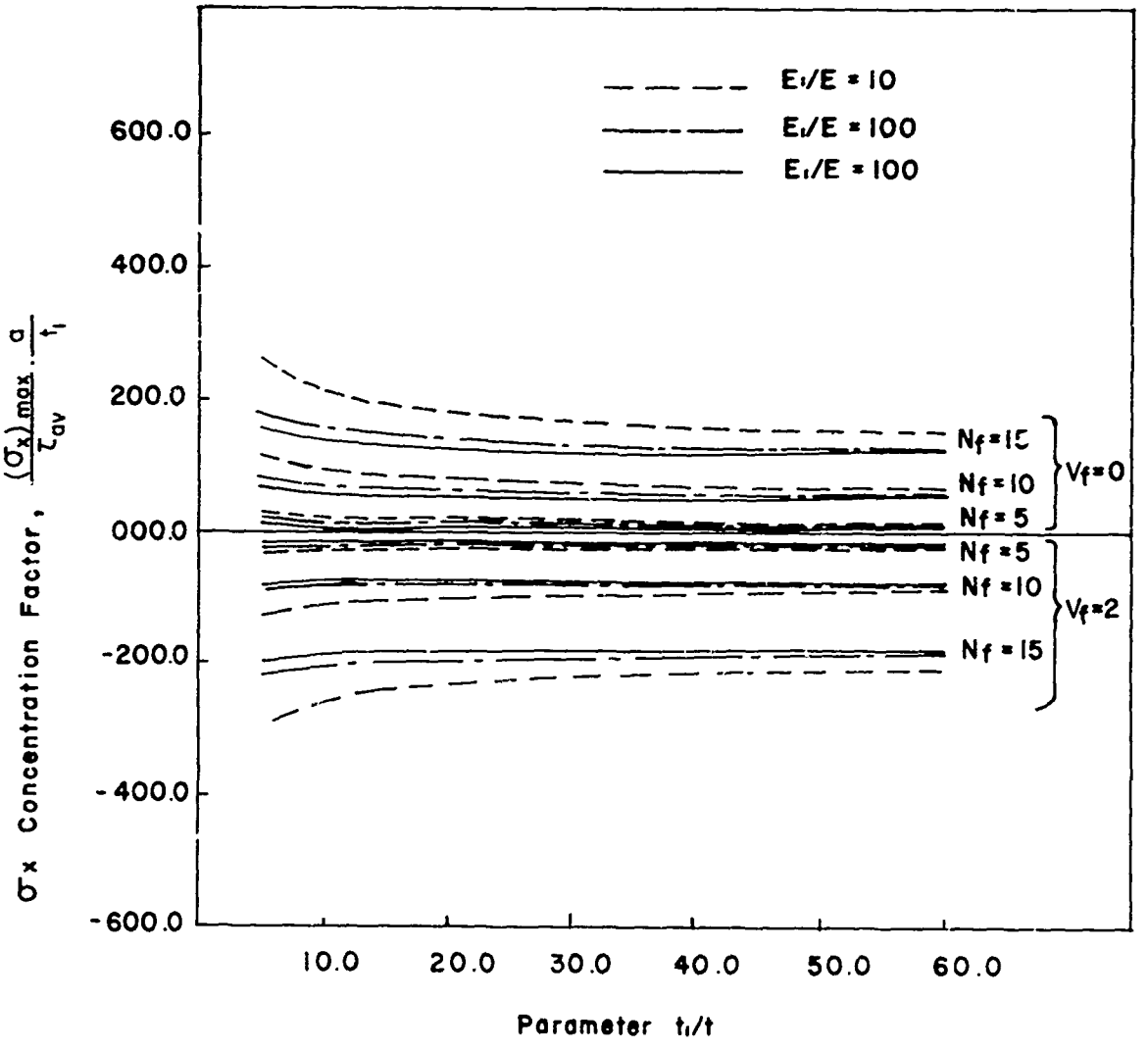

Fig. 43 σx Concentration Factor at the Interfacial plane as a Function of t_1/t, E_1/E, N_f, and V_f

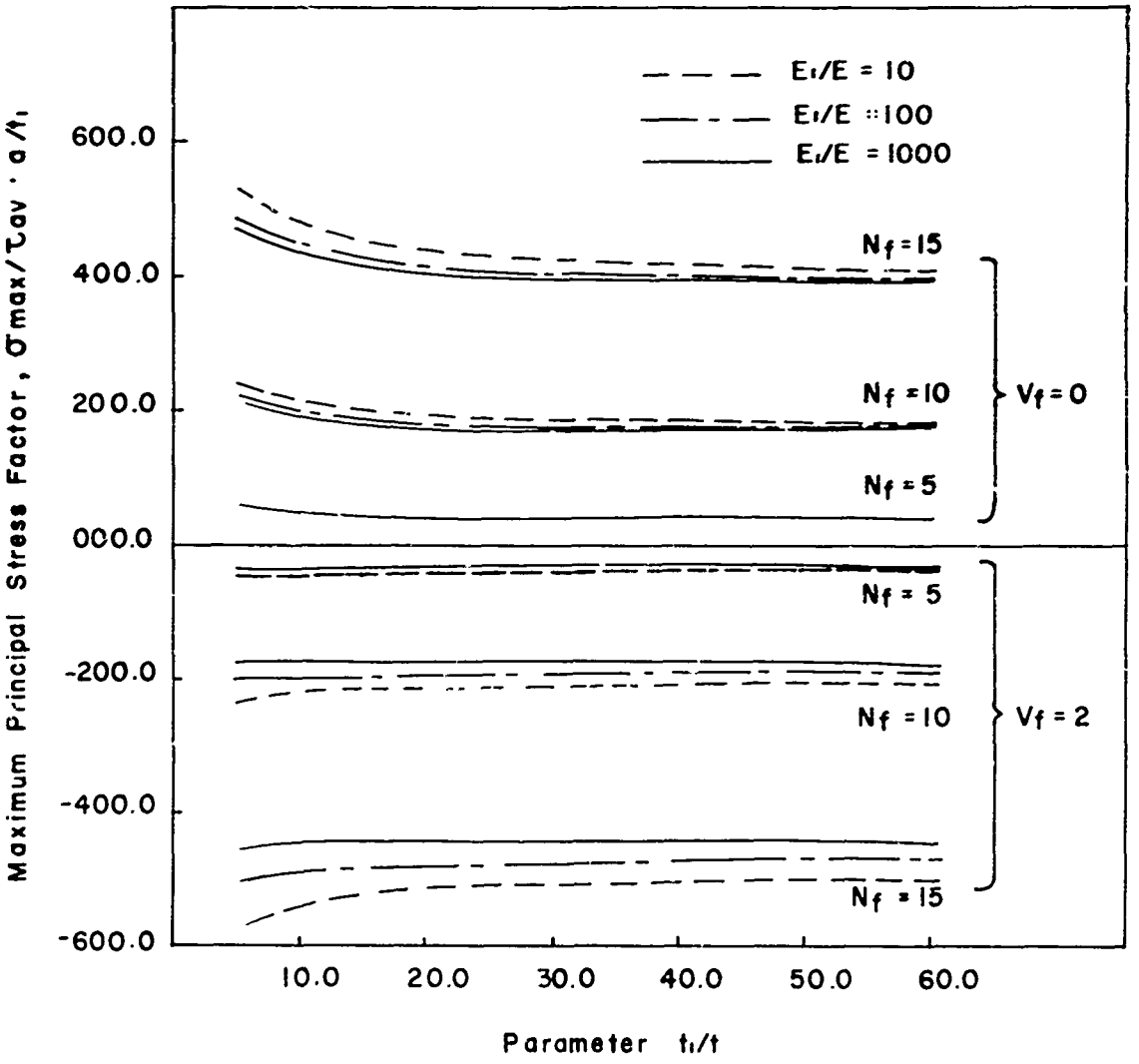

Fig. 44 Maximum Principal Stress Factor as a Function of t_1/t, E_1/E, N_f, and V_f

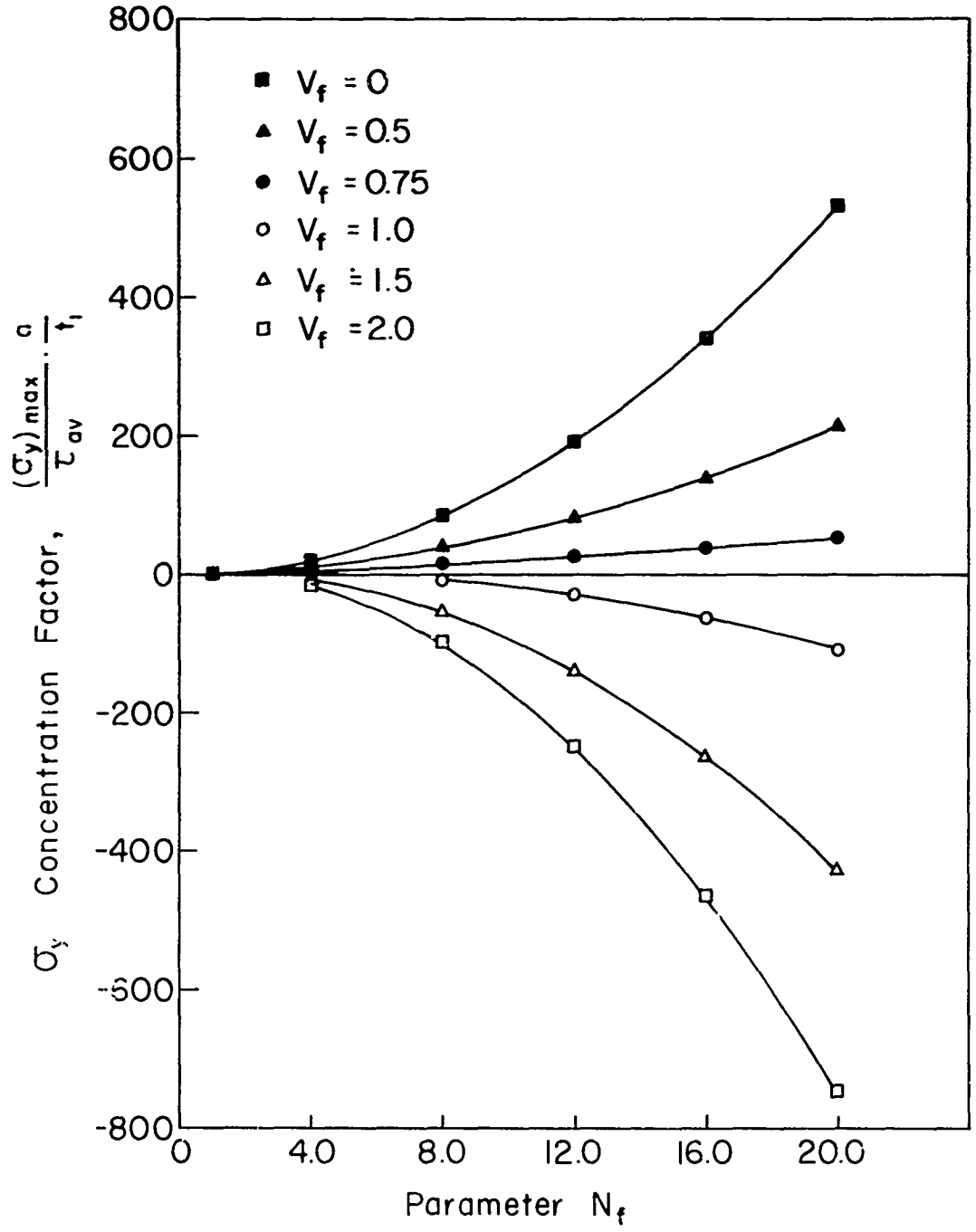

Fig. 45 σ_y Concentration Factor at the Mid-plane As a Function of N_f and V_f

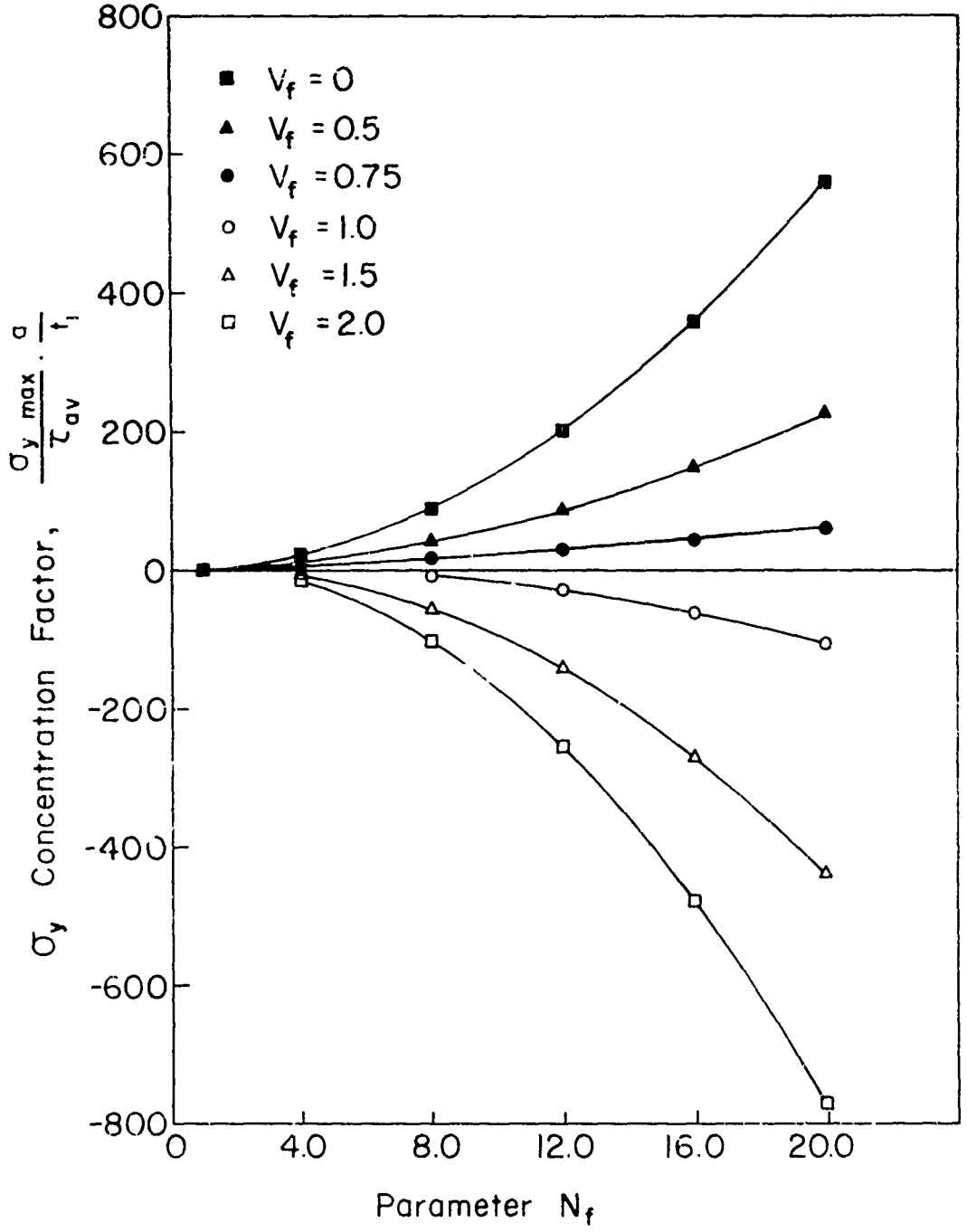

Fig 46 σ_y Concentration Factor at the Interfacial Plane As a Function of N_f and V_f

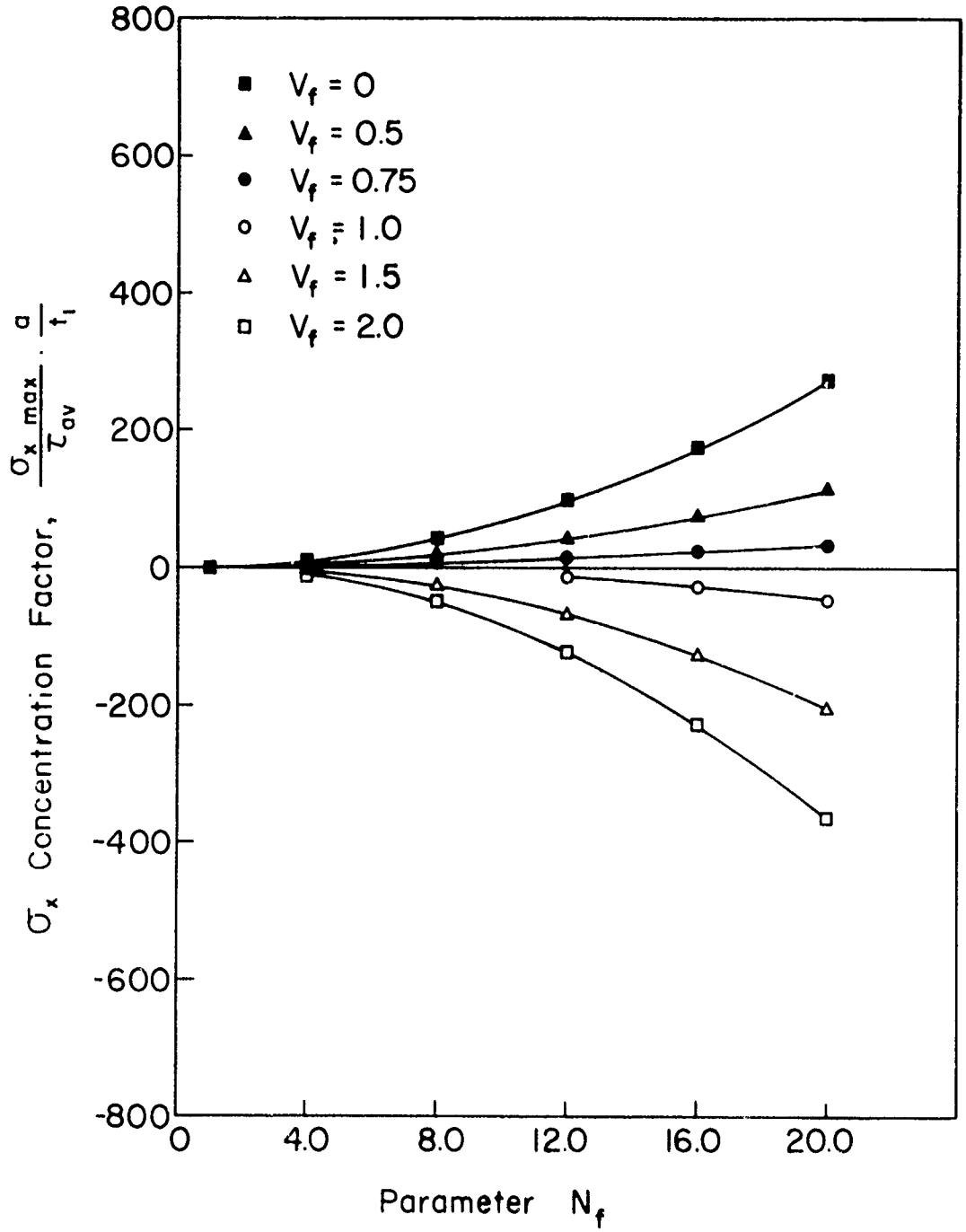

Fig. 47 σ_x Concentration Factor at the Mid-plane As a Function of N_f and V_f

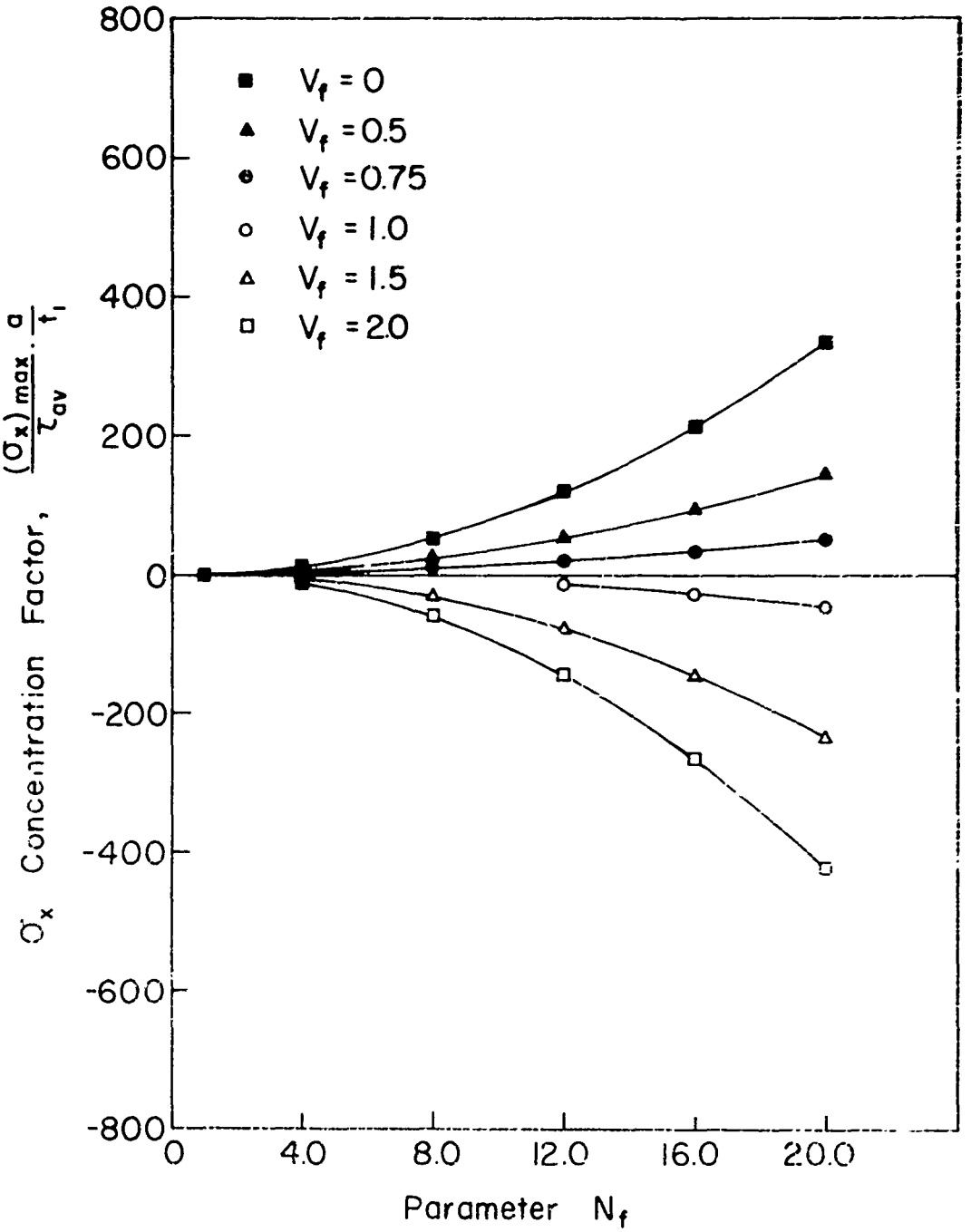

Fig. 48 σ_x Concentration Factor at the Interfacial Plane As a Function of N_f and V_f

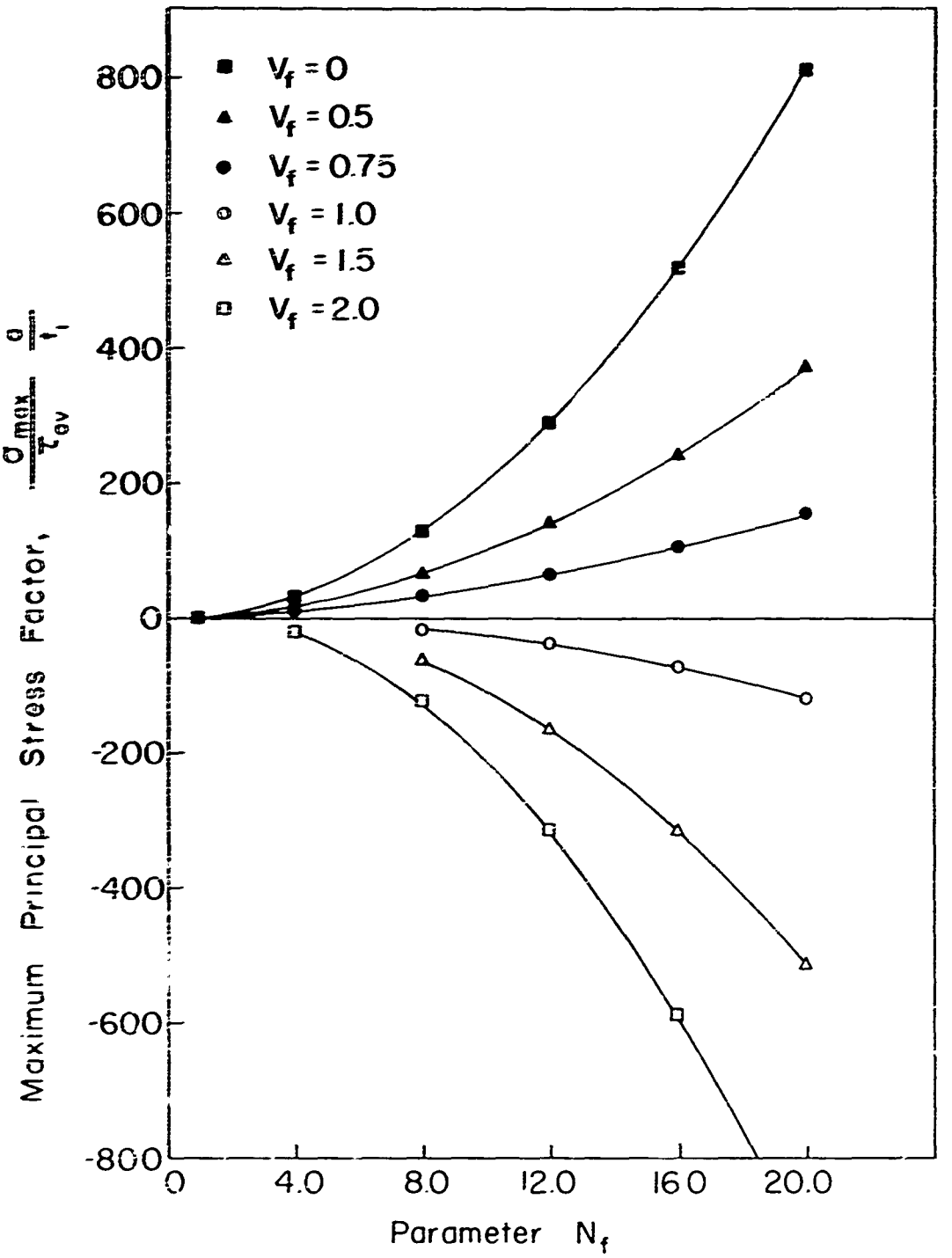

Fig. 49 Maximum Principal Stress Factor As a Function of N_f and V_f

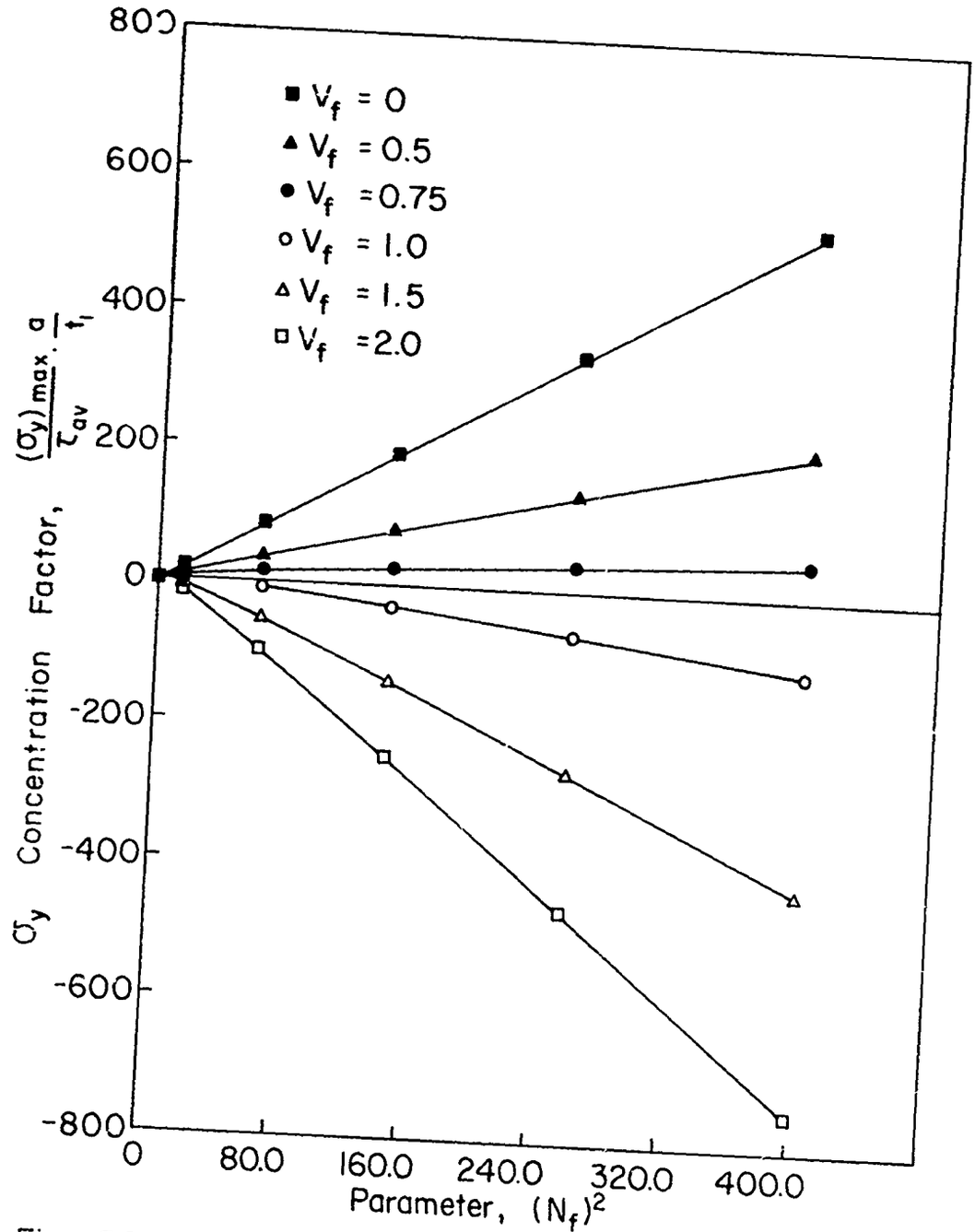

Fig. 50 σ_y Concentration Factor at the Mid-plane As a Function of $(N_f)^2$ and V_f

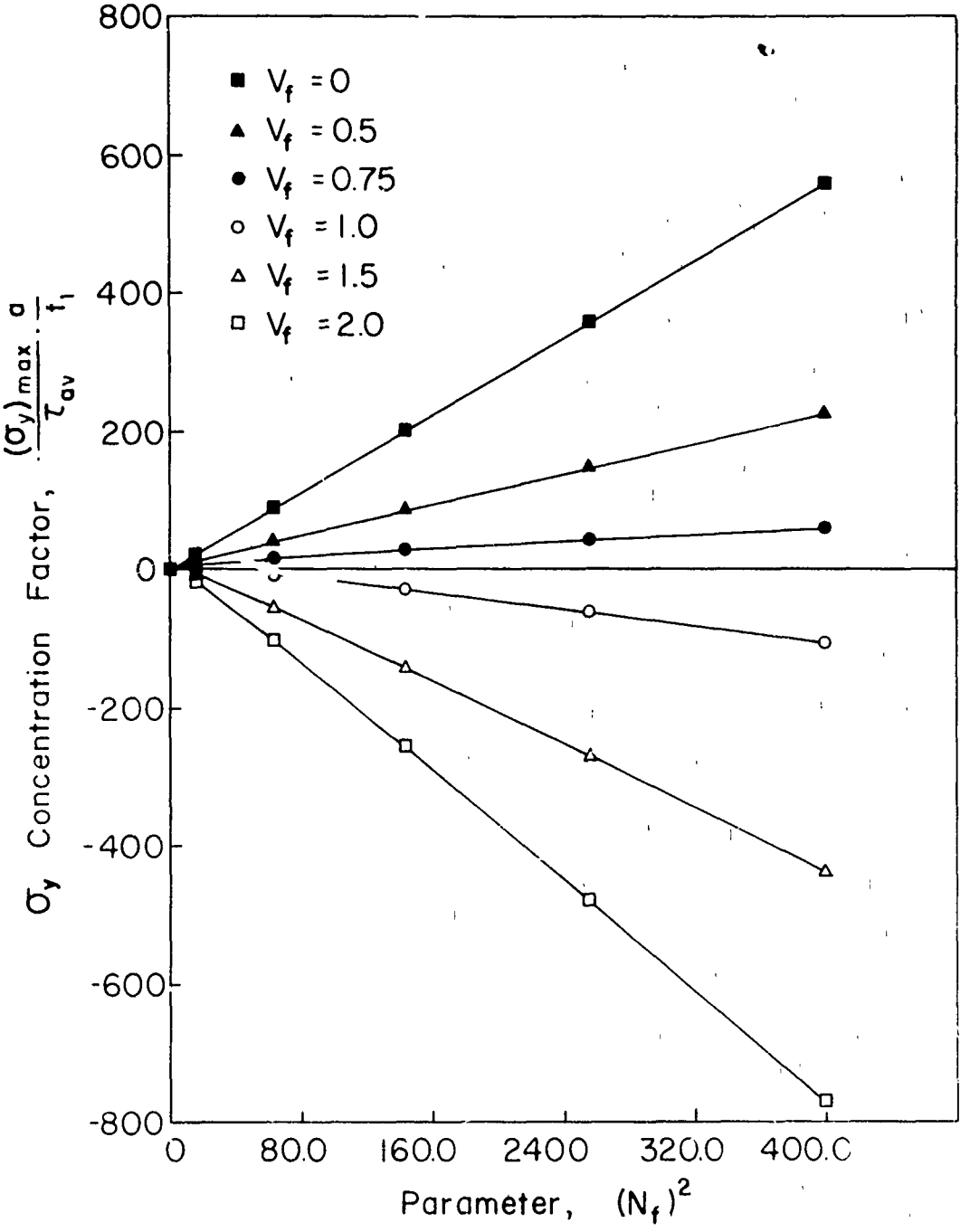

Fig. 51 σ_y Concentration Factor at the Interfacial Plane As a Function of $(N_f)^2$ and V_f

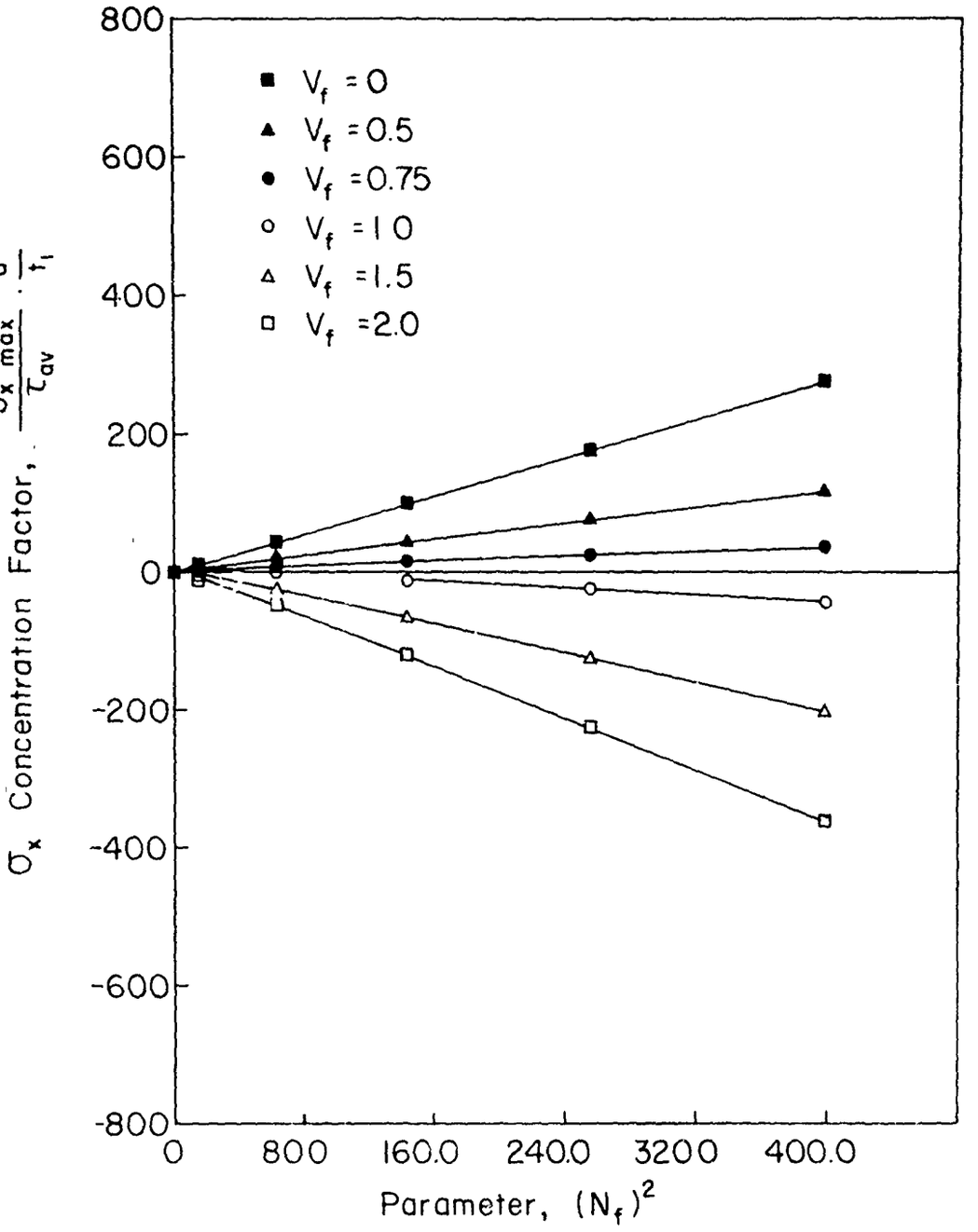

Fig. 52 σ_x Concentration Factor at the Mid-plane As a Function of $(N_f)^2$ and V_f

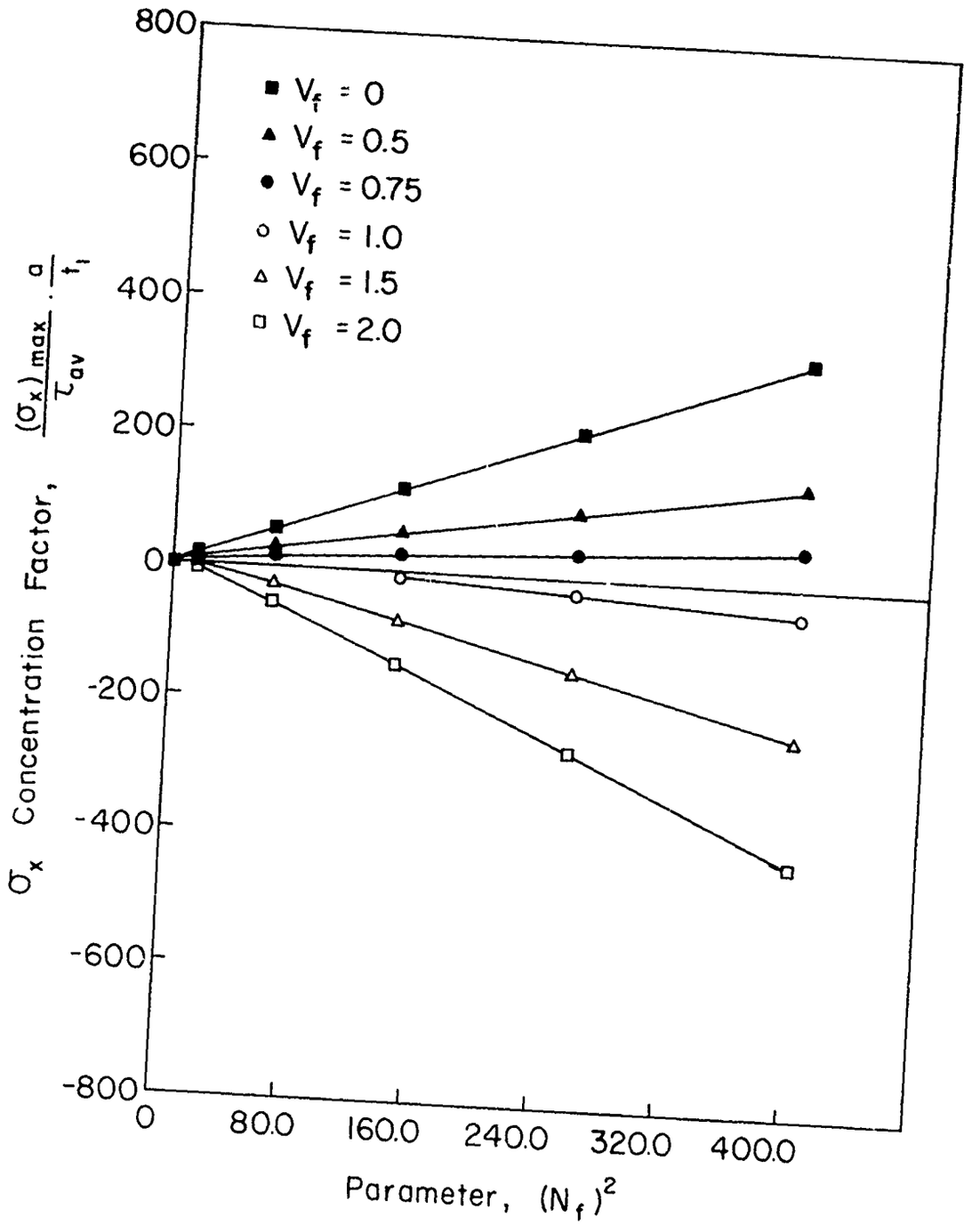

Fig. 53 σ_x Concentration Factor at the Interfacial Plane As a Function of $(N_f)^2$ and V_f

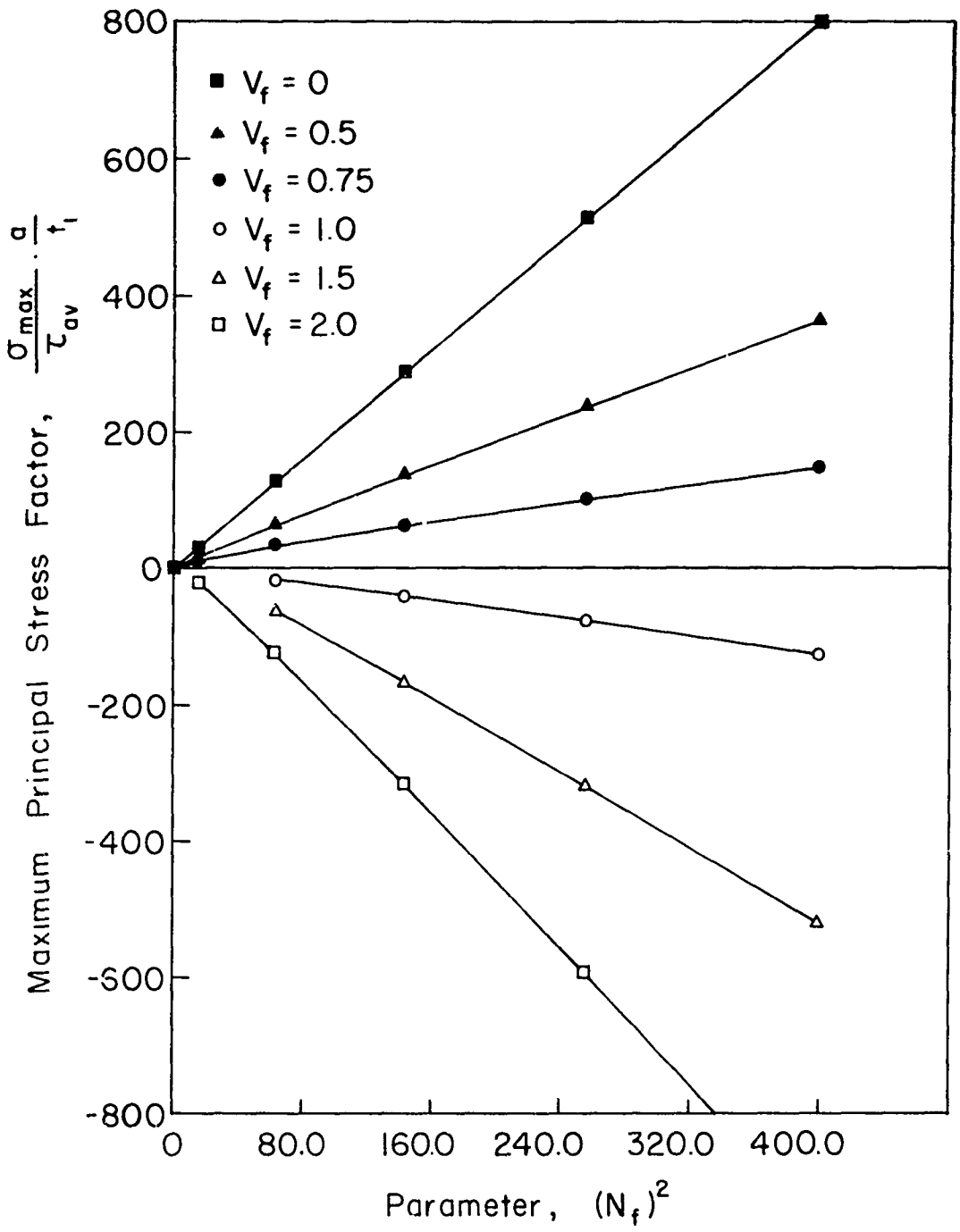

Fig. 54 Maximum Principal Stress Factor As a Function of $(N_f)^2$ and V_f

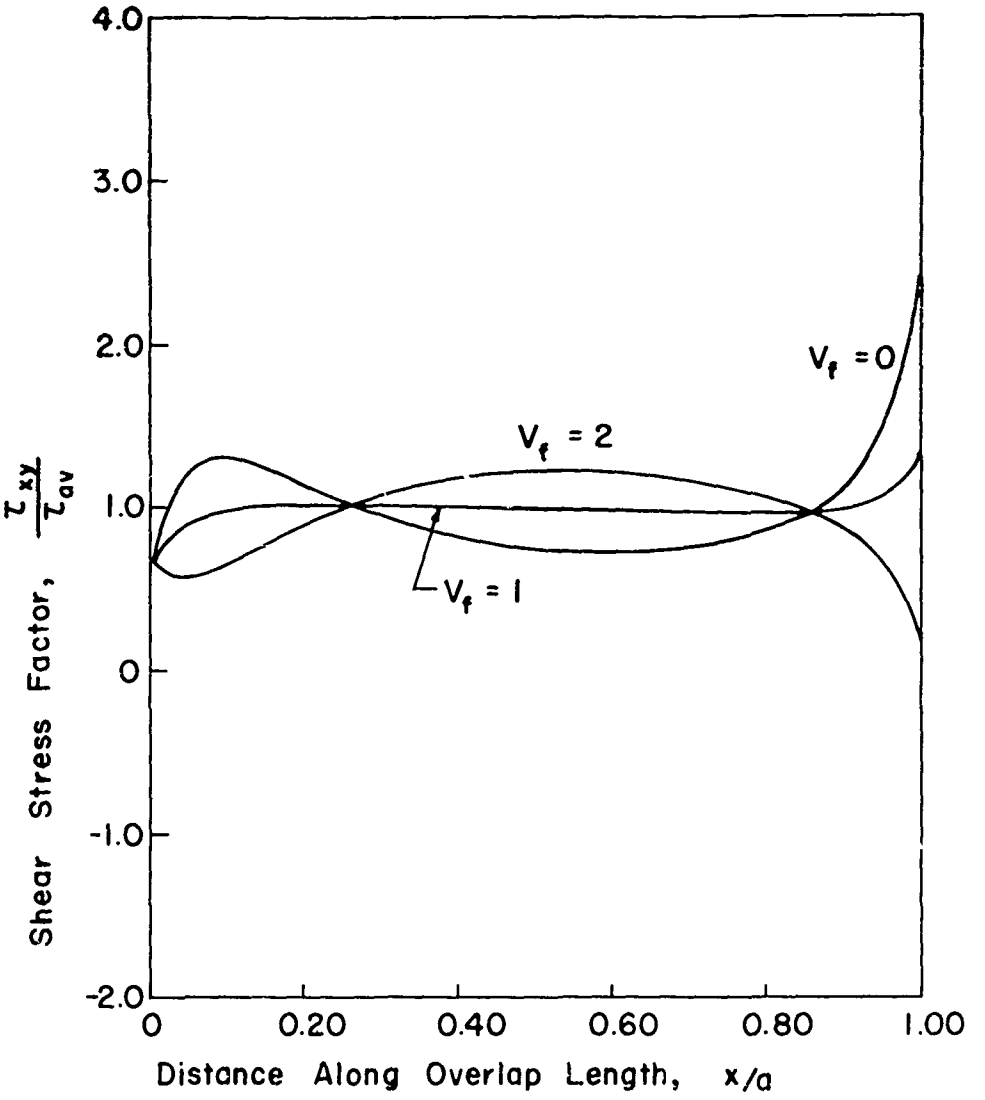

Fig. 55 τ_{xy} Distribution at Interfacial Plane ($y = t/2$) As a Function of V_f

($E_{l/E} = 20$, $t_{l/t} = 4$, $t_{l/a} = .3$, $m = 2$)

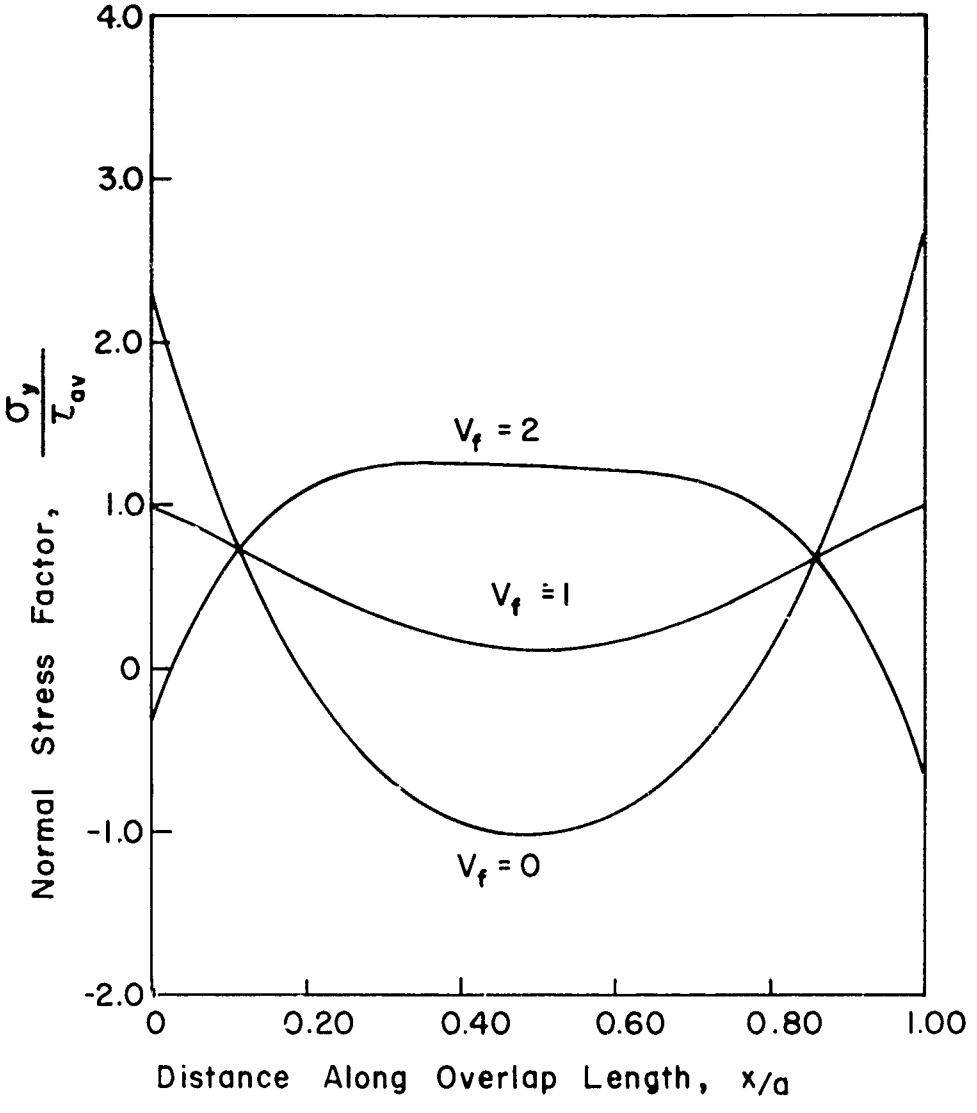

Fig. 56 σ_y Distribution at Interfacial Plane ($y = t/2$)
As a Function of V_f
($E_1/E = 20$, $t_1/t = 4$, $t_1/a = .3$, $m = 2$)

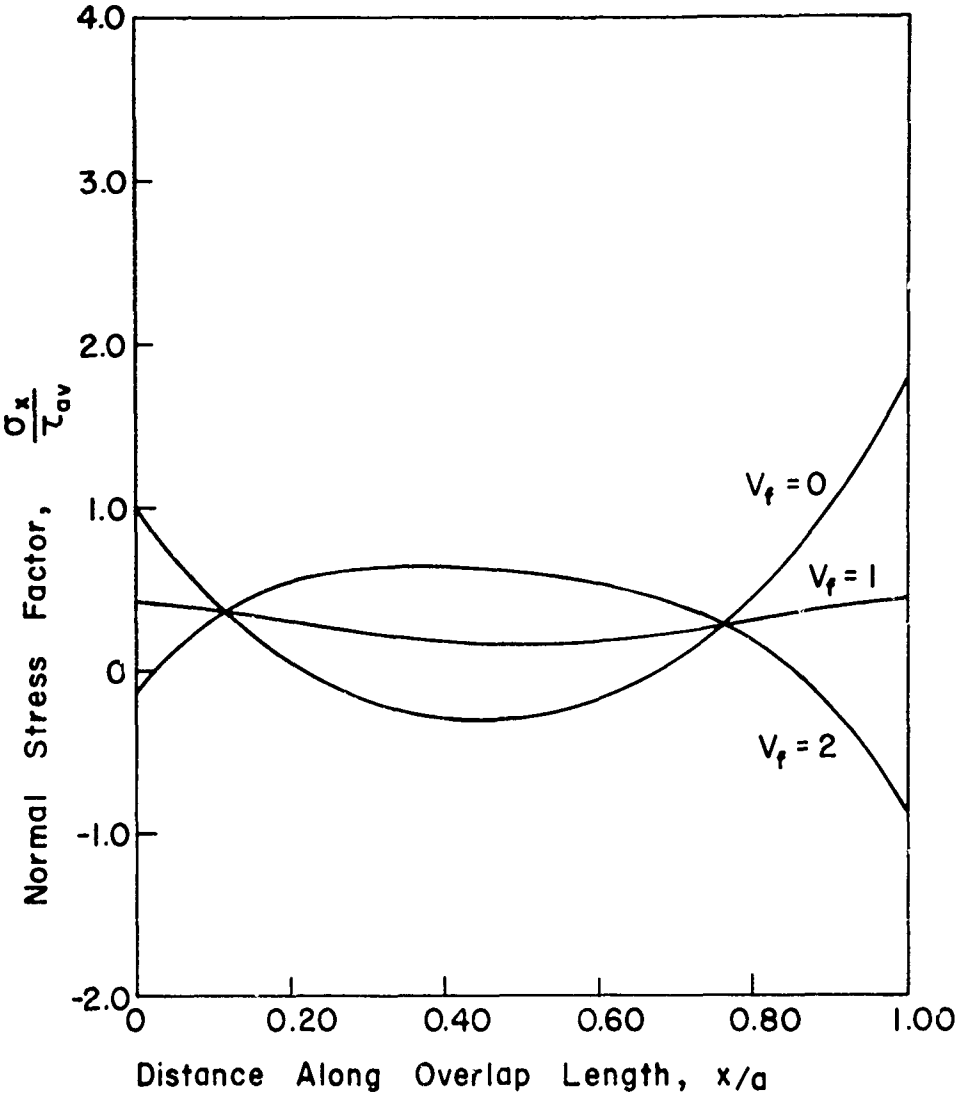

Fig. 57 σ_x Distribution at Interfacial Plane ($y = t/2$) As a Function of V_f ($E_{1/E} = 20$, $t_{1/t} = 4$, $t_{1/a} = .3$, $m = 2$)

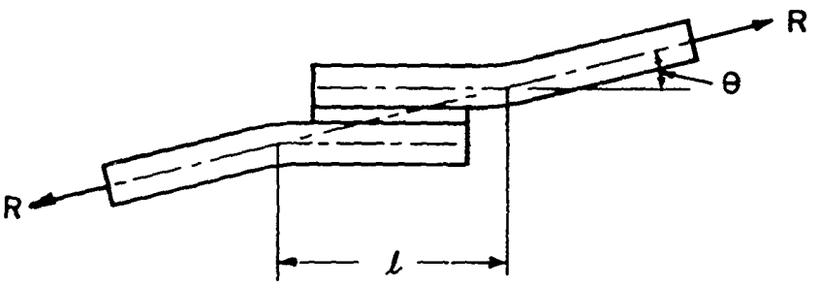

(a)

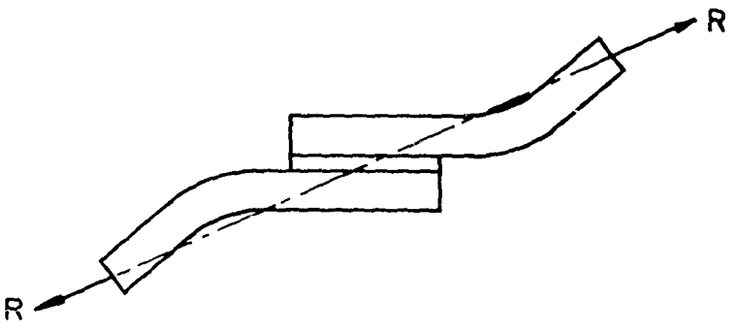

(b)

Fig. 58 Design of Lap Joint
(a) Pull Along the Adherends,
(b) Loading for $V_f = 1$

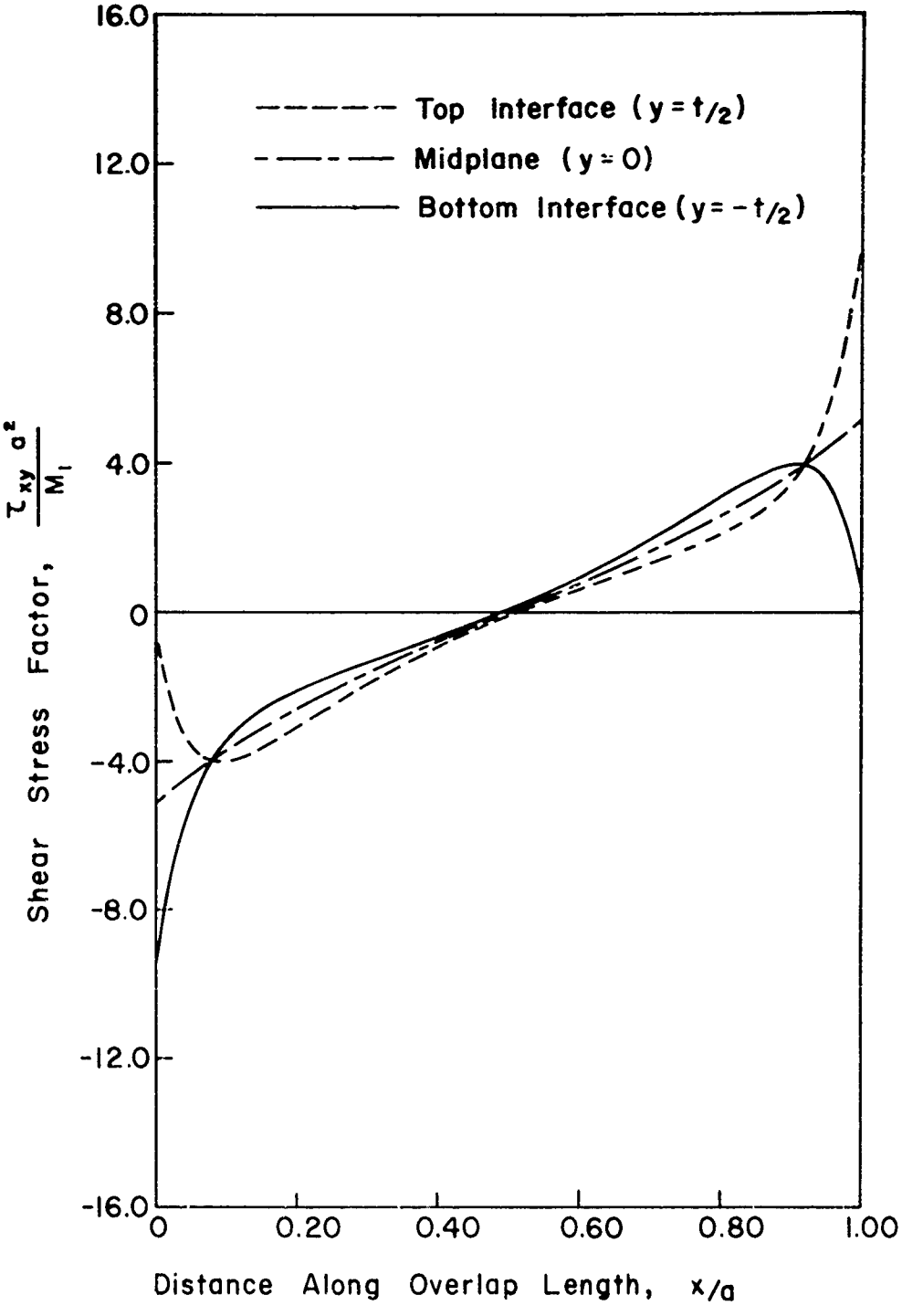

Fig. 59 τ_{xy} for Joint Loaded in Pure Moment
($E_{1/E} = 20$, $t_{1/t} = 4$, $\gamma_{1/a} = .3$, $m = 2$)

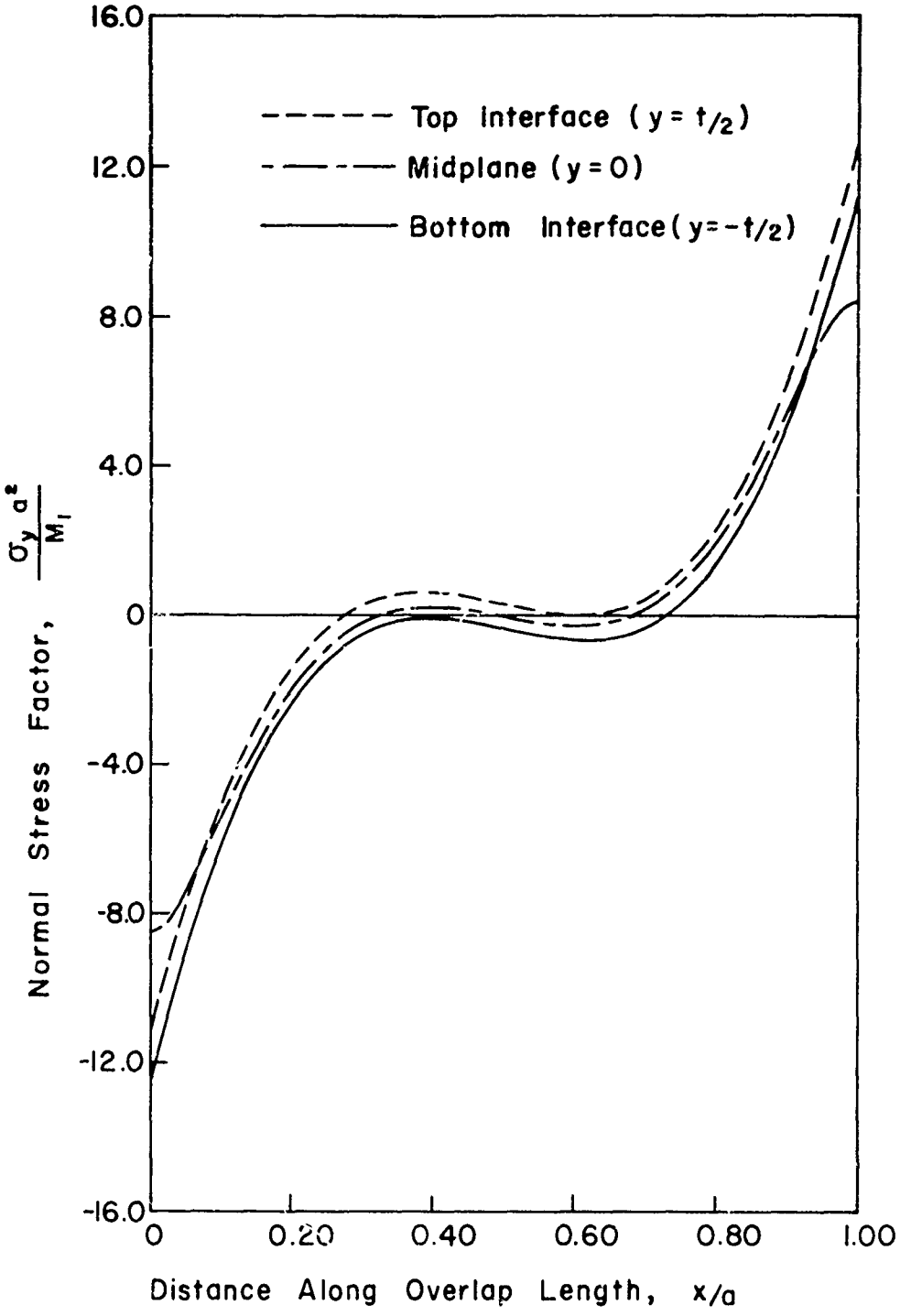

Fig. 60 σ_y for Joint Loaded in Pure Moment
($E_1/E = 20$, $t_1/t = 4$, $t_1/a = .3$, $m = 2$)

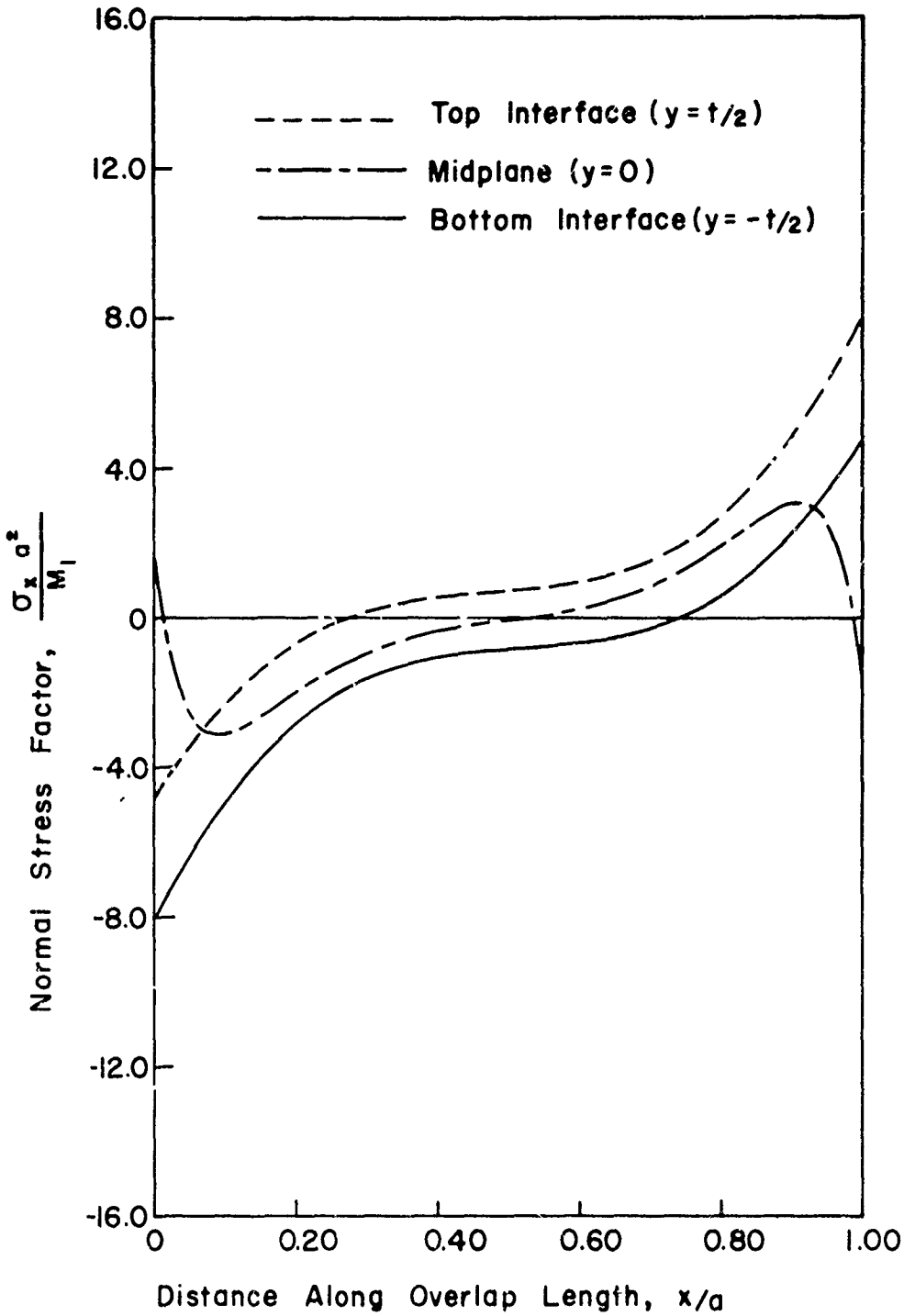

Fig. 61 σ_x for Joint Loaded in Pure Moment
($E_{1/E} = 20$, $t_{1/t} = 4$, $t_{1/a} = .3$, $m = 2$)

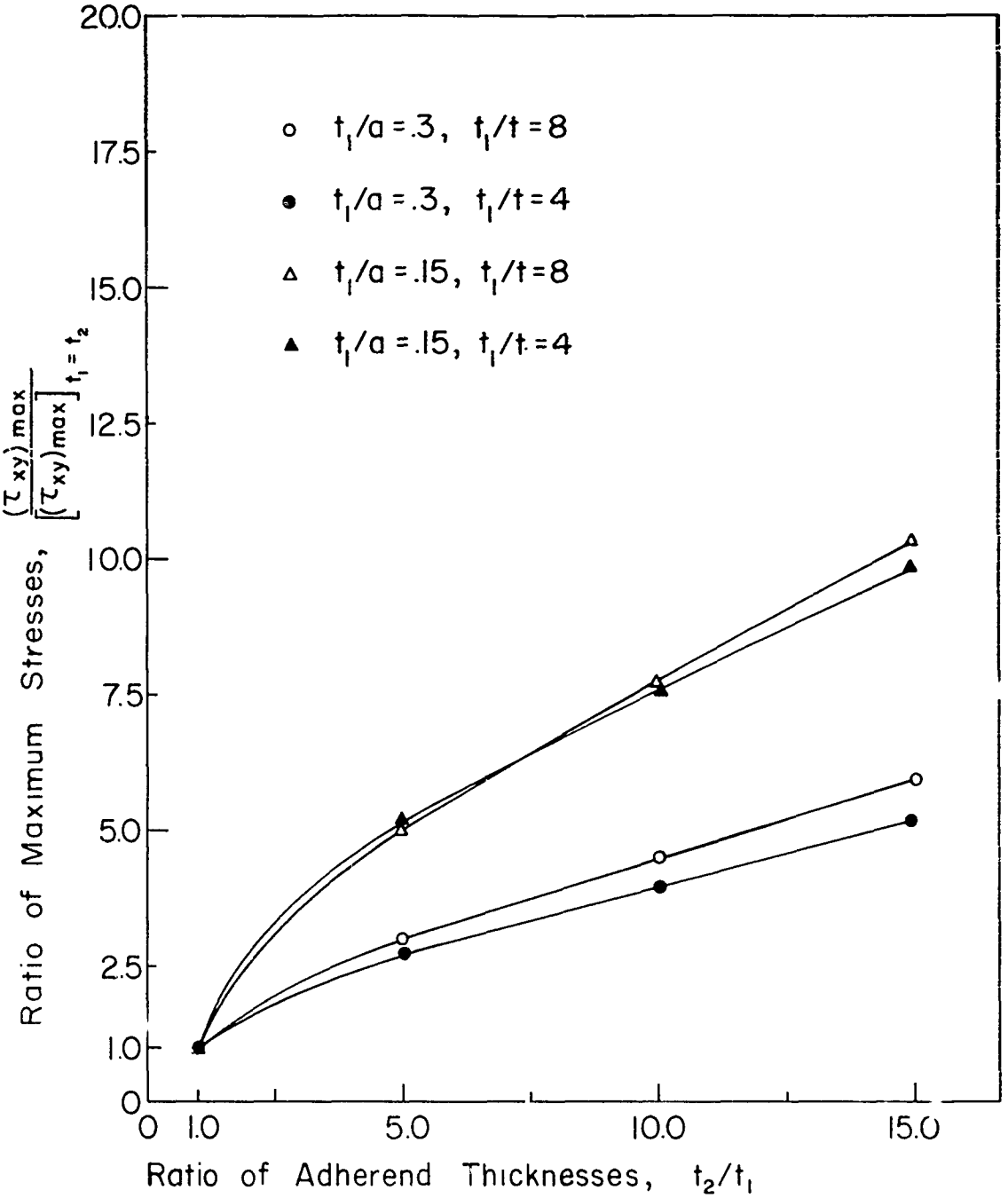

Fig. 62 $(\tau_{xy})_{max}$ in Non-Identical Adherend Joint for V=0

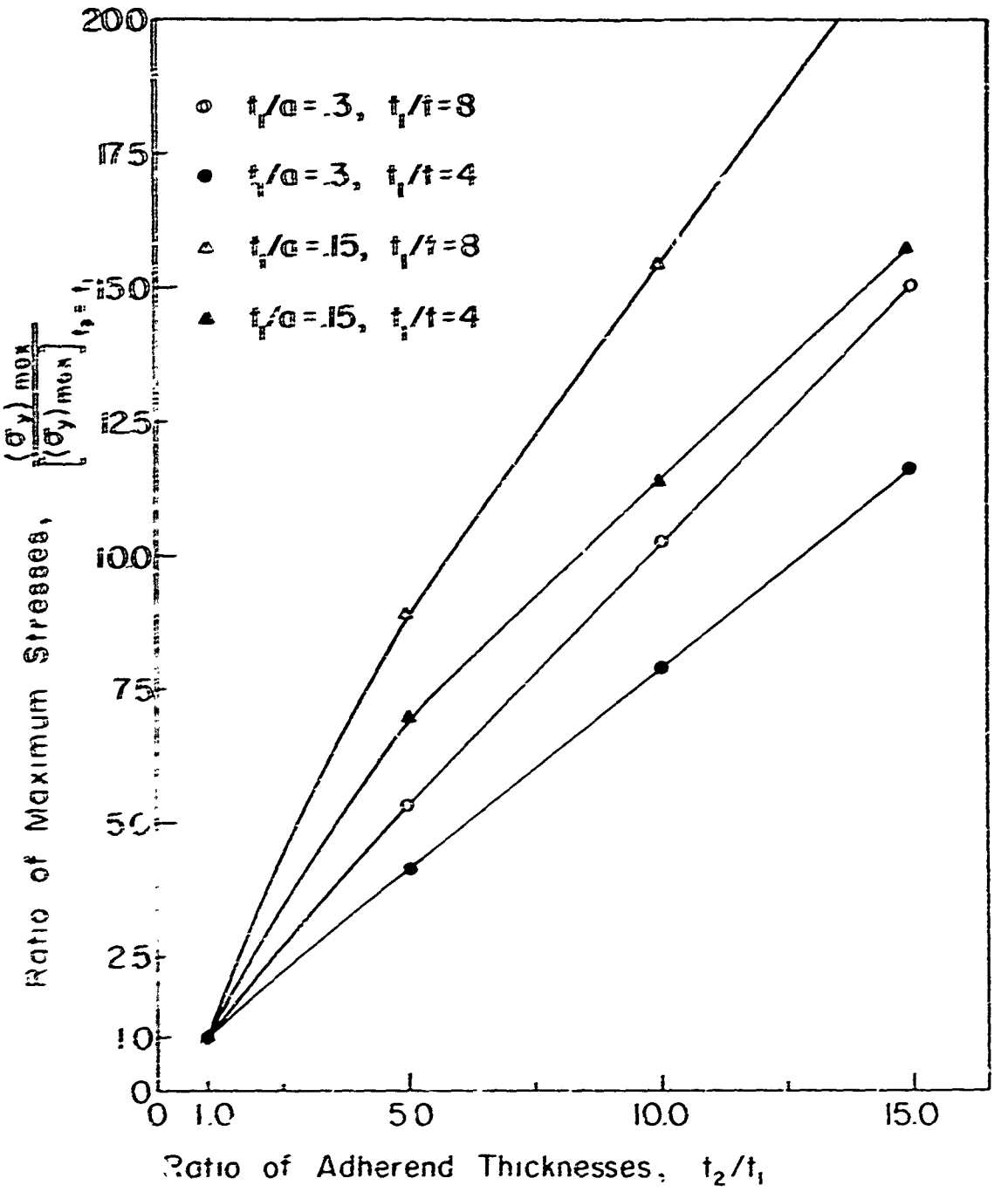

Fig 63 $(\sigma_y)_{max}$ in Non-Identical Adherend Joint or V = 0

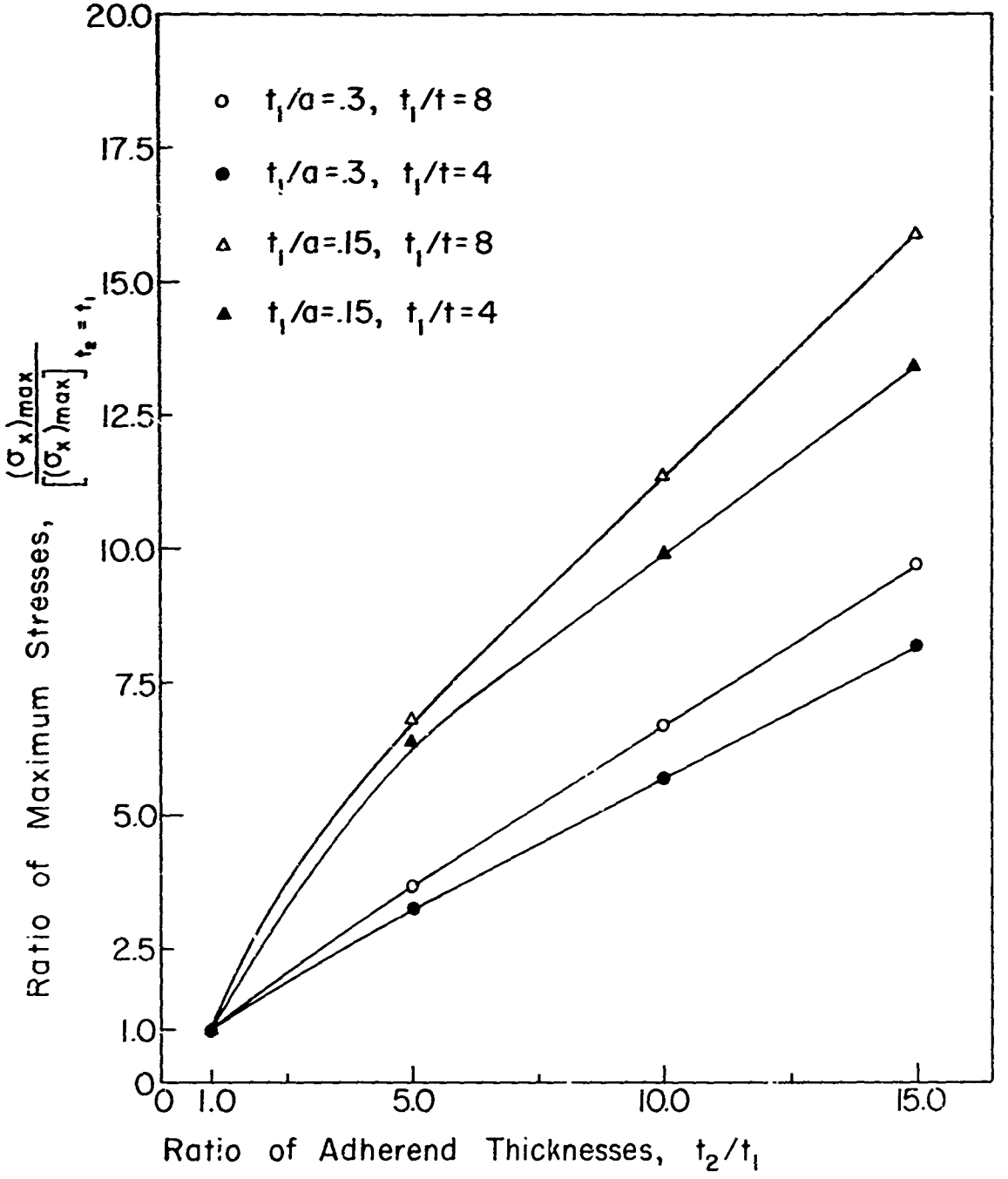

Fig. 64 $(\sigma_x)_{max}$ in Non-Identical Adherend Joint for V = 0

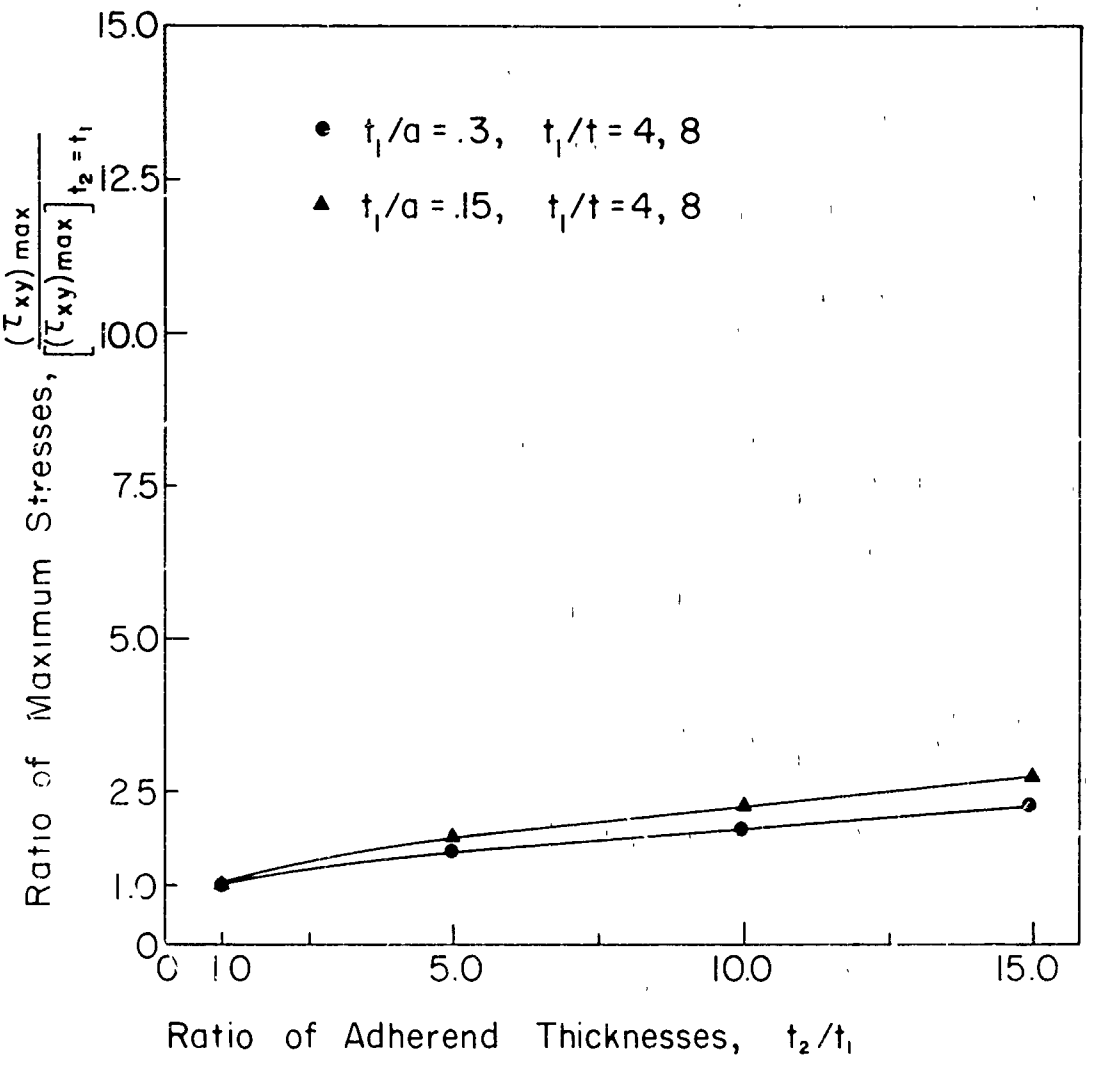

Fig. 65 $(\tau_{xy})_{max}$ in Non-Identical Adherend Joint for $M_1 = M_2 = 0$

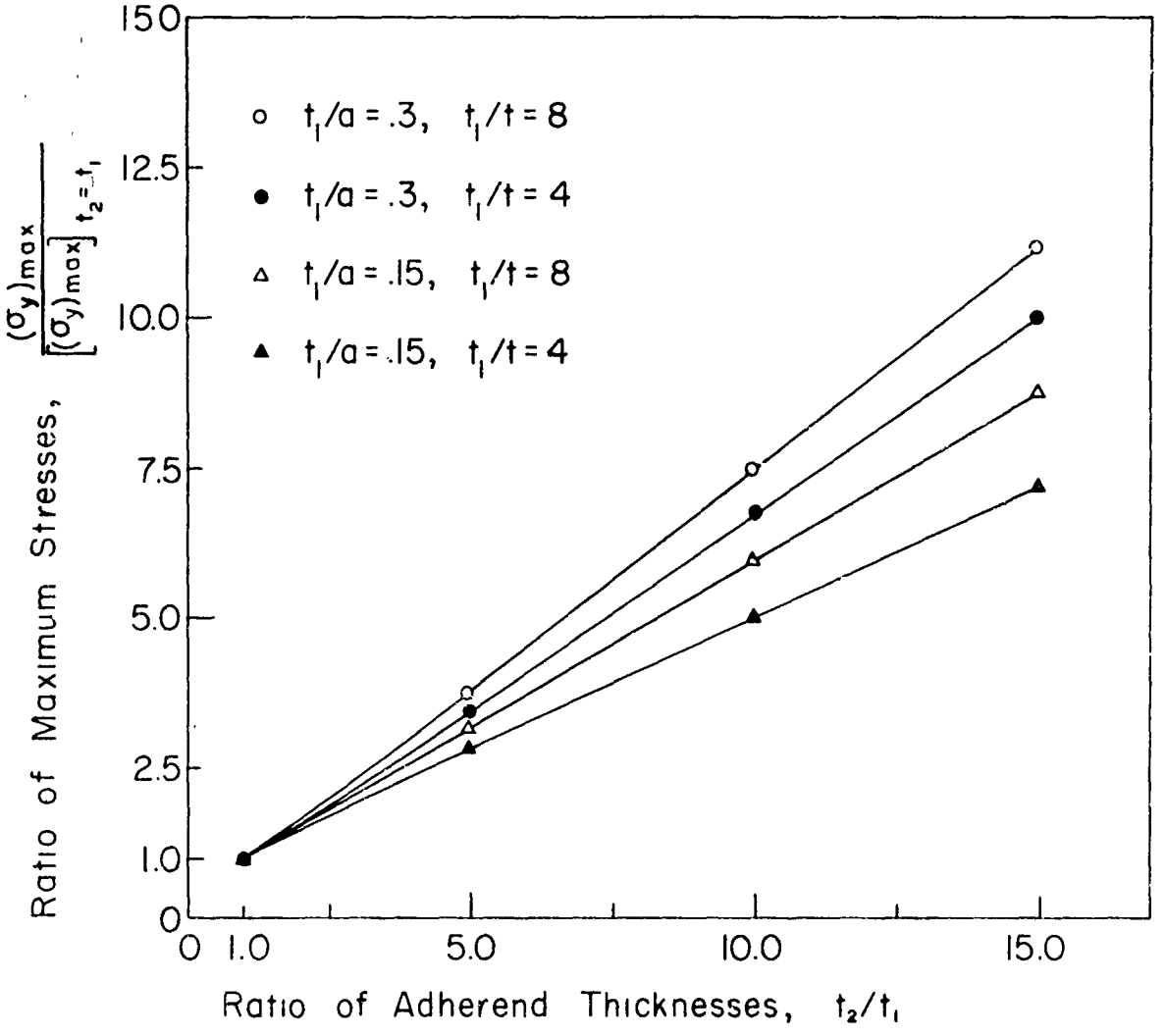

Fig. 66 $(\sigma_y)_{max}$ in Non-Identical Adherend Joint for $M_1 = M_2 = 0$

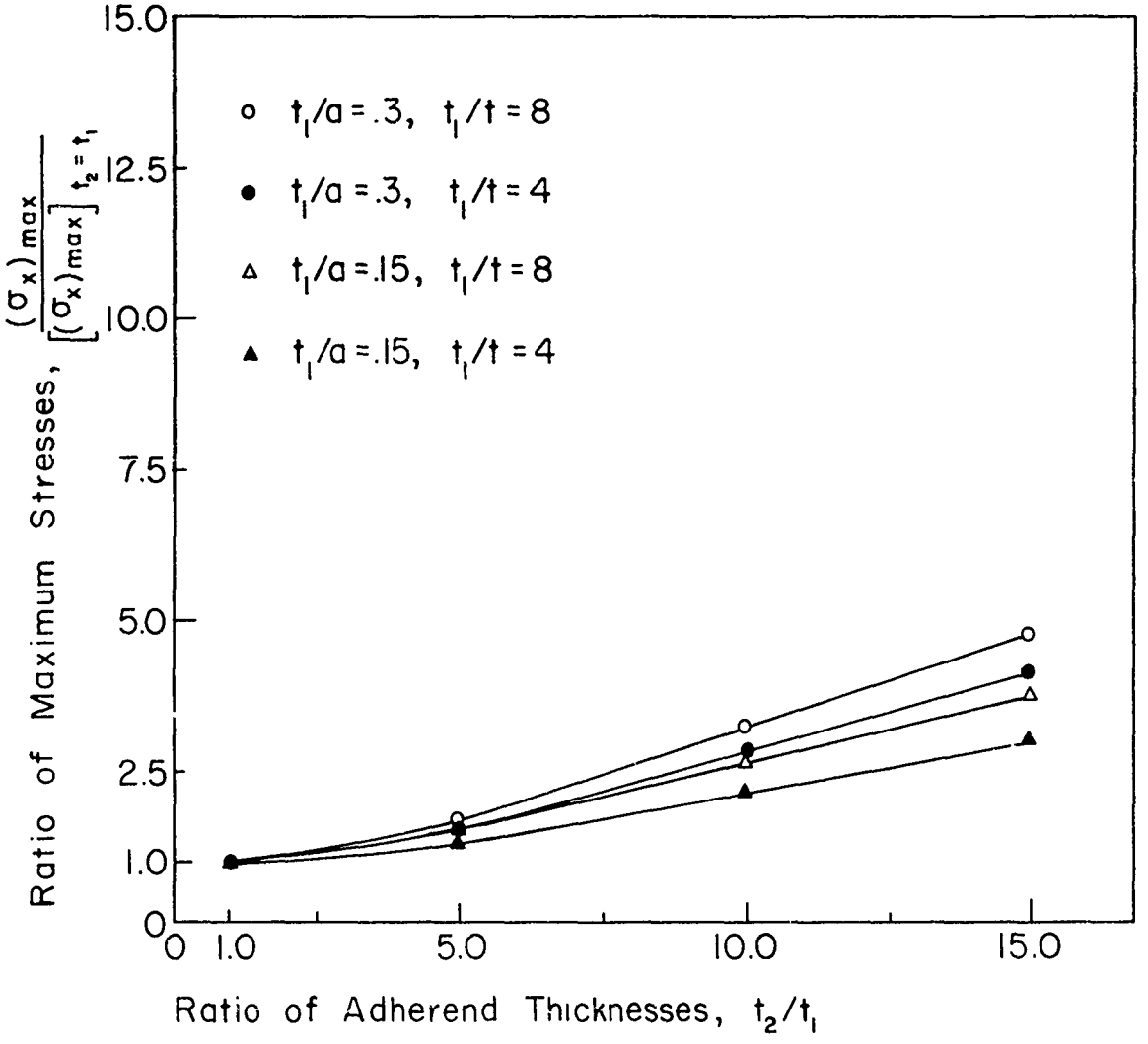

Fig. 67 $(\sigma_x)_{max}$ in Non-Identical Adherend Joint for $M_1 = M_2 = 0$